AALTO UNIVERSITY
School of Electrical Engineering
Department of Signal Processing and Acoustics

Juhana Jaatinen

PHASE ESTIMATION IN A NAVIGATION RECEIVER

The thesis was submitted in partial fulfillment for the degree of Licentiate of Science in Technology in Espoo ____ . ____ . 2011

Supervisor	Prof. Visa Koivunen
Second examiner	Prof. Risto Wichman

AALTO UNIVERSITY
SCHOOL OF ELECTRICAL ENGINEERING

ABSTRACT OF THE LICENTIATE'S THESIS

Author: Juhana Jaatinen

Title of thesis: Phase estimation in a navigation receiver

Date: April 11, 2011 **Language:** English **Number of pages:** 99

Department: Department of Signal Processing and Acoustics

Field of research: Signal Processing for Communications (S043Z)

Supervisor: Professor Visa Koivunen

Second examiner: Professor Risto Wichman

This thesis proposes a new method for estimating the unknown phase of a sampled sinusoid of known frequency. The method is called *phase corrected correlation (PCC)* and it is targeted specifically for the case, when there is a non-integer number of cycles in the measurement interval. Performance of the *PCC phase estimate* is studied by comparing its mean squared error (MSE) with the Cramér-Rao lower bound (CRLB). In order to simplify analysis and comparison with related methods, the selected signal model is a single sinusoid in additive white Gaussian noise. Two additional algorithms, *burst noise removal* and *partition outlier removal*, are proposed for decreasing the MSE of phase estimates in the presence of disturbances such as lightnings and interfering transmitters. *PCC frequency estimate* is obtained by observing signal phase change in consecutive measurement intervals. Frequency estimation performance and computational burden of the PCC is compared with Interpolated DFT (IDFT).

The application domain is a meteorological sounding system for upper-air wind finding using Very Low Frequency (VLF) navigation systems. The problem is to estimate a minute frequency offset caused by the Doppler effect. Frequencies transmitted especially by the Russian Alpha radionavigation system are challenging: the estimation algorithm must be able handle a non-integer number of signal cycles in the 400 ms measurement interval. Most of the related frequency and phase estimation methods are not applicable to this estimation problem. Interpolated DFT (IDFT) may be feasible and therefore it is used as a benchmark.

It is shown with computer simulations, that MSE of the phase estimate is close to the CRLB. The same applies to frequency estimates obtained by observing signal phase change in consecutive measurement intervals. Comparison with IDFT shows, that MSE of the PCC frequency estimate is closer to the CRLB as MSE of the IDFT frequency estimate. Moreover, PCC achieves this performance with lower computational burden, making it the preferred choice in this application. It is also shown that MSE of the phase estimate decreases as sampling rate or measurement interval is increased, and that MSE of the phase estimate decreases when interference is removed using burst noise removal and partition outlier removal algorithms. Finally, to achieve a computationally efficient digital signal processor (DSP) implementation, a number of implementation issues are covered.

Keywords: Phase corrected correlation, PCC, parameter estimation, MLE, phase, frequency, VLF, radionavigation, Alpha, Omega, upper-air wind finding

AALTO-YLIOPISTO **LISENSIAATINTUTKIMUKSEN**
SÄHKÖTEKNIIKAN KORKEAKOULU **TIIVISTELMÄ**

Tekijä: Juhana Jaatinen

Työn nimi: Vaiheen estimointi navigointivastaanottimessa

Päivämäärä: 11.4.2011 **Kieli:** Englanti **Sivumäärä:** 99

Laitos: Signaalinkäsittelyn ja akustiikan laitos

Tutkimusala: Tietoliikenteen signaalinkäsittely (S043Z)

Työn valvoja: Professori Visa Koivunen

Toinen tarkastaja: Professori Risto Wichman

Tässä lisensiaatintutkimuksessa esitetään menetelmä näytteistetyn sinimuotoisen signaalin vaiheen estimointiin silloin, kun taajuus on tunnettu. Menetelmän nimi on *vaihekorjattu korrelaatio (PCC)* ja sillä voi estimoida vaiheen myös niissä tapauksissa, joissa signaalista ei ole kokonaisluvullista määrää jaksoja mittausvälissä. *PCC-vaihe-estimaatin* suorituskykyä tutkitaan vertaamalla sen neliösummavirhettä (MSE) Cramér-Rao alarajaan (CRLB). Jotta menetelmän analysointi ja vertailu läheisten menetelmien kanssa olisi helpompaa, signaalimallina on yksi sinimuotoinen signaali valkoisessa Gaussisessa kohinassa. Työssä esitetään lisäksi kaksi menetelmää häiriöisen signaalin vaihe-estimaatin neliösummavirheen pienentämiseen. Tyypillisiä häiriölähteitä ovat salamat ja läheisellä taajuudella toimivat lähettimet; menetelmät ovat vastaavasti nimeltään *purskehäiriöiden poisto* ja *virheellisten ositteiden poisto*. *PCC-taajuusestimaatti* saadaan seuraamalla signaalin vaiheen muuttumista peräkkäisissä mittausväleissä ja sen suorituskykyä sekä laskentakuormaa verrataan Interpoloituun DFT:hen (IDFT).

Menetelmän sovellusalue on meteorologinen luotausjärjestelmä, joka käyttää VLF-navigointiverkkoja yläilmakehän tuulenmittaukseen. Estimointiongelmana on arvioida Doppler-ilmiön aiheuttama pienenpieni taajuussiirtymä. Venäläisen Alpha-radionavigointiverkon lähetystaajuudet ovat erityisen haasteellisia, koska käytetyssä 400 ms:n mittausvälissä ei ole kokonaisluvullista määrää signaalin jaksoja. Useimmat taajuuden- ja vaiheenestimointimenetelmät eivät ole soveliaita tähän estimointiongelmaan. IDFT saattaisi olla käyttökelpoinen ja siksi sitä on käytetty vertailukohtana.

Tietokonesimulaatioin osoitetaan, että vaihe-estimaatin MSE on lähellä CRLB:tä. Sama koskee taajuusestimaatteja, jotka on saatu seuraamalla signaalin vaiheen muuttumista peräkkäisissä mittausväleissä. Simulaatiot osoittavat myös, että PCC-taajuusestimaatin MSE on lähempänä CRLB:tä kuin IDFT-taajuusestimaatin MSE. Koska PCC saavuttaa tämän suorituskyvyn pienemmällä laskentakuormalla, se on soveliaampi kyseiseen sovellukseen. Lisäksi osoitetaan, että vaihe-estimaatin MSE pienenee, kun näytteenottotaajuutta tai mittausväliä kasvatetaan, tai kun salamoiden ja läheisellä taajuudella toimivien lähettimien aiheuttamat häiriöt poistetaan purskehäiriöiden poisto ja virheellisten ositteiden poisto -algoritmeilla. Lopuksi esitetään muutamia signaaliprosessoritoteutukseen (DSP) liittyviä yksityiskohtia, joilla voidaan pienentää laskentakuormaa.

Avainsanat: Vaihekorjattu korrelaatio, PCC, parametrin estimointi, MLE, vaihe, taajuus, VLF, radionavigointi, Alpha, Omega, yläilmakehän tuulenmittaus

Preface

Postgraduate studies leading to this thesis were started in the Laboratory of Signal Processing and Computer Technology at the Helsinki University of Technology in June 1991. At that time Professor Iiro Hartimo was the head of the laboratory together with Professor Jorma Skyttä. The great recession of 1991 changed plans and I ended up teaching engineering in the autumn and was hired as a digital signal processing expert to Vaisala Oy in January 1992 by Mr. Pentti Karhunen, R&D manager in the Upper Air Division. Thereafter I have studied the required credit points and written this thesis on the side of my full-time work.

The first major work assignment was given to me by Mr. Karhunen: "Design a new Navaid receiver". On one hand the assignment was very exact, and on the other hand gave a lot of freedom in implementation. For a recently graduated engineer this was a big challenge and a sign of trust. As it turned out, the work involved plenty of research, not just implementation of existing algorithms. I am very grateful to Mr. Karhunen for his support and this opportunity, which eventually led to the invention of a novel way to implement a particular navigation receiver [1], which is part of a meteorological sounding system [2]. This receiver was in many respects more versatile than existing implementations. Without the assignment from Mr. Karhunen the following thesis would not have been written.

During the years at Vaisala Oy, I had several interesting technical and historical discussions with designers of the previous generation receivers: Pentti Karhunen, Ilkka Ikonen, Keijo Luukkonen, Tapio Iivonen, Henry Andersson, Reijo Hämäläinen, Sakari Kajosaari, Osmo Roivainen, Ahti Sarvi, Pekka Vikman, Hannu Komulainen, and Arto Mahkonen. Some of them also took part in the design of the new receiver. The other end of the telemetry link is a radiosonde transmitter. In this respect I had warm relations with R&D manager Mr. Veijo Antikainen, and I also thank Ari Paukkunen and Kari Kalliokönnö for their patience in explaining sensor and transmitter details, respectively. Also to be thanked is Seija Sorvala who performed numerous soundings that were required to develop the system and to determine its performance. Many others were also involved in the development of the sounding system and daily work.

I would like to thank the three students who studied related topics under my supervision and wrote their Master's Theses during these assignments: an automatic VLF observing station in 1996 by Jussi Åkerberg [3], an extensive test series on VLF-Navaid wind finding accuracy in 1997 by Erkka Pälä [4], and a radiosonde PTU receiver and a study of various frequency estimation methods in 2000 by Ismo Haanaho [5].

I also wish to express my gratitude to Ritva Siikamäki who during the years at Vaisala diligently read and corrected my literary work for over a decade. Being a

linguist, her to the point questions on engineering topics have forced me to think matters from the readers point of view. In the course of years I may have learned something of the English language as well.

I would like to thank the personnel of the Laboratory of Signal Processing and Computer Technology, and Marja Leppäharju from GETA (Graduate School in Electronics, Telecommunications and Automation). Every time I visit the laboratory I feel very welcome, although it is now close to twenty years since I worked there myself.

Jarkko Vuori started working for the degree of Doctor of Technology in the Laboratory of Signal Processing and Computer Technology at the same time as I was there writing my Master's Thesis. We both had a keen enthusiasm for technology. Although our ways separated, we have kept contact and every few years Dr. Vuori has enquired about the progress of my thesis. His encouragement and support was one of the incentives to have this work finished.

The caring encouragement over the years from my lovely wife Sanna and our daughter Tiia has kept me going, and now the work is done.

The opportunity to finish off the literary work was made possible by my current employer ABB Oy, Drives.

Finally, I wish to express my gratitude to Professor Visa Koivunen for his endurance during this somewhat lengthy process.

Laaksolahti, Espoo
April 2011

Juhana Jaatinen

Contents

List of abbreviations

AC	Alternating current
CRLB	Cramér-Rao lower bound
ComVLF	Communications VLF
DFT	Discrete Fourier transform
DOA	Direction of arrival
DoD	U.S. Department of Defense
DoT	U.S. Department of Transportation
DSP	Digital Signal Processor
ECMWF	European Centre for Medium-Range Weather Forecasts
ESPRIT	Estimation of signal parameters via rotational invariance techniques
FSK	Frequency-shift keying
FFT	Fast Fourier transform
FRP	Federal Radionavigation Plan (DoT/DoD)
FTS	Frequency/Time Standard
GPS	Global Positioning System
IDFT	Interpolated DFT
LF	Low frequency, 30–300 kHz
MLE	Maximum likelihood estimator
MSE	Mean squared error
MSK	Minimum-shift keying
MUSIC	Multiple Signal Classification
NATO	North Atlantic Treaty Organization
NAVAID	Navigation Aid (e.g. Omega, Alpha, ComVLF, Loran-C, and GPS)
PCC	Phase corrected correlation
ppm	Parts per million
PSD	Power spectral density
PTU	Pressure (P), temperature (T), humidity (U)
RNS	Radio Navigation System
SNR	Signal-to-noise ratio
SPC	Samples per cycle
TDE	Time-delay estimation
USCG	United States Coast Guard
UTC	Universal Time Coordinated
VLF	Very low frequency, 3–30 kHz
WMO	World Meteorological Organization

List of symbols

A	Sinusoid signal amplitude
$ADev$	Average deviation
$ADev_x, ADev_y$	Average deviation of partitions, real and imaginary part
$C(f, m)$	Correlation at signal frequency for the mth measurement interval
D_{burst}	Burst detection threshold
$D_{cluster}$	Outlier detection threshold
E	Ensemble size in simulations
ϵ	Small positive number
f	Sinusoid signal frequency
$\hat{f}$	Frequency estimate
Δf	Frequency offset
$\Delta f_{doppler}$	Frequency offset caused by the Doppler effect
f_k	Sinusoid signal frequency, k cycles in the measurement interval
f_{rx}	Received frequency
f_s	Sampling rate, $f_s = 1/T$
f_{tx}	Transmitted frequency
η	Signal-to-noise ratio in CRLB
θ	Sinusoid signal phase
$\hat{\vartheta}$	Instantaneous sample-by-sample phase estimate
$\hat{\theta}$	Phase estimate of one measurement interval
$\hat{\theta}_m$	Phase estimate for the mth measurement interval
$\hat{\theta}_{all}$	Phase estimate using all partitions
$\hat{\theta}_{valid}$	Phase estimate using valid partitions
k	Integer part of K
Δk	Fractional part of K
K	Number of cycles in a measurement interval, $K = k + \Delta k$
L	Number of partitions in a measurement interval
Λ	Set of valid partitions
m	Measurement interval index, partition index
M	Length of correction term sequence
n	Discrete time sample index
N	Number of samples in a measurement interval
N'	Number of samples in a partition
$PC(m)$	Phase correction term for the mth measurement interval or partition
$PCC_m(f)$	Phase corrected correlation (PCC) for the mth measurement interval
$PCC_{partitioned}(f)$	Partitioned PCC
$PCC_{valid}(f)$	PCC constructed from valid partitions

$R(f)$	Correlation reference
r_{burst}	Zeroing range in burst noise removal
r_m	Distance of the mth partition from the center of the cluster
s_{burst}	Threshold scaling factor in burst noise removal
$s_{cluster}$	Threshold scaling factor in partition outlier removal
σ	Standard deviation
σ^2	Variance
T	Sampling interval, $T = 1/f_s$
T_{meas}	Measurement interval, $T_{meas} = NT$
w	Additive white Gaussian noise
ϕ	Apparent phase advance
$\phi(m)$	Apparent phase advance in the mth measurement interval
$x(n)$	Discrete time sampled signal
$X(f_k)$	Correlation (DFT) of a discrete time signal $x(n)$
x_C, y_C	Correlation at signal frequency, real and imaginary part
x_{med}, y_{med}	Center of partition cluster, real and imaginary part
x_{PC}, y_{PC}	Phase correction term, real and imaginary part
x_R, y_R	Correlation reference, real and imaginary part
z	Complex number, $z = x + jy = re^{j\varphi}$
ω	Signal frequency, $\omega = 2\pi f$ [rad/s]

Chapter 1

Introduction

1.1 Overview

Methods for estimating the frequency, frequency offset, or phase of a sinusoid signal from a finite set of discrete measurements are basic tools in a practising signal processing engineers toolbox. Frequency and phase estimation are also closely related, as frequency and frequency offset estimates can be obtained by observing signal phase change in consecutive time instants. Multiple approaches have been proposed over the years with emphasis on various details depending on the application and signal model. Some methods are targeted specifically for short data records and time varying signals, while other methods are better suited for stationary signals and longer measurement intervals. Applications can be found in many electronic signal processing systems, including navigation, radar, sonar, seismology, speech, digital audio, medical imaging, mobile communications, industrial control, renewable energy generation, and meteorology. The viewpoint in this thesis is on estimating sinusoid signal parameters from long data records in the presence of broad-band noise and nearby strong harmonic interference. Suitability of existing methods is also considered from this point of view.

Spectral analysis of sampled signals is usually based on the discrete Fourier transform (DFT), which can be efficiently calculated with the fast Fourier transform (FFT). Although this approach is popular and suitable for a wide range of signals, it does not offer a good solution for the very accurate measurement of the frequency of individual sinusoids [6]. To begin with, the frequency resolution in Hertz is approximately the reciprocal of the measurement interval in seconds. Secondly, spectral leakage of broadband noise and harmonic interference causes weak signals to be distorted and obscured [7]. These two performance limitations are particularly troublesome when analyzing short data records, which are present e.g. in radar and sonar. On the other hand, to achieve adequate frequency resolution in a navigation application, very long data records should be used, leading to prohibitive processing load and impractical memory requirements.

One approach to deal with this problem is based on interpolation between the discrete points of a DFT spectrum, thus achieving sub-bin resolution for frequency and phase estimates. This is attained at a cost of increased processing load [6]. Another approach is to assume, that the signal satisfies a known mathematical model and then estimate signal parameters based on this model. These methods (ARMA, AR, MA) may provide more details for shorter data lengths, assuming

that a proper model has been selected and signal-to-noise ratio is good. For low SNR they are no better than the FFT [8, p. 198].

Pitch or fundamental frequency estimation is essential in a variety of speech and audio processing systems. The problem is to estimate from a small number of samples the period of a speech or music waveform, which varies both in period and in the detailed structure within a period [9].

Phase locked loop (PLL) is the traditional and widely used method for estimating instantaneous frequency and phase, and to track periodic signals. Both analog [10, pp. 286–293] and digital [11, pp. 434–453] implementations exist. In communication systems the PLL is used among others for carrier and symbol synchronization, demodulation, and frequency synthesis. Frequency estimation accuracy of the PLL can be improved by using a narrower loop filter at a cost of increased processing load.

Time-delay estimation (TDE) and direction-of-arrival (DOA) estimation are basic tools in various array processing scenarios and have many applications, including tracking in sonar, range finding in radar, seismic exploration, positioning in navigation, synchronization in communications, and medical ultrasound imaging. Signal model is a single source and several time-delayed versions of the same signal. The quantities to be estimated are parameters upon which the sensors outputs depend, such as frequency, DOA of plane waves, or phase difference between sensors, and they are often estimated from a small number of samples. In such problems, the functional form and the number of the underlying signals can often be assumed to be known [12], [13].

When a signal is assumed to be a pure sinusoid in white Gaussian noise and only phase is unknown, the approximate maximum likelihood estimate of the phase can be obtained by correlation as described in [14, pp. 167–168]. This approach works also with long data records. When there is an integer number of cycles in the measurement interval, taking the argument of the discrete Fourier transform of the signal performs the same operation. Interpolated DFT has been developed for the case when there is a non-integer number of cycles in the measurement interval [6].

Methods for estimating phase difference of two equal frequency sinusoids have been developed in the fields of communications, control applications, and power-line signal processing. Time-domain methods are based on measuring the difference of zero-crossings of the two signals. More recent frequency-domain methods [15] are based on the interpolated DFT. Common to these methods is simultaneous sampling of the two equal frequency signals, and that the parameter of interest is the phase difference. These methods are not suitable for estimating the phase of a single sinusoid.

The rapid development of digital communications has motivated the development of several new methods [11], [16]. Typical to these applications are short data records, Doppler effect in mobile platforms, fading and multi-path effects, and rapidly time varying bandlimited signals. In order to enable reliable symbol detection, the receiver needs an estimate of the carrier frequency for frequency offset compensation. Typically perfect timing or symbol synchronization is assumed, and signal model is one-sample-per-symbol plus noise for a burst length of a few symbols. Phase estimation in the context of M-PSK modulated signals means symbol detection. In addition to single parameter estimation, joint estimation of several signal parameters has been widely studied.

1.2 Application domain

The application domain in this thesis is a meteorological sounding system [2]. Upper-air winds are commonly measured with a hydrogen or helium filled weather balloon and by measuring the velocity of the the radiosonde attached to it, one gets the wind velocity. The result is a vertical wind profile showing the horizontal component of the wind velocity (speed and direction). The focus in this thesis is on upper-air wind finding using Very Low Frequency (VLF) navigation systems. When a radiosonde flies relative to a fixed navigation transmitter, the observed frequency is changed by the Doppler effect, and by estimating this change in frequency, the radial motion of the radiosonde can be determined. By combining observations for several transmitters, the motion of the radiosonde relative to the earth can be determined as described in [17] and [18].

Although weather satellites and weather radars have developed in the recent years, radiosondes carried by weather balloons are still used in large numbers. Upper-air radiosonde observations are the most important inputs to the prediction model [19, pp. 242–253]. Typical measured parameters are wind speed and direction, pressure, temperature, and humidity.

In 1995 the prevailing technology in meteorological applications used Omega or Loran-C navigation networks for wind finding. Omega was the principal source for wind finding due to global coverage, excellent availability, good signal quality and low cost consumable measurement instrument, the radiosonde. Some receivers were also capable of receiving Russian Alpha signals and VLF band communication transmitters simultaneously with Omega signals [20].

Then the situation changed at short notice. The U.S. Department of Transportation (DoT) publishes the Federal Radionavigation Plan (FRP) together with the Department of Defense (DoD) every two years, providing the current U.S. government plans and policies for Federally-funded radionavigation systems. Past versions of the FRP called for a 10 to 15 year transition period prior to termination of radionavigation systems. When the 1994 FRP [21] was published in May 1995, there was an abrupt change in the policy between 1992 and 1994: the termination date for Omega radionavigation system was changed from the year 2005 to September 30, 1997 [22]. In two years there should be a global alternative to Omega based systems. The only alternative providing global coverage in all weather conditions was GPS, which was substantially more expensive to operate. The meteorological institutes were facing a major instrumentation replacement program and an unexpected raise in operating costs.

1.3 Scope of the thesis

Signal model in this thesis is a single unmodulated sinusoid in additive white Gaussian noise. A method for estimating the unknown phase of a sampled sinusoid of known frequency is proposed. The method is called *phase corrected correlation (PCC)* and it is targeted specifically for the case, when there is a non-integer number of cycles in the measurement interval. Performance of the *PCC phase estimate* is studied by comparing its mean squared error (MSE) with the Cramér-Rao lower bound (CRLB). *PCC frequency estimate* is obtained by observing signal

phase change in consecutive measurement intervals, and its performance and computational burden is compared with Interpolated DFT (IDFT). Two additional algorithms to be used in conjunction with the PCC are proposed. They are called *burst noise removal* and *partition outlier removal*, and are intended to be used in the presence of disturbances such as lightnings and interfering transmitters.

1.4 Contributions of the thesis

The meteorological sounding system [2] equipped with the navigation receiver by the author [1] was able to utilize more signals than existing [20] and earlier [23] implementations. This enabled wind finding without the Omega network, using only Alpha and Communications VLF signals. Even though the coverage was not quite global, many meteorological institutes could continue operations as before. To publicize this fact, the author wrote several papers during 1995 to 1998 about potential means to continue VLF-based wind finding without Omega: [24], [25], [26], [27], [28], [29], and [30].

To have continuous up-to-date status information, an automatic VLF observing station was designed in 1996 [3]. This observing station was based on receiver [1] and it monitored automatically the quality of Omega, Alpha, and Communications VLF signals and collected this data for further inspection. The receiver was slightly modified by adding a software based spectrum analyzer to make it easier to find new VLF transmissions for wind finding. One potential transmission from France was found and its location was later verified. The culmination of our VLF study was an extensive test series in 1997 [4]. This is probably the last study made on Omega-based wind finding and the results were presented by the author in 1998 [30], three months after Omega termination, in an American Meteorological Society (AMS) conference.

1.5 Structure of the thesis

Chapter 2 discusses the atmosphere, weather forecasting, meteorological measurements and instruments to the extent that is appropriate to give the reader an understanding of the application area. Description of navigation systems in *Chapter 3* and the brief discussion on various disturbances affecting the received signal gives a background for the estimation problem. *Chapter 4* summarizes properties of a number known methods for estimating the frequency, frequency offset, or phase of a sinusoid signal and assesses their applicability to the estimation problem faced by the navigation receiver. *Chapter 5* presents authors work: *phase corrected correlation (PCC)* algorithm. The discussion is started by presenting signal model and estimation problem, followed by a description of the proposed algorithm. Performance of the algorithm is studied by comparing its MSE with the CRLB, and with MSE of estimates obtained with Interpolated DFT (IDFT). Two additional algorithms to be used in conjunction with the PCC are proposed for decreasing MSE of phase estimates in the presence of disturbances. The conclusion in *Chapter 6* summarizes the main results. Finally, the *Appendix* contains a set of MATLAB scripts that illustrate the various algorithms which are presented in this thesis.

Chapter 2

Meteorological observations

2.1 Overview

Man has tried to predict the weather for ages. Before 1900's the predictions were largely based on folklore and the results were random. Weather map analysis and extrapolation of prominent characteristics was developed in 1920's. Up to 1970's meteorologists analyzed pressure changes and the observed trajectory of cyclones (low pressure) to predict the weather for 1–2 days ahead. This method is still valid for short periods up to 12 hours. Routine operational weather forecasts have been produced by computers since 1975. Today, numerical prediction using computers has practically replaced manual weather map analysis in *24-hour and longer forecasts*. Besides surface observations, the prediction model needs observations of the air flow and other parameters in the upper atmosphere. All measurements are important as the advantage of one method complements the weak point of another one. The variety of meteorological measurement systems is large, including surface weather stations, upper-air sounding systems, weather satellites, GPS meteorology, solar radiation monitoring, lightning detection, sea level and temperature monitoring, anchored and drifting buoys, en-route airplane and ship observations, and weather radars. Parameters such as cloud height, precipitable water vapor content, type of precipitation (e.g. water, snow, hail, mosquitoes), three-dimensional wind profile, and horizontal visibility can be monitored. Although weather satellites and weather radars have developed in the recent years, *upper-air radiosonde observations* are still the most important inputs to the prediction model [19, pp. 242–253].

The summary of the atmosphere and weather forecasting is based on the following books on meteorology [19], [31], [32], [33], and on web pages of the Finnish Meteorological Institute [34], European Centre for Medium-Range Weather Forecasts (ECMWF) [35], and World Meteorological Organization (WMO) [36]. The list of wind finding methods and the description of a VLF-band upper-air sounding system are based on authors work in this field.

2.2 Structure of the atmosphere

The atmosphere is a thin gaseous envelope which makes our planet habitable. Besides being a part in biological processes, the atmosphere affects our lives in many ways. Almost all weather related phenomena happen in the lowest 20 km of

the atmosphere, which makes up 95% of its mass. The atmosphere does not have a distinct upper boundary. Air density and air pressure decrease rapidly when going up, and above 100 km elevation one is practically in outer space. When this is compared to the 6400 km radius of the earth, one understands how very thin our protection against the void of the space is [32, pp. 1–9], [19, pp. 62–74].

Chemical composition of the atmosphere has changed little in the past few hundred million years. Dry air is mainly formed of nitrogen 78% and oxygen 21%. The remaining 1% is formed of several gases, mainly argon 0.93% and carbon dioxide 0.036%. The remainder is comprised of other gases such as neon, helium, methane, krypton, xenon, hydrogen, and ozone. The air also contains a variable amount of water vapor (0–4%), which is an invisible gas, various dust particles, and more recently, man-made air pollutants. Some of these gases (water vapor, carbon dioxide, methane, ozone, oxides of nitrogen, and CFC), are strong greenhouse gases, which affect the heat balance of the earth.

The atmosphere has several different layers, or *spheres*, in the vertical, and *pauses* that separate the spheres. Air density decreases almost evenly as elevation increases. Temperature, on the other hand, behaves quite differently as shown in Figure 2.1. Normally the temperature changes monotonically in one direction within a sphere and changes direction to the opposite at a pause. The weather phenomena and air motion are quite different from one sphere to the next one.

The lowest layer is called *troposphere*. Its upper boundary, *tropopause*, is typically at an elevation of 18 km over the equator and 8 km over the poles. *Almost all weather related phenomena, such as clouds and rain, take place in the troposphere.* The troposphere is heated from below by the heat radiation from the surface of the earth, which in turn is heated by the solar radiation. Normally the lowest part close to the surface is warmer and temperature decreases at an average rate of 6.5°C/km when going up. As warmer air is lighter than cold, it tends to rise up until it has mixed with the surrounding colder air. This vertical convection keeps the air fairly well stirred and affects the conditions in the whole troposphere. At tropopause air temperature is typically between -50 and -70°C and air density is only 10% compared to the sea level, consequently 90% of the mass of the atmosphere is below the tropopause. Most of the humidity in the atmosphere is found in the troposphere, especially in the lower parts of it.

The next layer is called *stratosphere*, and its upper boundary, *stratopause*, is at an elevation of 50 km. Temperature increases when going up in the stratosphere and reaches almost 0°C at the stratopause. About 10% of the mass of the atmosphere is in the stratosphere and air is very thin and dry. Winds in the stratosphere are normally strong and wind systems large, the size of the globe. Stratosphere contains most of the ozone of the atmosphere. It is heated from above by ozone absorbing sun's ultraviolet radiation. The amount of radiation and heating decreases when going down, which explains the thermal structure. Stratosphere protects us from excess ultraviolet radiation, cosmic radiation, and high-energy particles. The only visible phenomenon is rare stratospheric clouds in subpolar and polar regions.

The layer above is called *mesosphere*, and its upper boundary, *mesopause*, is at an elevation of 85 km where temperature is about -100°C and air pressure is comparable to a good vacuum. Mesosphere absorbs very little energy from the sun and hence, temperature decreases when going up. Mesopause is the coldest layer in the atmosphere. Meteors and luminous night clouds are visible phenomena

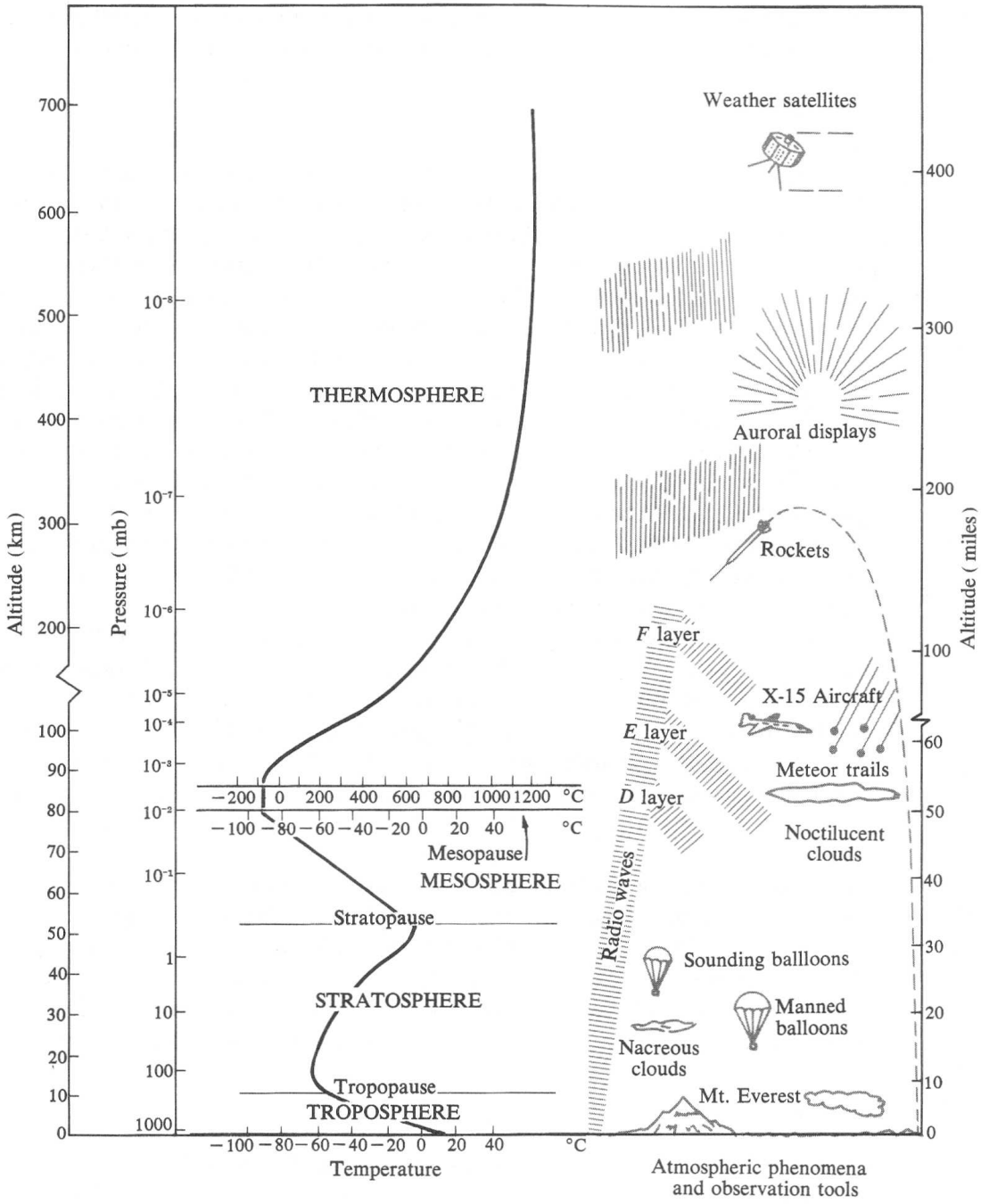

Figure 2.1: Vertical distribution of atmospheric temperature and phenomena [32, p. 8], the height of the ionosphere varies regularly each day from 70 to 90 km

taking place in the mesosphere. After mesosphere, above 85 km, are *thermosphere*, *ionosphere*, *exosphere*, and *magnetosphere*. These layers are practically in outer space.

The *ionosphere* is important for *VLF-band radio signal propagation*. Ultraviolet solar radiation ionizes atoms forming a large number of free electrons. This electrically charged part of the atmosphere reflects radio waves, making around-the-world transmissions possible. Reflective height of the ionosphere varies regularly each day and over the year from 70 to 90 km [37, pp. 180–186], [38, pp. 25–26]. Aurora borealis (northern lights) and aurora australis (southern lights) take place in the ionosphere.

2.3 Weather forecasting

The most well known weather forecasts are the ones in TV, radio, and newspapers, although professional weather services are financially more significant. These include road weather services, air traffic route planning, sea transport, and agriculture.

General circulation of the atmosphere

Temperature differences caused by uneven heating produce the basic force that drives the winds. The picture of the air flow is made complex by the rotation of the earth, friction and turbulence, and the variable character of the surface. To simplify analysis, it is convenient to categorize circulation systems according to size. The larger the circulation, the longer it lives [32, pp. 93–107], [19, pp. 176–221].

The largest and longest living are *planetary scale* weather systems, whose size is in the order of 5000–10000 km. The duration of planetary scale phenomena is from weeks to several months. These play an important role in determining the seasonal characteristics of the weather.

The size of *large scale* or *synoptic scale* weather systems is 500–5000 km and their duration is over one day. These are responsible for the day-to-day weather changes. One can observe a large scale weather system only by combining observations from a large area and analyzing them on a weather map. Figure 2.2 shows an example of a synoptic scale weather map.

Rain, fog, thunderstorms and land-sea breeze belong to *mesoscale* weather systems, whose size is 5–500 km. A weather radar is better suited for observing mesoscale phenomena. The lifetime of a large rain front can be over 12 hours, while individual rain clouds forming it can last only one hour. Small clouds, gusts of wind, formation of rain drops and ice crystals belong to *microscale* weather systems, whose size is 1 mm–5 km. Most of the phenomena in this category have their own interesting physical structure, but they are not particularly interesting in weather forecasting sense.

Synoptic observations

In meteorology, synoptic means coincident in time. About 10000 stations worldwide and 50 stations in Finland make a synoptic *surface observation* every three hours.

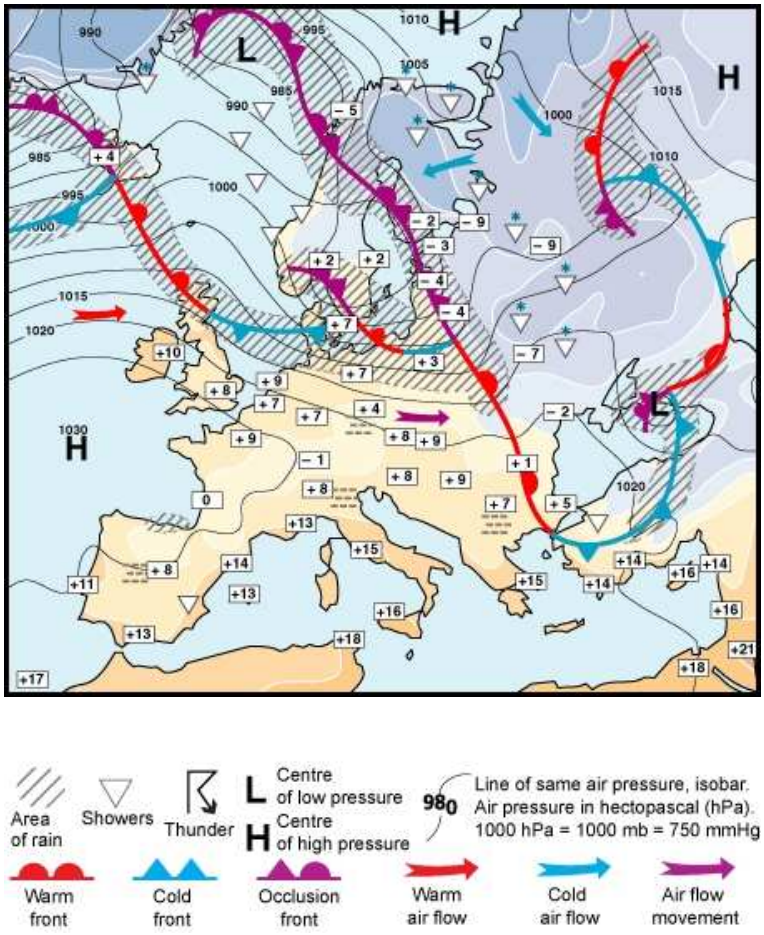

Figure 2.2: Synoptic scale weather map, 2007-01-31, 14:00 UTC [34]

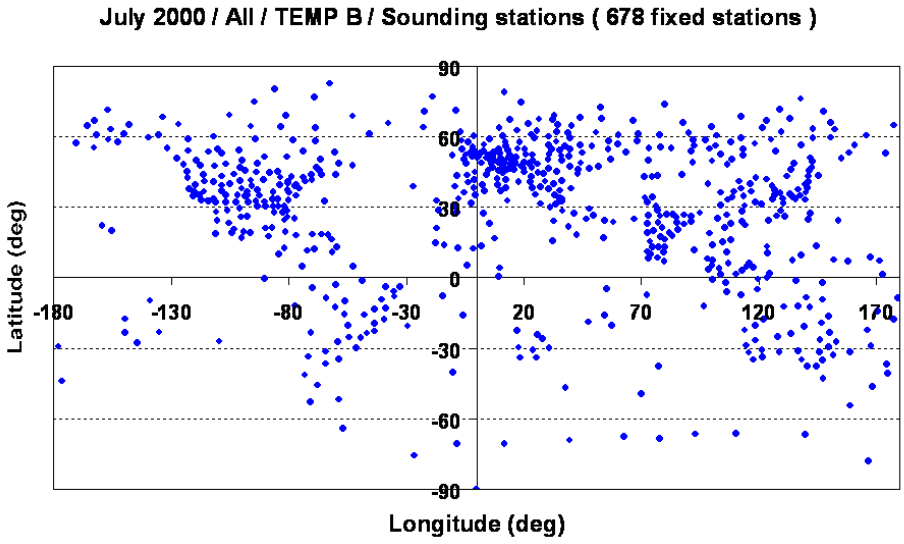

Figure 2.3: Synoptic upper-air sounding stations [39]

Additionally, there are over 600 synoptic *upper-air sounding stations* worldwide as shown in Figure 2.3. Three of them are in Finland: Jokioinen (close to Forssa), Luonetjärvi (close to Jyväskylä), and Sodankylä. The information about wind, pressure, temperature, humidity, clouds, rain, visibility, and other parameters are transferred to all participating meteorological institutes to be used in numerical weather prediction [19, pp. 132–163].

Prediction models benefit from an evenly populated observation grid. Since two thirds of the earth is covered by sea, it is very important to get observations from this area. Surface observations over the seas are obtained from ships, anchored and drifting buoys, and fixed platforms. Upper-air observations are obtained from ships using automatic weather balloon release systems and en-route airplanes equipped with meteorological instruments.

Numerical prediction

The basic principle of large-scale numerical weather prediction is to write predictive equations for the variables that represent the weather. The atmosphere is represented as a number of grid or calculation points, and weather as the various properties of these points. The dependency of a grid point property on neighboring points can be written into an equation, which represents the variation of the property as a function of time. *Prediction equations* vary, but most models are based on the following equations from flow dynamics: Newton's second law of motion, ideal gas equation, continuity equation, hydrostatic equation, and the first law of thermodynamics [32, pp. 131–149], [33, pp. 311-332], [31, pp. 84–114].

There are three phases in the *forecast process*. First the weather observations from irregular locations and times around the world are transformed into a regular grid of initial conditions. Second is the the actual computerized weather forecast. Finally, post-processing is performed to refine and correct the forecasts. The grid points are typically 20–100 km apart horizontally and in 20–30 layers vertically. As the grid is over the whole earth, the number of grid points is huge. Consequently, weather forecasting computers are among the most powerful ones in the world.

Traditionally, all the computing capacity was used to make one forecast. In recent years, instead of computing one forecast, several are computed using slightly different initial conditions. This technique is called *ensemble prediction*. By analyzing the consistency of the ensemble of forecasts, the meteorologist can judge the probability of a certain development taking place.

The two most significant *error sources* in numerical weather forecasts are insufficient initial conditions and imperfect forecast models. A short 2–3 day forecast is usually rather accurate and a 5–10 day forecast has more uncertainties. Although planetary scale equations do not model millimeter scale vortices, the energy from the small vortices does spread into planetary scale in about two weeks. In practice this means, that it is not possible to make accurate weather forecasts for longer than two weeks. The reliability of long term, over 24 hours, weather forecasts relies primarily on synoptic radiosonde measurements [19, pp. 242–253].

Figure 2.4: Wind vane and cup anemometer [40]

Figure 2.5: Ultrasonic wind sensor [40]

2.4 Wind finding methods

There are two main classes of wind finding: surface wind and upper-air wind. *Surface winds* are commonly measured with a wind vane and cup anemometer, and more recently, with an ultrasonic wind sensor. Examples are shown in Figures 2.4 and 2.5, respectively. Surface wind sensors are ground based and typically installed to a mast, away from obstructions. *Upper-air wind finding* falls into two main categories: *in situ measurements* performed with a radiosonde, and *remote sensing* with weather radars and satellites.

In situ upper-air wind finding

As the name implies, the instrument is taken in situ to make the measurement. Typically a weather balloon carries a radiosonde, but a parachute or a rocket can also be used. The advantage is a very accurate measurement of local conditions, and the downside is the limited spatial and temporal coverage.

GPS radiosondes provide global coverage and have excellent wind finding accuracy (0.1 m/s) which exceeds numerical forecast requirements. GPS has mostly displaced other upper-air wind finding methods.

Dropsonde is a radiosonde with a parachute and it is dropped from an aircraft at an altitude of 5 to 10 km. As the dropsonde falls carried by its parachute, it measures vertical profiles of pressure, temperature, humidity, and wind. Dropsondes are used to predict the trajectory of hurricanes. Forecast capability is being improved by being able to deploy dropsondes from high altitude over large areas of open sea, where few observations would otherwise be available. Omega was the wind finding method from 1982 until 1997, and current models use the more accurate GPS.

Radiotheodolite tracks a radiosonde electronically. The measurement principle is passive (the antenna does not transmit) and independent of navigation networks. Wind is calculated from the azimuth and elevation measurements and height, which is calculated from the pressure, temperature, and humidity measurements. Wind

finding accuracy (1 m/s above 15-degree-elevation) depends on the range and elevation angle to the radiosonde, and a practical lower limit is 10-degree-elevation. The use of radiotheodolite has declined in civil meteorology, but it is still widely used by military forces to generate meteorological reports for the artillery.

Loran-C is a regional radionavigation system utilizing transmitters transmitting pulses in the 90 to 110 kHz band. Wind finding accuracy (1 m/s) meets numerical forecast requirements. Even though Loran-C is still used on areas where it is available, it is being replaced by GPS in new installations.

Wind finding accuracy using *Omega, Alpha,* and *Communications VLF* signals (2 m/s) met numerical forecast requirements of the World Meteorological Organization (WMO) [41]. These Very Low Frequency navigation systems are no longer used for upper-air wind finding. Other obsolete wind finding methods include *primary radar*, *secondary radar* or *transponder*, and *optical theodolite*.

Remote sensing

Remote sensing has the advantage of covering large areas and being able to provide measurements continuously. Depending on the method the weakness can be in measurement accuracy, vertical resolution, or in the ability to perform well in all weather conditions.

Weather radar is an important instrument for short term weather forecasts, from 3 to 6 hours. Local rain showers can be detected up to a 250 km radius. A rotating radar antenna sends high energy microwave pulses, which echo from obstacles such as rain drops, and measures the return time and power of the echo. Recent dual-polarization radars can also detect the size and velocity of the raindrops, and the form of the water, e.g. rain, hail, snow, or supercooled water. They can also distinguish the meteorologically interesting echoes from mosquitoes and flocks of birds.

Wind profiler is an upward looking radar which creates a three-dimensional profile of the wind speed and direction. Applications include airport wind shear detection, space launch support, special research programs, and tactical artillery support. Depending on the model, the upper limit of the measurement range is from 1 km up to about 10 km height. The range from surface up to a height of a few hundred meters can not be measured due to ground clutter. A rainy and cloudy day is good for measurement accuracy as there are a lot of particles and turbulence for radar echoes, while a nice and sunny day is difficult.

Weather satellites complement the other measurements in weather forecasting but can not replace them. Detection of cloud fronts in satellite pictures is one of the important, and certainly the most known application of satellite meteorology. Satellite measurements can also be used to detect cloud types, measure upper-air ozone, and to calculate some meteorological parameters, such as wind velocity, temperature, and precipitable water content. Although satellites can cover wide areas of the earth rapidly, they have some limitations in measurement accuracy and vertical resolution. In situ radiosonde measurements are required for satellite data calibration.

2.5 VLF-band upper-air sounding system

Upper-air winds are commonly measured with a hydrogen or helium filled weather balloon that ascends freely, about 5 m/s. The common assumption is that the balloon travels at the same velocity as the wind, and by measuring the velocity of the balloon or the radiosonde attached to it, one gets the wind velocity. This operation is called *wind finding* and the result is a vertical wind profile showing the horizontal component of the wind velocity (speed and direction) as a function of air pressure, height, or time. A weather balloon with a radiosonde provides wind profiles up to a height of about 30 km. Determination of wind speed and direction is based on navigation signals received and relayed by a radiosonde to a ground receiving station during the ascent of a weather balloon. The radiosonde receiver does not calculate wind velocity, it merely relays the signal to the ground receiver for further processing.

A VLF-band upper-air sounding system [2] is comprised of a ground receiving station and a radiosonde transmitter carried by a weather balloon. Sounding systems from other manufacturers have a similar configuration. Several physical quantities are measured during the ascent of the weather balloon: wind speed and direction, atmospheric pressure, temperature and relative humidity. Additional sensors can be attached to the radiosonde to measure radioactivity and ozone.

Figure 2.6 shows two hydrogen filled 800 g weather balloons, which have a bursting height of about 30 km. Free lift is adjusted to 1 kg to carry a 250 g radiosonde. Weight of the balloon varies from 200 g to 2 kg depending on the payload and desired bursting height. Figure 2.7 shows a weather balloon launch, Figure 2.8 shows a sounding operator entering unique calibration coefficients for the radiosonde sensors with a paper tape, and Figure 2.9 shows an example of a wind profile which has been measured using Omega, Alpha, and Communications VLF signals.

Radiosonde

The Finnish radiosonde was invented by professor Vilho Väisälä in 1931. Testing and development continued after the first flight and the radiosonde was presented internationally to the meteorological community in 1935. At that time only a very few types of radiosonde existed, all of which were heavier and considerably less advantageous than the Finnish instrument. Vaisala has been selling radiosondes since 1936, when the company was founded [40]. A VLF-band radiosonde is shown in Figure 2.10, this RS80-type was in use from 1981 till 2005 [42]. The main parts of the radiosonde are capacitive sensors, VLF receiver, UHF telemetry transmitter, and water activated battery. Figure 2.11 shows a paper tape containing unique sensor calibration coefficients and Figure 2.12 shows a water activated battery.

The radiosonde measures meteorological quantities in situ with its sensors. Sensors are connected in sequence to an oscillator. The measured physical quantity changes the capacitance of the sensor, and hence, the frequency of the oscillator between 7 and 10 kHz. The measurement sequence contains also two constant capacitances and an internal temperature measurement, which are used to improve measurement accuracy. Depending on the radiosonde type the connection time for each sensor is approximately 250 ms or 110 ms.

Figure 2.6: Two hydrogen filled 800 g weather balloons

Figure 2.7: Weather balloon launch

Figure 2.8: Sounding operator entering radiosonde calibration coefficients

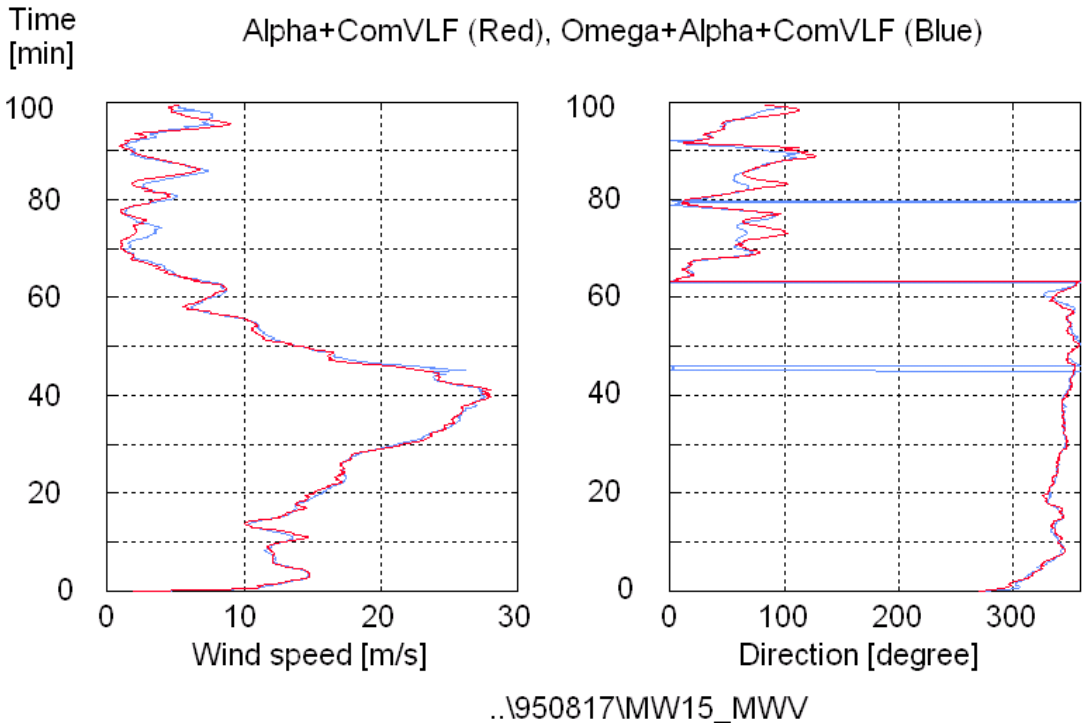

Figure 2.9: Upper-air wind profile (speed and direction) as a function of time

The radiosonde receives and retransmits a 10–30 kHz band of the VLF signal together with the 7–10 kHz sensor signal on the same 400–406 MHz FM-modulated carrier. An important property of FM-modulation is, that the frequency content of the baseband signal is preserved unchanged after demodulation at the receiver. Telemetry range with a 250 mW transmitter is between 200 and 300 km [43].

Ground receiving station

The ground receiving station shown in Figure 2.13 has two input channels: *remote* channel for radiosonde telemetry, and *local* channel for receiver synchronization and reference oscillator correction. Radiosonde motion, i.e. the wind, is detected from the remote channel signal. The receiving station is comprised of a 400 MHz UHF Receiver, a VLF-Navaid Processor, and a Main Processor Unit. Supporting functions, such as power supply and console processor, are not shown. A directional UHF antenna provides radiosonde telemetry up to a distance of 300 km, which is sufficient even under high wind conditions. A local VLF-antenna receives Omega, Alpha, and Communications VLF signals (10–30 kHz), and LF-band Loran-C signals (100 kHz).

Figure 2.14 shows *VLF-Navaid Processor* [1], which is a single-board software-defined navigation receiver. An earlier implementation [20] contained six circuit boards to execute the same tasks. There are two operating modes, one for the VLF-band and the other for Loran-C. A DSP-processor executes the phase estimation algorithm which is described in Chapter 5. The processor calculates continuously *fifty phase estimates* in real time ($2\ Channels \cdot (8\ Omega + 5\ Alpha + 2 \cdot 6\ ComVLF)$). These estimates are further processed in the Main Processor Unit to get a wind profile as described in [17].

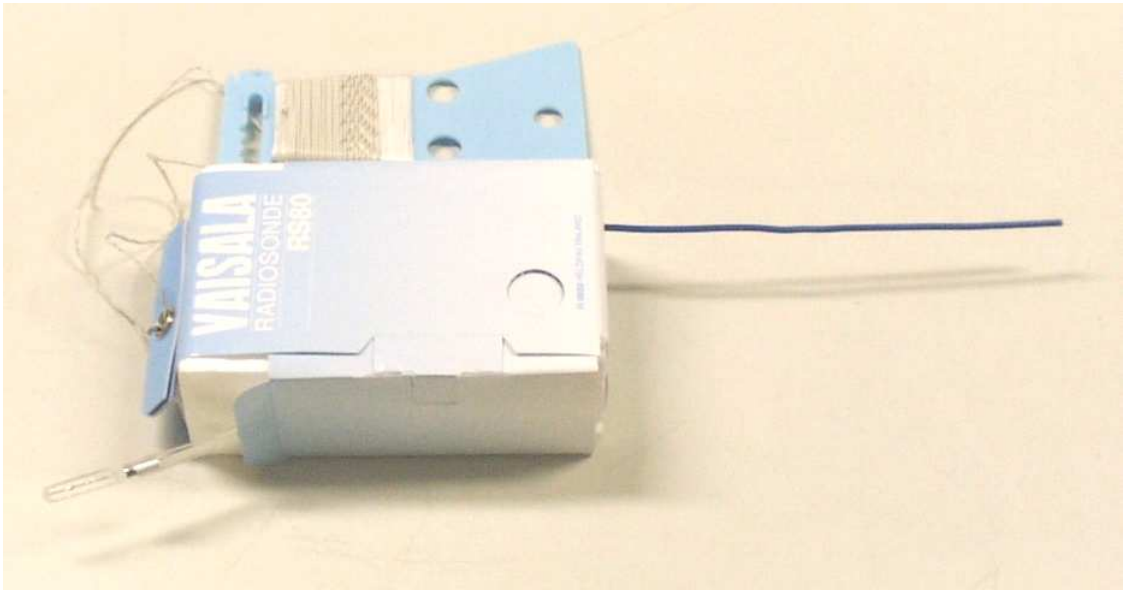

Figure 2.10: A VLF-band radiosonde for receiving Omega, Alpha, and Communications VLF signals has also pressure, temperature, and humidity sensors

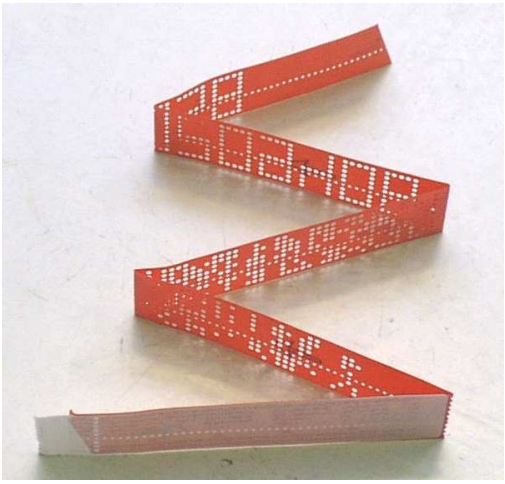

Figure 2.11: A paper tape containing unique sensor calibration coefficients

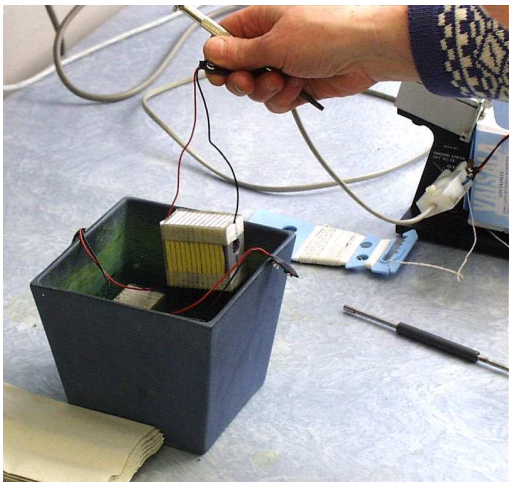

Figure 2.12: Radiosonde is powered by a water activated battery

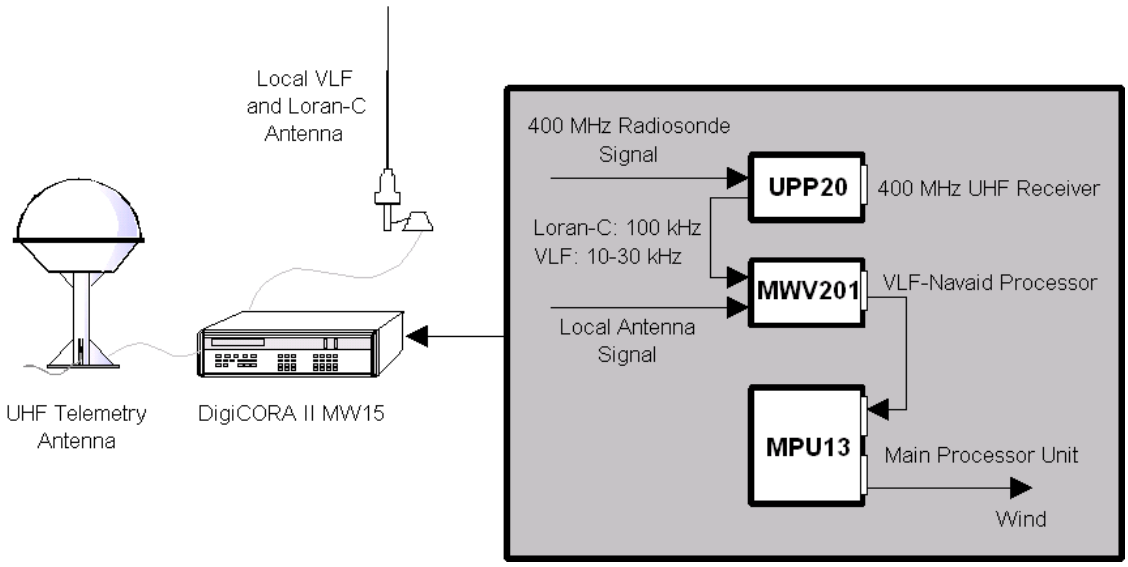

Figure 2.13: Ground receiving station is comprised of UHF and VLF antennas, UHF Receiver, VLF-Navaid Processor, and Main Processor Unit

Figure 2.14: VLF-Navaid Processor [1] executes the phase estimation algorithm described in Chapter 5

The author started the development of the VLF-Navaid Processor in 1992. Besides reducing the size of the receiver, the goal was to improve wind finding accuracy on the fringe of the navigation network coverage area. The existing [20] and earlier [23] implementations received all but one of the twelve Omega frequencies but only one of the five Alpha frequencies. The reason for not using all the frequencies in these early receivers was in the peculiar way in which the navigation transmitters generate the frequencies (see Tables 3.1, 3.4, and 3.5). It is not possible to set up such a measurement interval that there would be an integer number of cycles of every transmitted frequency. This thesis describes a new phase estimation method, which enabled VLF-Navaid Processor to receive every transmitted frequency. This in turn made it possible to use VLF based wind finding on areas previously unavailable.

The VLF-Navaid Processor contains four software-defined navigation receivers, which were introduced as follows:

- Omega (10.2–13.6 kHz) and Communications VLF receiver (16.4–28.5 kHz), April 1995
- Alpha receiver (11.9–14.9 kHz), August 1995, [2]
- Lightning removal and five-station-Alpha receiver, November 1995, [1]
- Loran-C receiver (90–110 kHz), June 1996, [27]

The next two years were spent improving receiver performance and adding new features. Since Russian Alpha returned from the five-station-regime back to the three-station-regime, the receiver was also updated to take this change into account.

- Synchronization from Loran-C secondary stations, April 1997
- Alpha frequency correction, October 1997
- Improved three-station-Alpha receiver, November 1997, [44]
- Differential phase calculation, January 1998
- Automatic Loran-C chain selection, June 1998, [45]

Wind finding accuracy of the VLF-Navaid Processor was studied in three major test series [4], [30], and [46]. The results met the numerical forecast requirements set by the World Meteorological Organization [41], and they were in line with other research on the same subject in [47] and [48].

2.6 Discussion

In meteorology wind data is needed to support weather forecasts and in climatology to predict long-term changes in global climate. Although weather satellites and weather radars have developed in the recent years, radiosondes carried by weather balloons are still used in large numbers. Merely the wind finding method has changed from VLF to GPS.

Chapter 3

Very Low Frequency navigation systems

3.1 Overview

Weather forecasts in the 1980's to 1990's were largely based on radiosonde measurements using very low frequency (VLF) navigation systems. Omega radionavigation system was the principal source for measuring upper-air winds in meteorological applications for over two decades. The major benefits of VLF navigation in meteorological applications are global coverage, excellent availability, good signal quality, and low cost consumable measurement instrument, the radiosonde.

The receiver by the author [1] could also use Alpha and Communications VLF signals simultaneously with Omega, thus providing better coverage and measurement accuracy. The challenge presented in particular by the the *Alpha navigation system frequencies* led to the invention of the phase estimation algorithm presented in Chapter 5.

VLF signals propagate in a waveguide formed by the conductive surface of the earth and the ionosphere as shown in Figure 3.1. The ionosphere is a layer of electrically charged particles which bend and reflect the signals along the curvature of the earth. Some of the transmitted power leaks out of this waveguide, which causes attenuation. Further instability is caused by several factors, including the height of the ionosphere, which varies regularly each day and over the year from 70 to 90 km [37, pp. 180–186], [38, pp. 25–26]. Figure 3.2 shows the frequency bands occupied by VLF navigation systems and Figure 3.3 shows a typical 3–30 kHz VLF spectrum.

When Omega network was shut down in 1997, the previously global coverage achieved by using eight Omega, three Alpha, and six Communications VLF transmitters was then limited to the Northern Hemisphere only. Wind finding using only Alpha and Communications VLF signals [26] was possible with receiver [1]. Even though the coverage was not quite global, many meteorological institutes could continue operations as before [28].

Figures 3.4 and 3.5 show the estimated number of available navigation transmitters prior to and after Omega termination in September 1997, respectively [27]. The availability estimate is based on a model that takes into account receiver sensitivity and signal attenuation over the sea, land, and freshwater ice. The calculation grid is 1000 km. A big blue number indicates an adequate number of transmit-

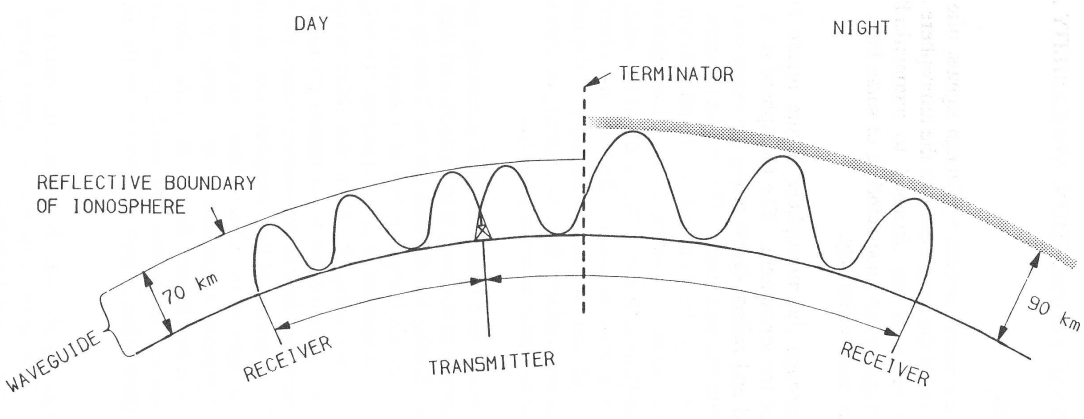

Figure 3.1: VLF frequencies travel in a waveguide formed by the conductive earth and the ionosphere [38, p. 26]

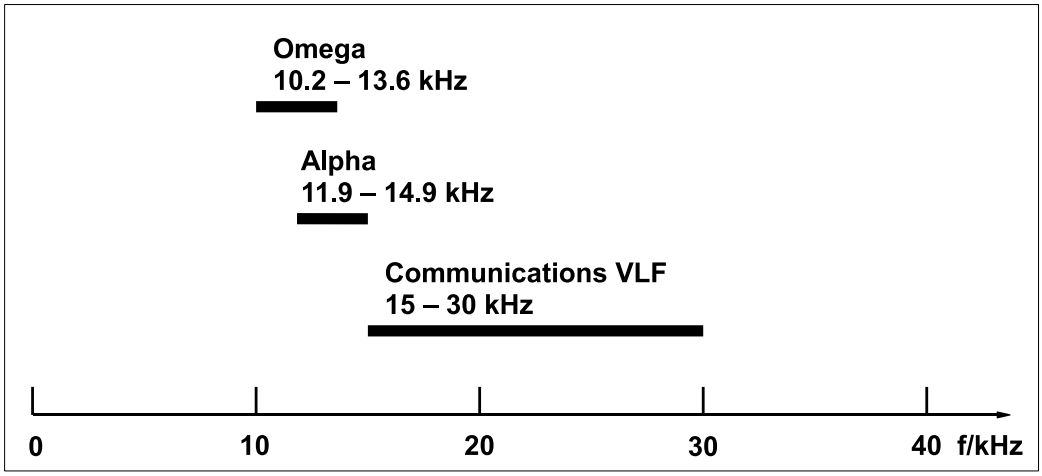

Figure 3.2: Frequency bands occupied by VLF navigation systems

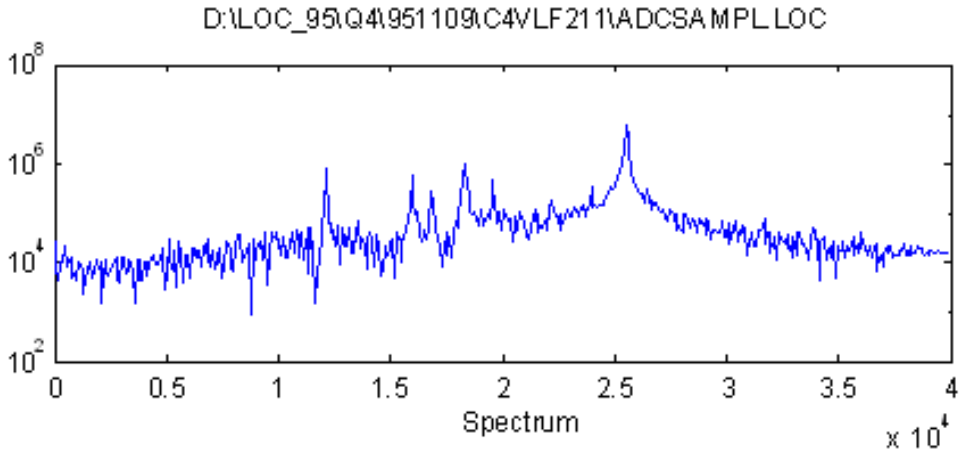

Figure 3.3: Typical VLF spectrum

ters for wind finding, and a small green number indicates too few transmitters. The red asterisks indicate the location of the Omega, Alpha, and Communications VLF transmitters. The estimated numbers are in line with the observed number of transmitters in various locations using receiver [1]. The number of available transmitters varies $(-1 \ldots +2)$ depending on the time of the day and time of the year. At least three transmitters are required for wind finding, but in practice four to five should be available.

3.2 Alpha radionavigation system

Alpha is a long range radionavigation system that is used for aviation, maritime and submarine navigation. Some receivers can use it for meteorological wind finding [2], [49], [50]. Alpha radionavigation system is also known as RSDN-20, Russian VLF, Soviet VLF, or Sigma. Even today very little information on the system has been published and most references are based on observations on the Russian navigation system. A number of details were confirmed by Russian authorities to the author and his colleagues during a visit to the Committee Internavigation, Moscow, in 1995 [51]. The following summary is based on an unpublished internal report [52] and a relevant part of it (transmission frequencies, transmission sequence, and transmitter locations) has also been published in a sounding system user's guide [53].

The Alpha system consists of three widely spaced transmitting stations in Novosibirsk, Krasnodar, and El 'Ban (Khabarovsk). This is known as the three-station-regime [54], [55]. There was a plan to change to a five-station-regime by the end of 1995 [56]. At first, four stations would be used: Novosibirsk, Krasnodar, El 'Ban (Khabarovsk) and Revda (Murmansk). The fifth station, Seyda (Turkmenistan), was delayed because of the political situation. Negotiations were going on to have the station operational and there was a common understanding between the nations of the use of common property [51]. The three-station-regime was still operational in 2006. Alpha transmitters emit unmodulated continuous wave VLF signals between 11.9 and 14.9 kHz, and they use a cesium frequency standard with an accuracy in the order of 10^{-12} [57]. An Alpha receiver determines position either by making range measurements based on the phase of the received signals, or by making phase comparisons between signals of selected transmitter pairs.

Transmitted frequencies

Alpha transmission frequencies are derived from $f_0 = 744\ 1/21$ Hz as shown in Table 3.1. The three common Alpha frequencies used by the present three-station-regime and the five-station-regime are f_1, f_2, and f_3. Transmission frequency f_{3P} is intended for synchronization of stations. Transmission frequency f_{1k} $(= f_1)$ is intended for synchronization of stations in the three-station-regime, five-station-regime does not use it. The two new stations in the five-station-regime can be identified from transmitter specific frequencies f_4 and f_5 [51], [54], [55], [57].

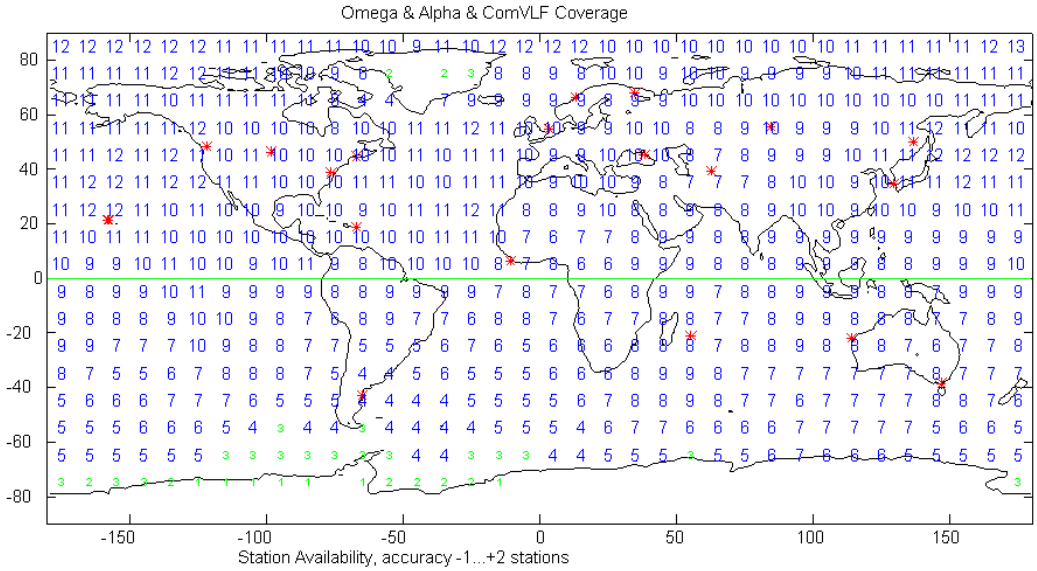

Figure 3.4: Combined coverage of all three VLF navigation systems [27] using receiver [1]

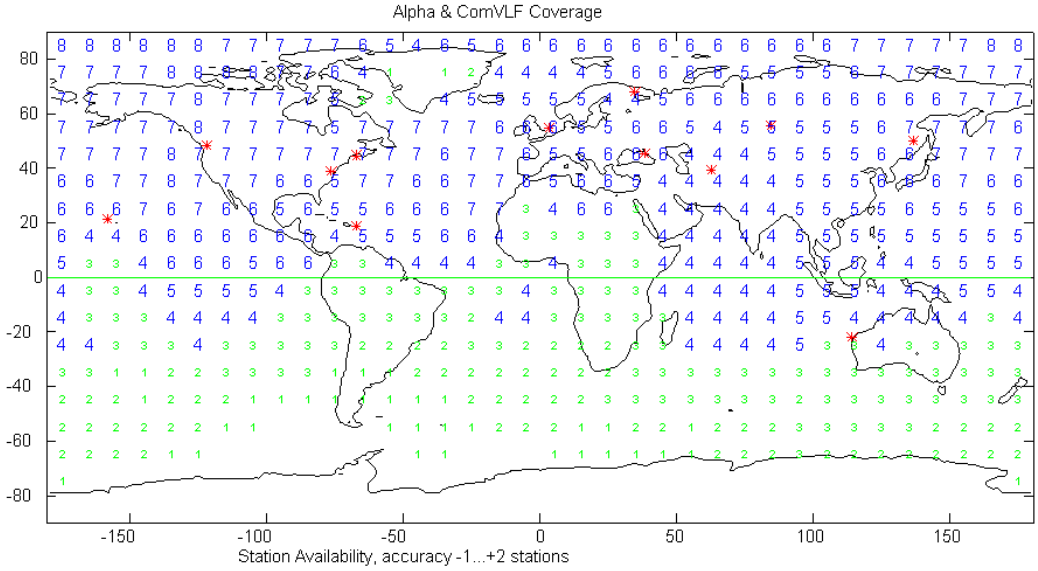

Figure 3.5: VLF navigation system coverage after Omega termination in 1997 [27] using receiver [1]

	Frequency	Exactly [Hz]	Approximately [Hz]
f_1	$16 \cdot f_0$	$250,000/21$	11904.76190476
f_2	$17 \cdot f_0$	$265,625/21$	12648.80952381
f_3	$20 \cdot f_0$	$312,500/21$	14880.95238095
f_4	$260/16 \cdot f_0$	$1,015,625/84$	12090.77380952
f_5	$259/16 \cdot f_0$	$578,125/48$	12044.27083333
f_{3P}	$f_3 + 5/36$	$3,750,035/252$	14881.09126984
f_0		744 1/21	744.04761904

Table 3.1: Alpha transmission frequencies are derived from f_0

Station	Designator	Latitude	Longitude
Novosibirsk (region) Bolotnoye (station)	A, 1	55° 45′ 22.0″ N	84° 26′ 52.4″ E
Krasnodar (region) Red Army (station)	B, 2	45° 24′ 17.9″ N	38° 09′ 29.0″ E
El 'Ban (town) Khabarovsk (region) (Komsomolskamur)	C, 3	50° 04′ 23.9″ N	136° 36′ 24.1″ E

Table 3.2: Alpha station coordinates in the *three-station-regime*

Transmission sequence

Alpha system uses a 3.6 s transmission sequence, which contains six 600 ms segments where a 400 ms transmission is followed by a 200 ms pause. This sequence is repeated continuously by all stations. The three-station and five-station transmission sequences are illustrated in Figures 3.6 and 3.7, respectively, and corresponding station coordinates in Tables 3.2 and 3.3 [51], [54], [55], [58]. Stations are identified by the name of the region or city where they are located as shown in Figure 3.8. Also a letter (A, B, C, D, and I) or digit is being used as a designator.

The *three-station-regime* (A, B, C in Table 3.2) was in use till the end of 1995, and it returned into use at some point during 1996–1997. Pulses f_{1k} in Figure 3.6 are sent by the master station, Novosibirsk. These pulses are used for synchronization of the two other stations to the master station, and they are not used by the Russian navigation receiver [51].

The first four stations (A, B, C, and D in Table 3.3) of the new *five-station-regime* were on-air for test purposes during 1995–1997. The fifth station (I), Seyda (Turkmenistan), did not transmit. At some point during 1996–1997 the test transmissions ended and the format returned back to the three-station-regime. In case station A is off-air, transmission frequency f_{3p} can be switched over to station D or I [51].

Coverage area

Alpha navigation system coverage area (hyperbolic coverage) is shown in Figure 3.8. This map was received from the Committee Internavigation in 1995. Coverage area

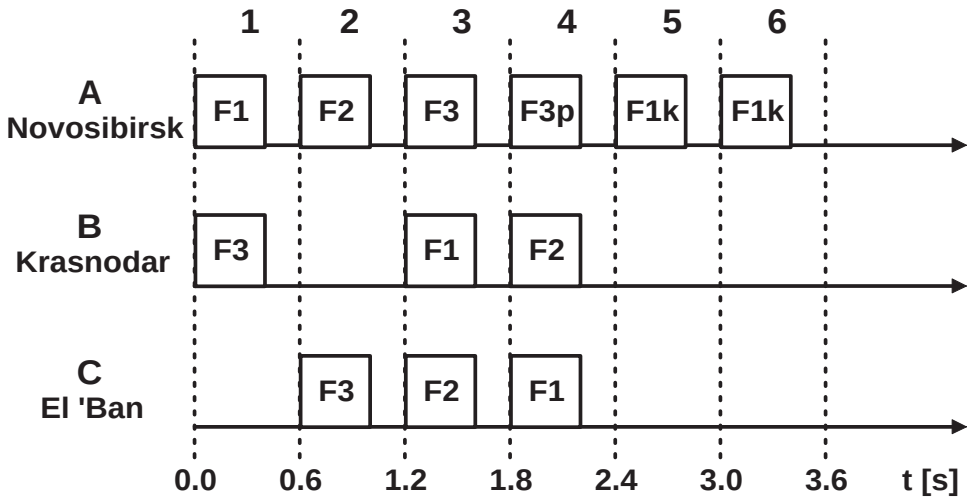

Figure 3.6: Alpha transmission sequence in the *three-station-regime*, a 400 ms transmission is followed by a 200 ms pause in each 600 ms segment

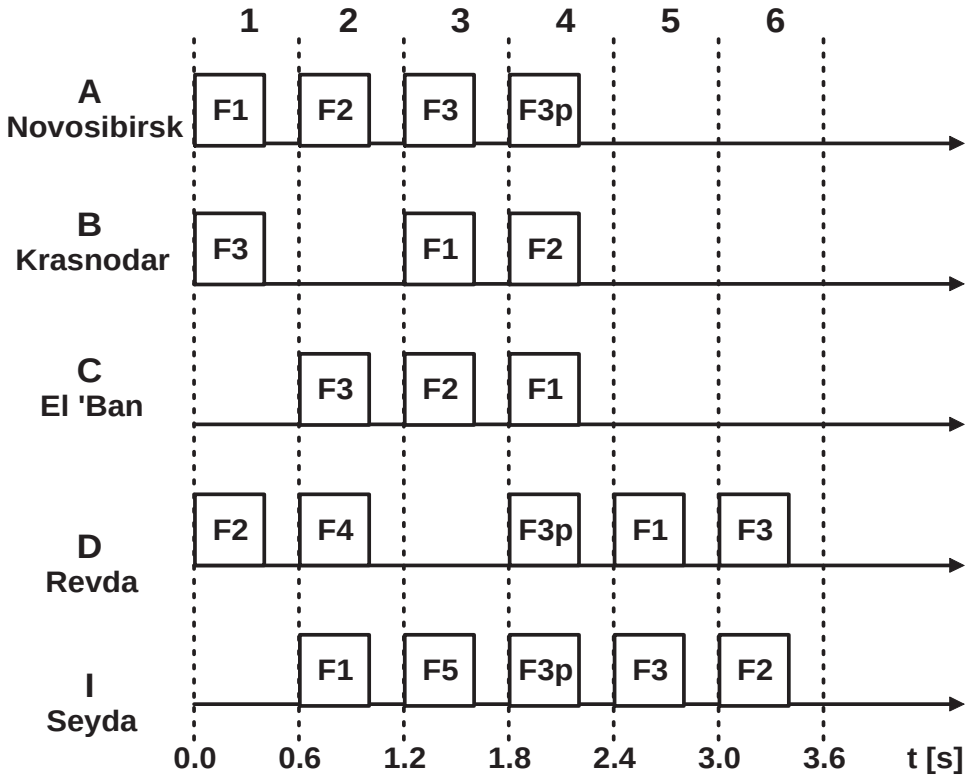

Figure 3.7: Alpha transmission sequence in the *five-station-regime*, a 400 ms transmission is followed by a 200 ms pause in each 600 ms segment

Station	Designator	Latitude	Longitude
Novosibirsk (region) Bolotnoye (station)	A, 1	55° 45′ 22.0″ N	84° 26′ 52.4″ E
Krasnodar (region) Red Army (station)	B, 2	45° 24′ 17.9″ N	38° 09′ 29.0″ E
El 'Ban (town) Khabarovsk (region) (Komsomolskamur)	C, 3	50° 04′ 23.9″ N	136° 36′ 24.1″ E
Revda (town) Murmansk (region)	D, 4	68° 02′ 07.8″ N	34° 41′ 00.0″ E
Seyda (city) Turkmenistan (region)	I, 5	39° 28′ 16.0″ N	62° 43′ 07.3″ E

Table 3.3: Alpha station coordinates in the *five-station-regime*

of the *three-station-regime* is North Polar region, North America, Southern Asia and Indian Ocean, covering 140 million km^2 and 27% of the earth's surface, as the area of the earth is 510.2 million km^2. The average annual and daily positioning accuracy in hyperbolic mode is 2.3–10 km over 100 million km^2. Two-station-positioning is accessible over 50% of the surface of the earth [51], [54], [55].

The two additional stations in the *five-station-regime*, Revda (Murmansk) and Seyda (Turkmenistan), enable navigation also within Russia. The coverage area will increase significantly, including Europe, North America, Asia, Africa, North Atlantic, Indian Ocean, North Pacific, and North Polar regions, covering 350 million km^2 and 69% of the earth's surface. The coverage area of *four stations*, Novosibirsk, Krasnodar, El 'Ban (Khabarovsk), and Revda (Murmansk), will be approximately the same as for five stations, but there may be some geometrical limitations [51]. An accuracy of 1.5–10 km will be available over 120 million km^2 [54], [55].

Russian Alpha receivers use a correction model to mitigate the effects of radio wave propagation errors. The correction model is formed in several steps. First, supplementary phase measurements are made at points with known coordinates, and this data is used to construct a global model for predicting propagation errors. Then the values predicted by the model are compared with the measured ones and additional correction parameters are determined for day and night conditions. Interpolation is used for calculating correction values for other points [54], [55].

Transmitting station description

Each station is continuously staffed with a watch consisting of three to five persons in duty and communication is done via secure telephone and radio connections. *Transmitting antenna* is comprised of a central 300 m insulated mast with 6 peripheral masts supporting 6 interconnected horizontal conductors which serve as the radiating element. *Transmission power* conducted to the antenna circuit is between 200 and 250 kW, and radiated power is approximately 80 kW. The efficiency of the antenna system is between 0.27 and 0.46 depending on the output frequency. The primary 3-phase *mains power* to the station is 10 kV at 50 Hz. Electricity is

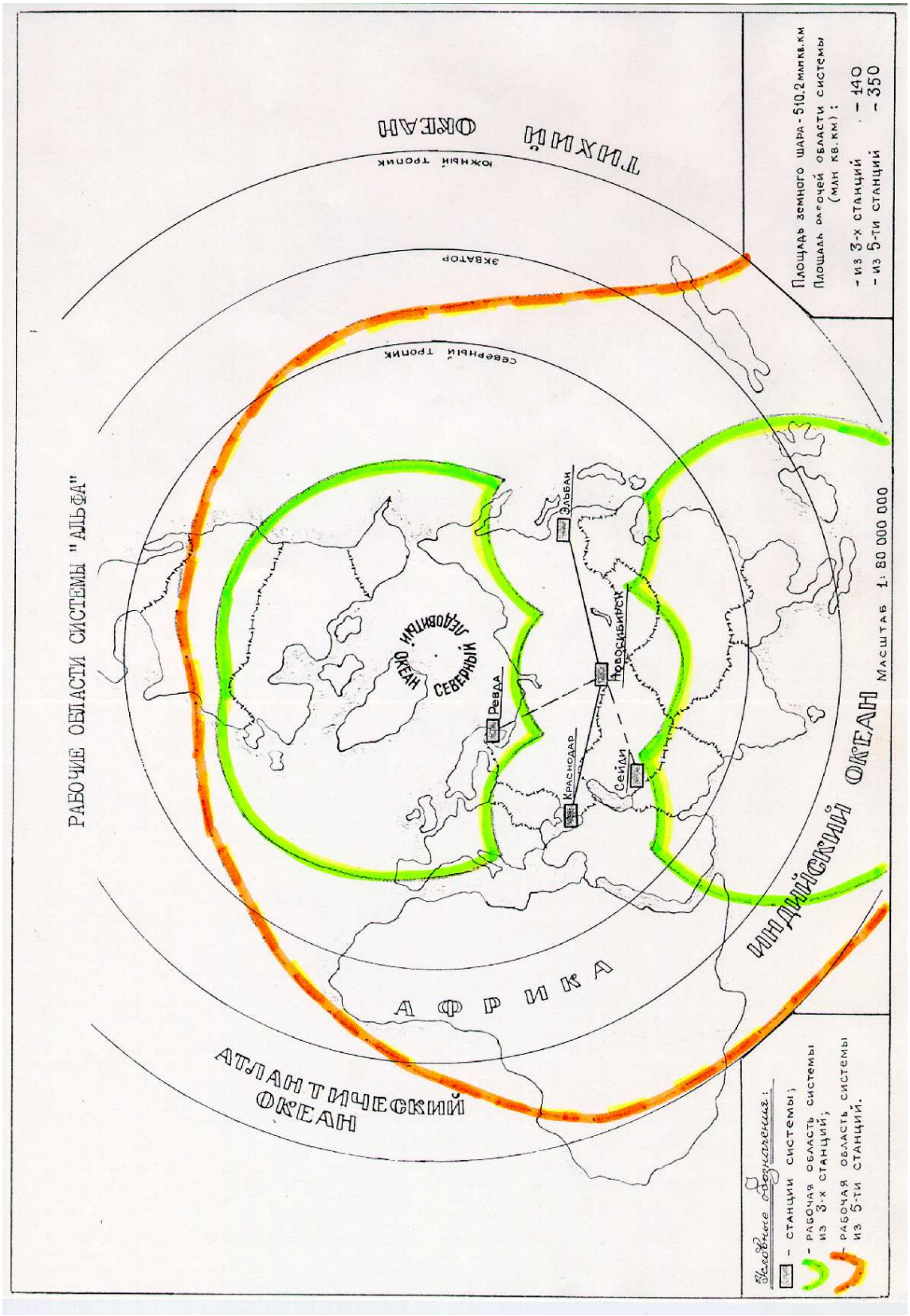

Figure 3.8: Alpha station locations and coverage area in the *three-station-regime* and *five-station-regime* [51]

supplied from two separate nets, primary and standby, each capable of providing 1500 kW. Two diesel generators serve as a reserve [51], [54], [55].

Frequency/Time Standard (FTS) is based on a synchronized ensemble of four cesium frequency standards grouped as two sub-assemblies. Output frequency of the cesium standard is 5 MHz. Amplitude, phase, and frequency of each frequency standard is analyzed automatically. Leading standard is selected based on frequency deviation from the average drift of all four standards. Phase of the remaining three standards is adjusted automatically to the phase of the leading standard. In case the leading standard is rejected, a reserve is selected automatically. Root mean square error of the frequency reproduction from switch to switch is not greater than $2.5 \cdot 10^{-12}$. In six hours after the station has been turned on, the relative error in the 5 MHz signal has been stabilized below $1 \cdot 10^{-11}$. Time scale of the FTS can be corrected in 50 ns steps [57], [54], [55].

Synchronization to the UTC is performed by external means, using satellite navigation systems, LF radionavigation systems, VLF communications stations, and TV transmissions. Stations are synchronized every day at 21:00 UTC causing a phase jump in the operating frequency [58]. This phase jump has been detected also at a western monitoring station [59].

There are provisions for two planned semi-annual *service breaks* causing the station to be off-air. Their duration is determined by the amount of work to be done, normally between one and two weeks. Additionally there are planned monthly service breaks which normally last two days [54], [55].

Alpha in meteorological applications

Russian Alpha radionavigation system has been operational since 1970 [58]. Vaisala started development of their Alpha receiver in 1972, gave a public demonstration during Meteorex exhibition in 1973 [60], and presented the results in 1974 [61]. Transmission frequencies and transmitter coordinates were found from the International Frequency List [62], and the transmission sequence was studied and resolved with a self-built directional antenna [60]. Alpha navigation receiver was commercially available as part of a sounding system in 1975 [49]. These early systems received $f1 \approx 11.905$ kHz frequency of the three-station transmission format, which is described in a 1991 article [17]. The history of the Alpha system and an experimental two-station single-frequency receiver is described in a 1991 paper [59], and a three-frequency-receiver is proposed in a 1993 paper [63].

The receiver by the author [1] needed more detailed information on the Alpha system covering both the three- and five-station transmission formats and all transmitted frequencies. The most comprehensive references are a 1993 fax by USCG with a set of questions [54] and the Russian answer to it and its translation [55]. These two unpublished references cover most of the system features including transmitter coordinates, transmitted frequencies and three-station transmission sequence. Synchronization and control system is discussed in a 1992 paper [57]. The five-station transmission sequence can be found in a Russian-United States Coordination Council meeting protocol from 1992 [58] and the schedule for the augmented system in an unpublished document from 1995 [56].

Four stations of the five-station-regime were indeed on-air for test purposes in 1995, and this was verified by the author using a five-station Alpha receiver [1].

Measurements confirmed the new transmission format and the fourth station at Revda (Murmansk). The fifth station, Seyda (Turkmenistan), was never received. At some point during 1996–1997 the transmission format returned from the five-station-regime back to the three-station-regime. When this was noticed by the author, the receiver was updated back to the three-station format in November 1997 [44].

3.3 Omega radionavigation system

The U.S. Coast Guard (USCG) Omega radionavigation system was the western equivalent to the Russian Alpha radionavigation system. The following brief system description is based on Omega Navigation System User's Guide [38] and Omega brochure [64]. Termination of the Omega radionavigation system in 1997 and its history is covered in the 1994 Federal Radionavigation Plan [21] and in a few Radionavigation Bulletins published by the USCG [65], [66], [67], and [68].

Omega was a very low frequency (VLF) radionavigation system that was used for aviation, maritime, and submarine navigation, meteorological wind finding, wildlife tracking on both land and sea, time and frequency dissemination, and scientific research in VLF ionospheric propagation [65]. If you have taken a transoceanic flight in 1980's or 1990's, the aircraft you flew on most likely used Omega as the primary en route navigation system. The system consisted of eight widely spaced transmitting stations around the world. Omega transmitters emitted unmodulated continuous wave VLF signals between 10.2 and 13.6 kHz, and they used a cesium frequency standard with an accuracy in the order of 10^{-12}. An Omega receiver determined position either by making range measurements based on the phase of the received signals, or by making phase comparisons between signals of selected transmitter pairs [38, pp. 5–15].

Transmitted frequencies

Four transmission frequencies were common to all eight Omega stations and they are listed in Table 3.4. In addition to these, each station had a unique frequency, which is listed in Table 3.5. The eight Omega transmitting stations are shown in Figure 3.9 and their coordinates are listed in Table 3.6 [38, pp. 2–3].

Transmission sequence

Omega system used a 10 s transmission sequence, which contained eight segments as shown in Figure 3.10. Each transmission lasted between 0.9 and 1.2 seconds and was followed by a 0.2 second pause. This sequence was repeated continuously by all stations. [38, pp. 3–4]

System description

Operational Omega stations began broadcasting navigation signals in the mid-1970's, and the system reached its final eight-station configuration in 1982. Omega was operated as an international partnership between the United States, Argentina,

	Frequency [kHz]
1	10.2
2	11.05
3	11 1/3
4	13.6

Table 3.4: Common Omega frequencies

	Station	Frequency [kHz]
A	Norway	12.1
B	Liberia	12.0
C	Hawaii	11.8
D	North Dakota	13.1
E	La Reunion	12.3
F	Argentina	12.9
G	Australia	13.0
H	Japan	12.8

Table 3.5: Unique Omega frequencies

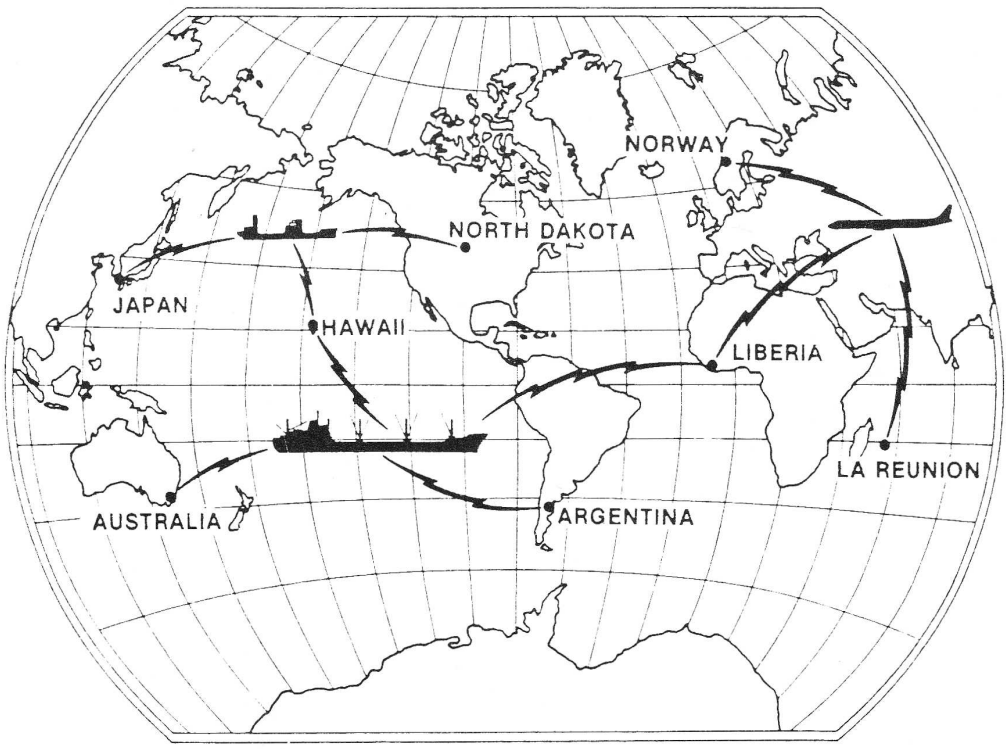

Figure 3.9: Omega station locations [38]

	Station	Position	Operating Agency
A	Norway	66° 25′ 12.68″ N 13° 8′ 13.07″ E	Norwegian Telecommunications Administration
B	Liberia	6° 18′ 19.26″ N 10° 39′ 51.85″ W	Liberian Ministry of Transport
C	Hawaii (USA)	21° 24′ 16.92″ N 157° 49′ 50.96″ W	U.S. Coast Guard
D	North Dakota (USA)	46° 21′ 57.40″ N 98° 20′ 8.22″ W	U.S. Coast Guard
E	La Reunion (France)	20° 58′ 26.90″ S 55° 17′ 23.62″ E	French Navy
F	Argentina	43° 3′ 12.79″ S 65° 11′ 26.81″ W	Argentine Navy
G	Australia	38° 28′ 52.42″ S 146° 56′ 7.06″ E	Australian Department of Transport and Communications
H	Japan	34° 36′ 53.06″ N 129° 27′ 13.12″ E	Japanese Maritime Safety Agency

Table 3.6: Omega station coordinates

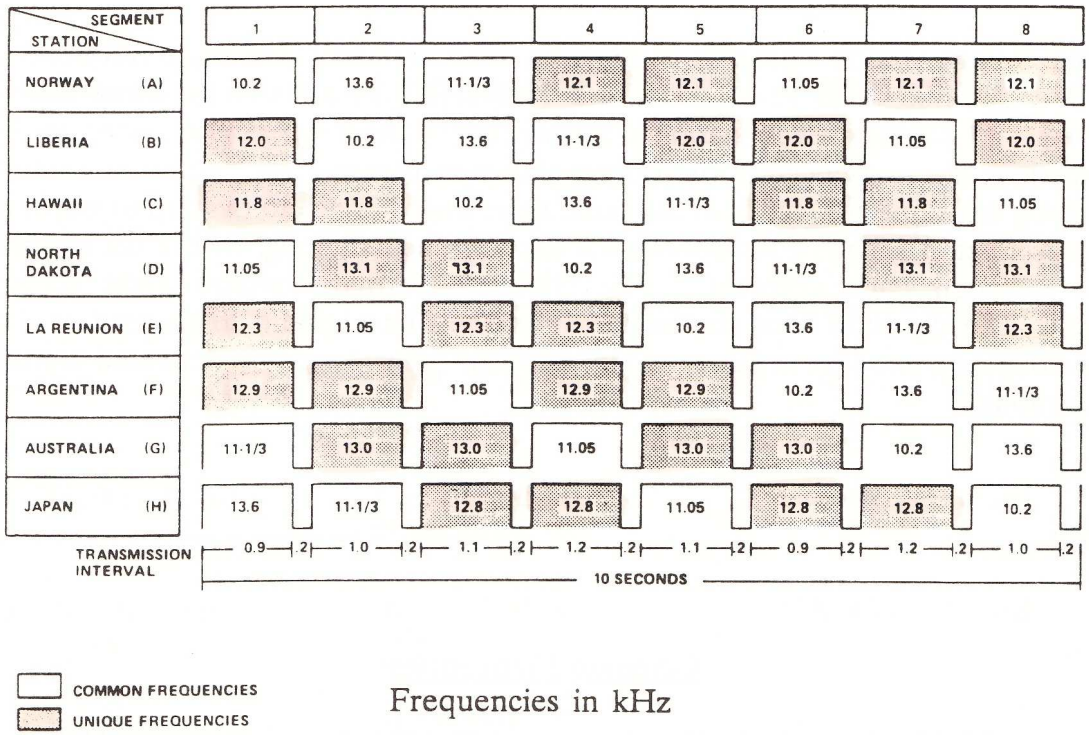

Figure 3.10: Omega transmission sequence, a 0.9 to 1.2 second transmission is followed by a 0.2 second pause in each segment [38, p. 4]

Australia, Liberia, France, Japan, and Norway. Each station was staffed and operated by the nation in which it was located. The Japanese Maritime Safety Agency was responsible for synchronization of the transmitted signals of all stations. The U.S. Coast Guard, through the Omega Navigation System Center (ONSCEN), had operational control of the system and was responsible for electronics engineering and logistics support of the transmitters. Overall coordination of operations and policy was governed by the International Omega Technical Commission, which was composed of one member from each of the partner nations [38, p. 1].

The nominal fix accuracy of Omega was two to four nautical miles (3.7–7.4 km, 1 n.mi.=1852 m) at 95% confidence level. The obtained accuracy dependeds on several factors, including signal propagation anomalies, geographic location, number of available stations, season, time of day, and receiving equipment [64]. It should be noted, that Omega was the only navigation system of its time which provided practically global coverage.

Omega in meteorological applications

Omega was the principal source for measuring upper-air winds in meteorological applications for over two decades due to adequate wind finding accuracy [41], global coverage, and low cost consumable measurement instrument, the radiosonde. Some receivers [1], and [50], could also use Alpha and Communications VLF signals simultaneously with Omega, thus providing better coverage and measurement accuracy [4]. Weather forecasts in the 1980's to 1990's were largely based on these measurements.

This all was to end when the U.S. Department of Transportation (DoT) gave a notice of intent in October 1996, that the U.S. Coast Guard intends to terminate its involvement in the Omega radionavigation system on September 30, 1997 [69]. Figure 3.11 shows a recording of the Omega signal on the day of termination of the navigation system. A weather balloon was released in Vantaa, Finland, at 02:00 UTC (05:00 local time), one hour prior to the announced termination. All stations worldwide ceased transmission of the Omega signal at 03:00 UTC (06:00 local time), except Liberia, which stayed on-air a few minutes overtime.

3.4 Communication transmitters

All major military powers have communication transmitters in the very low frequency (VLF) band. The fact that VLF signals propagate also under the surface of the earth and sea is important for land-based missile sites and submarines with ballistic missiles. As these transmitters are intended for military communication, not for navigation, they can change phase, frequency, format, broadcast schedule, or cease transmissions with no advance notice. According to the International Frequency List [70], many countries have frequency allocation for VLF band communication transmitters, including the United States, Russia, France, Britain, Italy, Germany, India, Poland, Japan, Chile, Brazil, and South Africa. The most well known transmitters are the ones operated by the U.S. Navy for submarine communication. In the 1960's the U.S. Navy started using airborne VLF communication systems (TACAMO) [71] and later also satellite-to-submarine communication. This

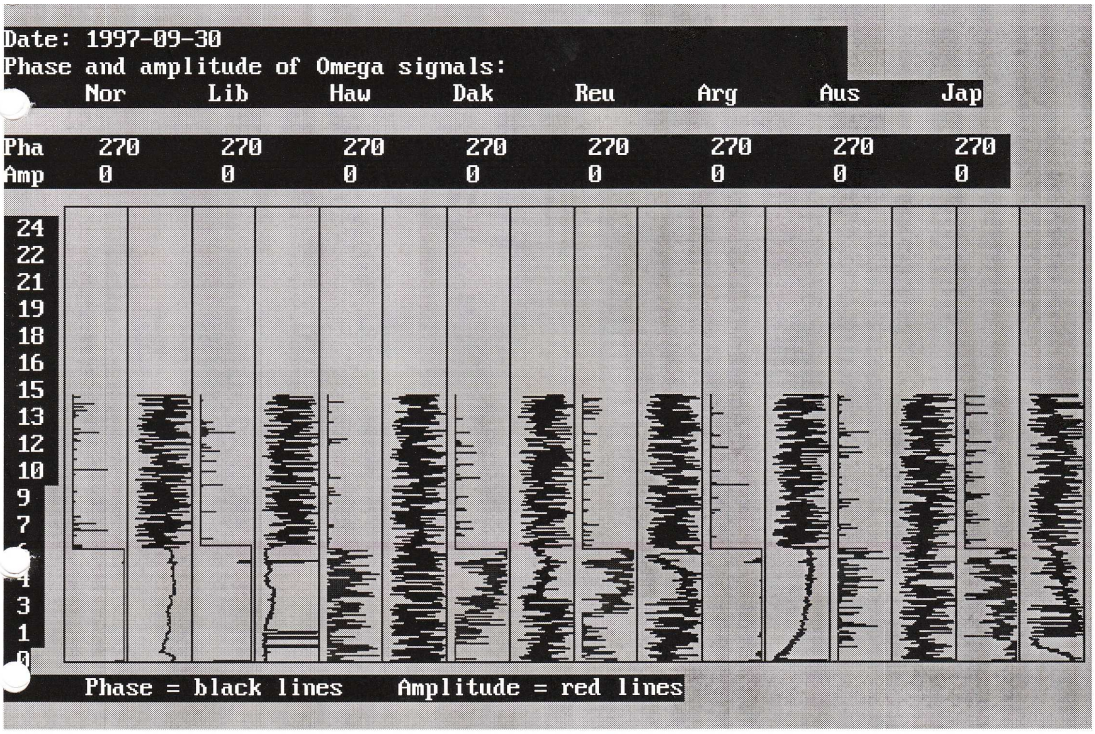

Figure 3.11: Termination of the Omega radionavigation system on September 30, 1997, at 06:00 local time

has resulted in terminating some of the existing fixed ground installations [72].

Communications VLF (ComVLF) stations transmit continuous-wave signals between 15 and 30 kHz, with frequency-shift keying (FSK) or minimum-shift keying (MSK) modulation. Two MSK data rates are in use: 200 baud and 100 baud with respective 100 Hz and 50 Hz spectral deviation. The transmissions are controlled by cesium beam frequency standards which makes them very phase stable. The U.S. Navy ComVLF stations were fairly reliable, maintaining their normally assigned frequency and signal format. Because of their stability and long range, ComVLF transmissions could be used for wind finding similar to the way that Omega and Alpha signals were used. Despite their unpredictability, the few communications VLF transmitters were a valuable supplement for a meteorological sounding system, especially on the fringe of Omega and Alpha navigation system coverage area.

Being a military system it was very hard to find information and it was collected and kept up-to-date in much the same way as Alpha information: from bits and pieces. An unpublished internal report [73] contains this information and a relevant part of it (transmission frequencies, modulation, and transmitter locations) has also been published in a sounding system user's guide [53].

3.5 Disturbances

There are several man-made and natural disturbances affecting the received VLF-band signal. These disturbances can depend on the atmosphere, climate, time of the day, time of the year, signal propagation direction, characteristics of the propagation path, system electronics, system software, and the geometry of the

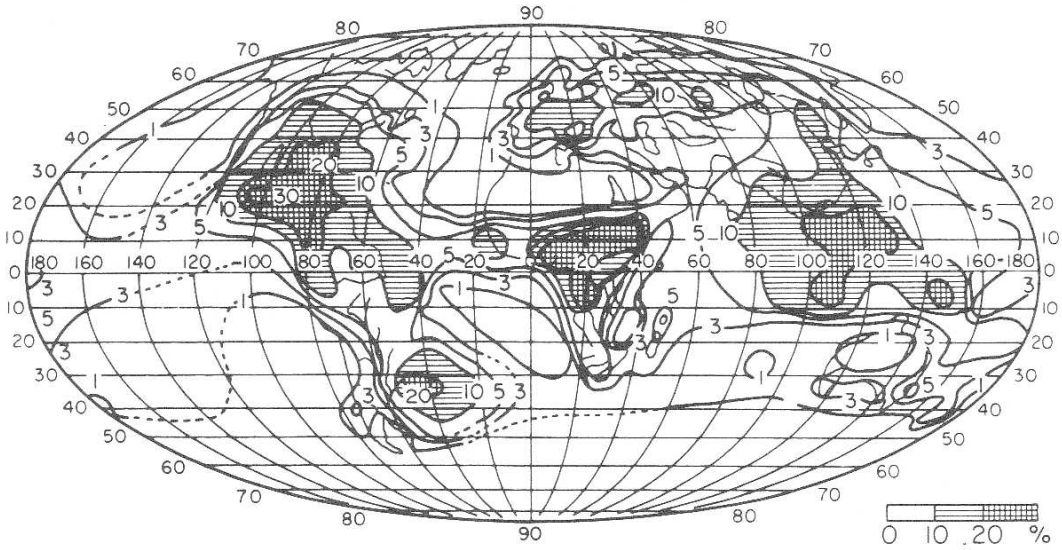

Figure 3.12: Thunderstorm distribution in June-August, lightning activity is highest at the equatorial band [37, p. 250]

transmitting stations relative to the receiver. Some of them have short duration, in the order of milliseconds (lightnings), and some have longer, diurnal, or even seasonal variation (ground conductivity). A thorough discussion on signal propagation phenomena can be found in references [37], [74], and [75, pp. 33-3 thru 33-6]. Factors affecting specifically VLF-band navigation are discussed in [38, pp. 25–31].

Lightnings

Lightnings are always present. There are approximately 50000 thunderstorms yearly on the Earth. At every moment there are some 2000 storms underway, which cause about 100 lightning strokes each second. A lighting stroke has two parts: a 100–300 A current flows in a pre-discharge, which is followed by a 10–100 kA main discharge. The discharge channel is some 2–4 km long and is heated momentarily to about 15000 K (compare to the 6000 K surface temperature of the sun). A lightning discharge actually consist of multiple strokes, each lasting about 1 ms, with about 40 ms between successive strokes [32, pp. 107–112], [37, pp. 250–251].

Lightings cause wide band additive noise, which is the result of different frequency components propagating at different velocities from several lightnings at several locations. The maximum of the radiated radio frequency energy is at 10 kHz and the amplitude decreases with increasing frequency. Lightning activity is the dominant noise source below 20 MHz. Noise level is highest at the equatorial band due to the high lightning activity as shown in Figure 3.12. Burst noise removal described in Section 5.5 is one solution for dealing with lightning disturbances.

Narrow band interference

The frequency band from 9 to 14 kHz is reserved for navigation use [75, p. 1-6]. Transmissions within a navigation system are sequenced so that no two stations are

Alpha	Omega	Separation [Hz]
12090.77	12100.00	9.23
12044.27	12000.00	44.27
12090.77	12000.00	90.77
11904.76	12000.00	95.24

Table 3.7: Some Alpha and Omega frequencies are close to each other

transmitting the same frequency at the same time. Although Alpha and Omega frequencies do not overlap, their transmissions do overlap. As some of the frequencies are very close to each other, they may cause interference in the receiver. Table 3.7 shows Alpha and Omega frequencies which are closest to each other. Furthermore, Alpha $F3$ and $F3_p$ are separated by only 5/36 Hz ($\sim$139 mHz)!

In case signals from two transmitters fit into the receiver band width, the stronger one will be detected. Both single system (Alpha or Omega) and multi-system (combined Alpha and Omega) receivers are affected by narrow band interference. Partition outlier removal described in Section 5.6 is one solution for overcoming this problem.

Radiosonde signal

The radiosonde transmits both the frequency coded sensor measurements (7–10 kHz) and VLF-band navigation signals (10–30 kHz) on the same FM-modulated carrier. For the navigation receiver the 7–10 kHz sensor signal in Figure 3.13 is a strong interference. After filtering the sensor signal away, the signal in Figure 3.14 is ready to be processed by the navigation receiver.

Sampling clock

The effect of sampling clock can not be neglected when a frequency difference in the order of 10^{-5} to 10^{-3} Hz has to be estimated. There is always some error in the oscillator frequency which is seen as a common mode error in the received signals. Although common mode errors, such as sampling clock, vanish when the wind equation is solved, incorrect sampling clock causes increased noise level to the estimate. Another inconvenient side effect of a sufficiently large offset in the sampling clock is, that the navigation receiver can no longer synchronize to the received signals.

Sampling clock in navigation receiver [1] is derived from an oven controlled oscillator which has an accuracy in the order of 10^{-7}, which corresponds to a 10^{-3} Hz error in a 10 kHz signal. VLF navigation systems use cesium frequency standards with an accuracy in the order of 10^{-12}. The receiver uses navigation signals as a reference and corrects sampling clock accordingly. An accuracy of 10^{-9} can be achieved, which is small compared to disturbances in the propagation channel.

Alpha transmitter frequency offset

In 1997 Alpha navigation network cesium frequency standard was repeatedly offset from the Omega and Communications VLF frequency standards: the error was in

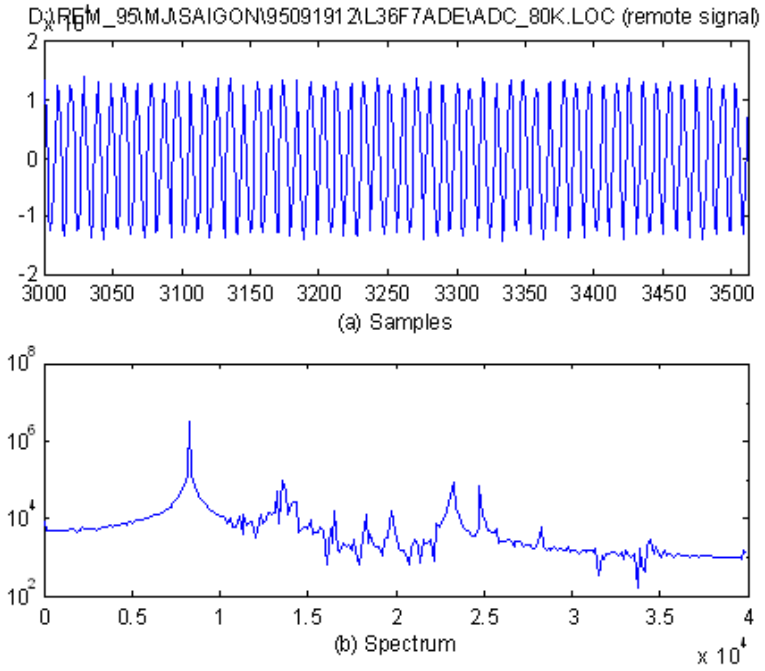

Figure 3.13: A 7–10 kHz sensor signal together with 10–30 kHz VLF navigation signals enters the receiver

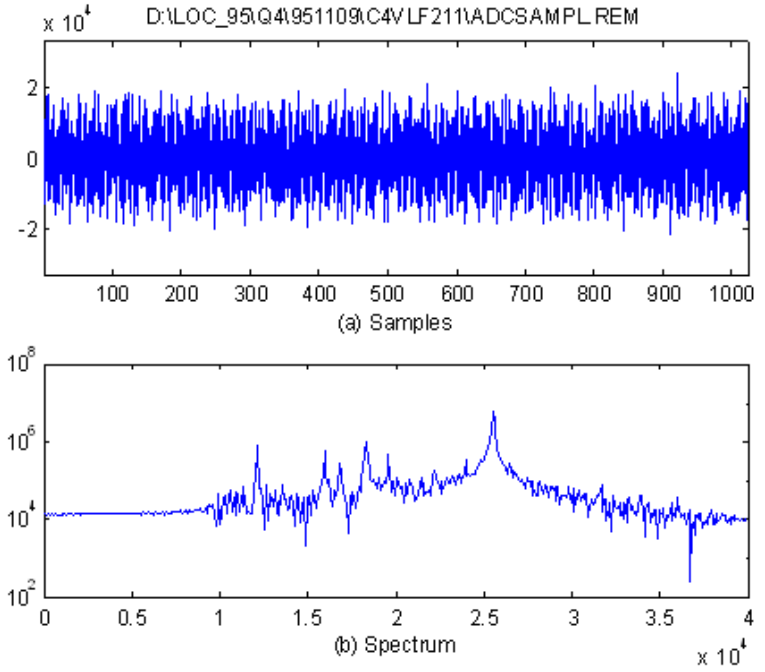

Figure 3.14: Only VLF navigation signals are left after removing the interfering sensor signal

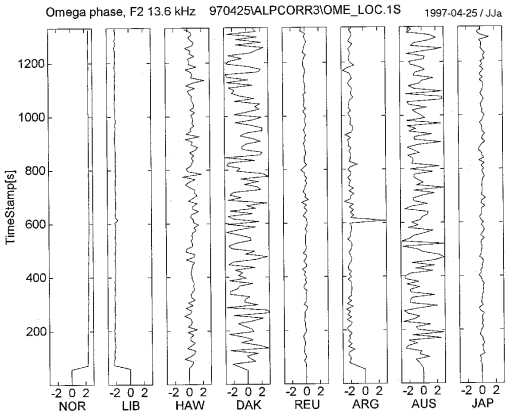

Figure 3.15: Omega phase estimates are used as a reference

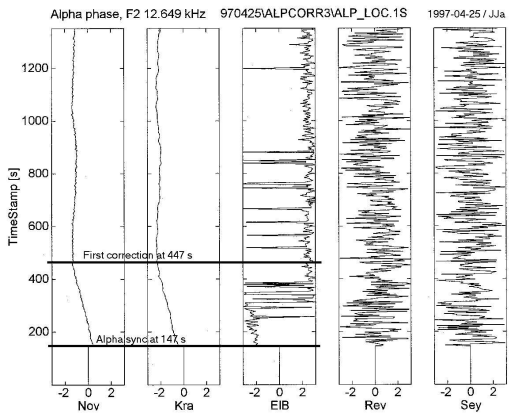

Figure 3.16: Alpha frequency correction is switched on at 447 s, after which the error is eliminated

the order of 10^{-8} to 10^{-7}. Wind estimate error in test soundings was in the order of 10 m/s in speed and up to 180 degrees in direction. Occasional frequency standard adjustments were also observed at our VLF observing station. A correction algorithm was introduced in 1997 and it is briefly described here. Similar behavior was also reported earlier by the U.S. Coast guard in 1991 [59] and in 1993 [63].

Wind finding procedure assumes that every transmitter has an identical frequency standard. Any frequency offset in one of the transmitters causes an error in the calculated wind. *Alpha frequency correction* is based on comparing Alpha signals to the the Omega and Communications VLF signals, and correcting Alpha phase estimates accordingly. Figure 3.15 shows an example of Omega phase estimates which were used as a reference. After Alpha receiver synchronization at 147 s, a $-8 \cdot 10^{-8}$ error is clearly visible in in Figure 3.16. Alpha frequency correction is switched on 300 s after synchronization at 447 s, after which the error is eliminated.

Figure 3.17 from May 1997 shows a set of wind profiles, which clearly illustrate the effect. The same radiosonde was received with two receivers, one of the receivers implemented Alpha frequency correction and the other one did not. The Omega-only wind profile and the Omega+Alpha(corrected)+ComVLF wind profile correlate very well. Without correction, Omega+Alpha(not corrected)+ComVLF, there is a ± 10 m/s difference in wind speed and a long duration of 180 degree difference in wind direction.

Signal path

All daylight path: The signal is most stable when the entire signal path from transmitter to receiver is in daylight as shown in Figure 3.1. The reflective boundary of the ionosphere remains fairly constant at a hight of about 70 km.

All nighttime path: Signals can normally be received at greater distance during the night, since attenuation rate is lower. In the absence of solar radiation the height of the ionosphere increases to about 90 km, but the reflective boundary is more diffuse, which causes uncertainty in the signal.

Transition path: The transition of the ionosphere from its daytime to nighttime

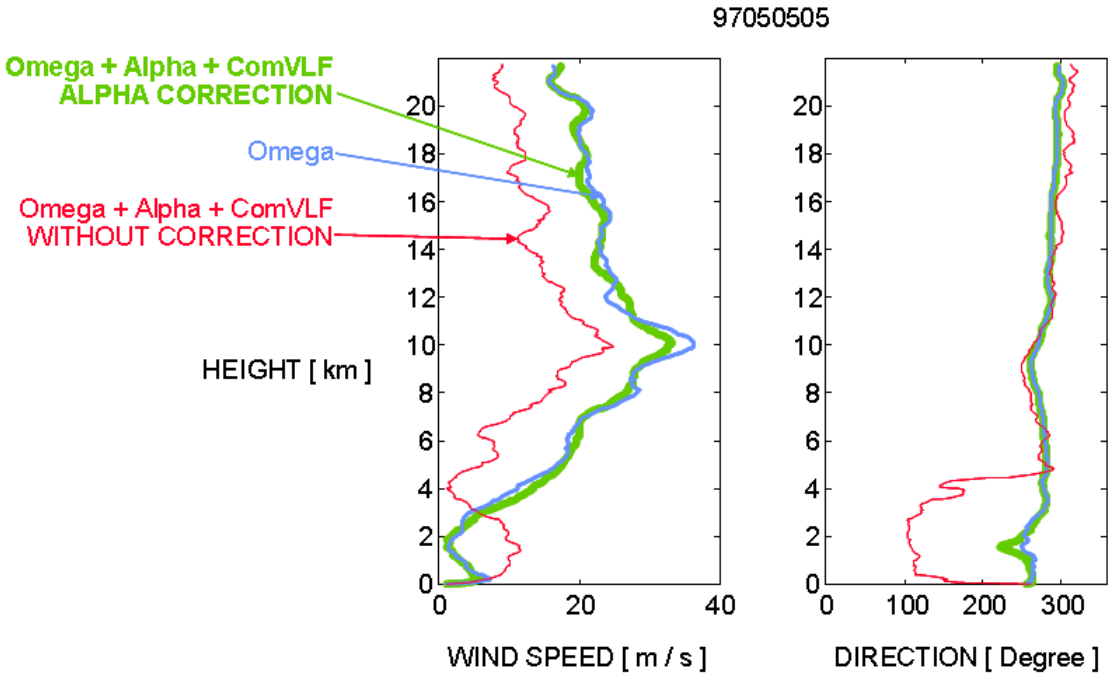

Figure 3.17: Without Alpha frequency correction there is a ±10 m/s difference in wind speed and a 180 degree difference in wind direction

height causes changes in phase of the signal. The longer the signal travels in the transition zone, the more pronounced is the disturbance. The transition effect is least apparent when the signal path is at right angles to the sunrise-sunset line as shown in Figure 3.18.

Ground conductivity

Signal attenuation is dependent on ground conductivity: attenuation rate decreases as conductivity increases [75, p. 33-5]. Greatest distance is achieved over sea water paths where conductivity is high. Medium distance is achieved over wet land and least distance over dry tundra and freshwater ice, e.g. Greenland and Antarctica. The effect of freshwater ice was clearly visible, when receiving Omega signals from North Dakota and Argentina in Finland. The more distant transmitter in Argentina was received loud and clear as the signal propagated mostly over the sea, while the signal from North Dakota was useless as the path crossed the ice-sheet of Greenland.

Magnetic field

The magnetic field of the Earth has a distinct effect on VLF signals. Signals travelling from west-to-east have lowest attenuation rate. In the opposite direction the attenuation rate is greater by about 1 dB/1000 km [75, p. 33-4]. Signals travelling from north-to-south or south-to-north have an attenuation rate in between the two extremes.

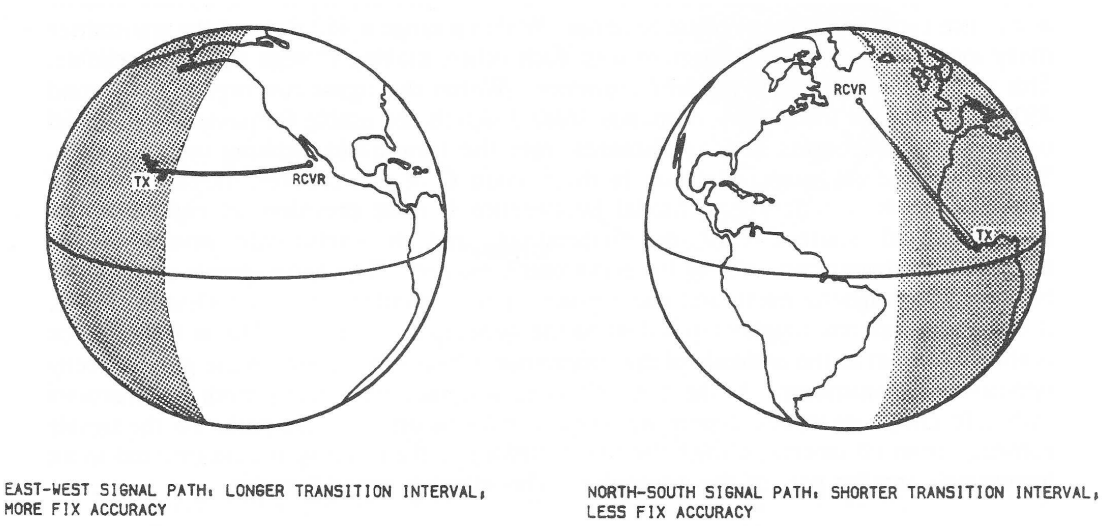

Figure 3.18: When signal path crosses the sunrise-sunset line, this is called a transition [38, p. 27]

3.6 Discussion

VLF band navigation systems, Alpha and Omega, transmit sinusoid signals according to a predetermined transmission sequence. VLF band communication stations transmit modulated continuous-wave signals. When the modulation is removed, e.g. by squaring, the resulting sinusoid signal can be used in the same manner as signals from Alpha and Omega navigation networks.

Chapter 4

Review of related work

4.1 Overview

This chapter summarizes properties of a number known methods for estimating the frequency, frequency offset, or phase of a sinusoid signal. Multiple approaches have been proposed over the years with emphasis on various details depending on the application and signal model. In addition to single parameter estimation, joint estimation of several signal parameters has been widely studied especially in the field of digital communications.

This discussion is started by noting that *frequency* and *frequency offset estimates* can be obtained by observing signal *phase* change in consecutive time instants. *Frequency estimation* methods include classical power spectrum estimators, high resolution methods, pitch estimation, and phase locked loop. DFT resolution improvement using interpolation has also been proposed. *Phase estimation* methods include correlation based phase estimates, time-delay estimation, and methods that have arisen from three-phase power line phase estimation. Various frequency and phase estimation methods used in *communication systems* are discussed, including carrier Doppler, carrier frequency and phase estimation of M-PSK signals. Finally, applicability of known methods to the estimation problem is assessed.

Multidimensional methods, higher order statistical analysis and spatial spectral analysis are out of the scope. Their applications can be found e.g. in sensor array and image processing. Multiresolution wavelet analysis is also out of the scope.

4.2 Frequency estimation using phase estimates

Instantaneous *frequency estimate* $\hat{f}_{inst}$ can be obtained by observing sinusoid signal phase change on a sample-by-sample basis:

$$\hat{f}_{inst} = \frac{\hat{\vartheta}_2 - \hat{\vartheta}_1}{2\pi(t_2 - t_1)} = \frac{\Delta\hat{\vartheta}}{2\pi T} \tag{4.1}$$

where $T = t_2 - t_1$ is the sampling interval and $\hat{\vartheta}_i$ are the instantaneous phase estimates of the sinusoid as shown in Figure 4.1. Sampling interval must fulfill the Nyquist condition for the frequency of interest. A digital phase locked loop uses this approach together with a narrow band loop filter, which suppresses interfering frequency components and guarantees a high signal-to-noise ratio.

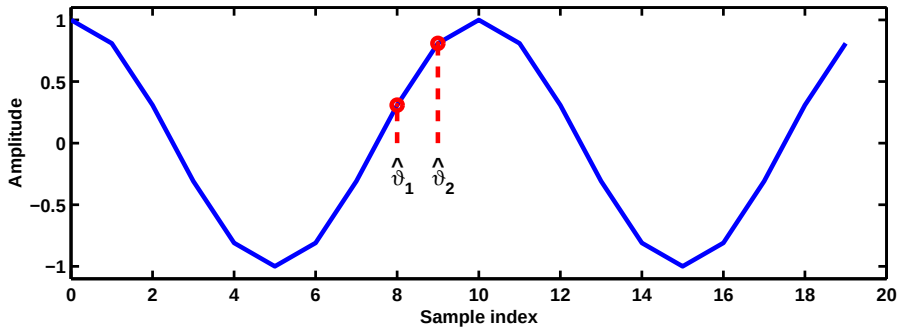

Figure 4.1: Instantaneous frequency estimate can be obtained by observing sinusoid signal phase change on a sample-by-sample basis

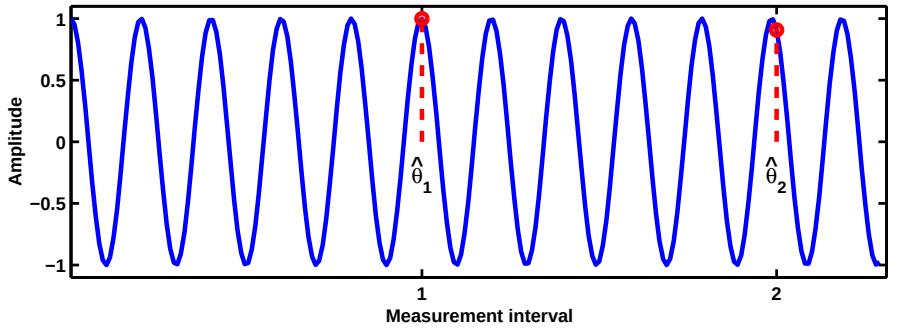

Figure 4.2: Frequency offset estimate can be obtained by observing sinusoid signal phase change in consecutive measurement intervals

Frequency offset is the difference between a received signal and a known transmitted signal. Assuming that the frequency offset is small ($f = f_{rx} \approx f_{tx}$) and by using the notation of the signal model (5.1)

$$x(n) = A\cos(2\pi n f/f_s + \theta) + w(n)$$

a *frequency offset estimate* $\Delta\hat{f}$ can be obtained by observing sinusoid signal phase change in consecutive measurement intervals relative to the known reference f

$$\Delta\hat{f} = \frac{\hat{\theta}_2 - \hat{\theta}_1}{2\pi(t_2 - t_1)} = \frac{\Delta\hat{\theta}}{2\pi T_{meas}} \tag{4.2}$$

where $T_{meas} = t_2 - t_1$ is the measurement interval and $\hat{\theta}_i$ are the phase estimates of the received sinusoid as shown in Figure 4.2. The corresponding *frequency estimate* $\hat{f}$ of the received signal is

$$\hat{f} = f + \Delta\hat{f} \tag{4.3}$$

When there is an integer number of cycles of the signal $x(n)$ in the measurement interval T_{meas}, phase can be estimated using a maximum likelihood estimator as described in Section 4.4. Otherwise PLL, interpolated DFT, high-resolution methods, or phase corrected correlation as described in Chapter 5, can be used. In one study [5] frequency offset estimation using phase estimates outperformed PLL, classical DFT-based methods, and high-resolution methods. Estimation problem in this study was similar to the one presented in Section 5.3.

4.3 Frequency estimation

Classical power spectrum estimators

Classical frequency estimation methods are based on the Fourier transform of the data sequence or its autocorrelation function. They do not require any knowledge of the data sequence, i.e. they are nonparametric. These methods are straightforward to use and provide reasonably high resolution for sufficiently long data sequences. The Fast Fourier Transform (FFT) makes it convenient to calculate the periodogram spectral estimate or any of its variations [7], [76, pp. 23–68].

Periodogram and correlogram methods have high variance, which does not decrease with increasing data length. Modified methods with lower variance have been developed, but with the cost of decreased resolution. They exploit averaging (Bartlett), windowing (Blackman-Tukey) or both (Welch) to lower the variance. All of these methods have more or less equal properties and performance for long data lengths. Frequency resolution of the DFT, also known as bin width, is defined by sampling rate f_s and length of the DFT N, i.e. measurement time.

$$BinWidth = \frac{f_s}{N} = \frac{1}{N \cdot T} = \frac{1}{T_{meas}} \tag{4.4}$$

Hence, to increase frequency resolution, a longer measurement time must be used. In order to achieve sub-Hertz resolution with the DFT, a measurement time of several seconds is required!

Classical nonparametric spectral estimators are still the most robust for low signal-to-noise ratio, but they can not exploit high SNR conditions [8, p. 167]. Classical methods are applicable to all signal classes and the estimated PSD is directly proportional to power. The main disadvantage of classical methods is that their resolution is limited by windowing effects. *Smearing* causes two peaks in the spectrum to appear as a single broader peak in the spectral estimate, whereas spectral *leakage* causes weak signals to be masked off by sidelobes of strong signals.

Parametric methods

Parametric methods (ARMA, AR, MA) assume, that the signal satisfies a known mathematical model, then they estimate signal parameters based on this model. Usually, the observed data is considered to be a realization of a linear filter, whose input is white noise. Model parameters are estimated from the observed data with linear modelling methods. Once the model parameters have been determined, a spectral estimate can be computed, e.g. with the FFT [76, pp. 85–126].

The resolution of nonparametric methods is ultimately limited by the length of available data. Parametric methods may provide more details and less sidelobe artifacts for shorter data lengths, assuming that a proper model has been selected and signal-to-noise ratio is good. For low SNR they are no better than nonparametric methods [8, p. 233]. In the ARMA (autoregressive moving average) class the AR method is most frequently used. Applications can be found in the fields of speech, communications, radar, sonar, and geophysical seismology.

High-resolution methods

Pisarenko harmonic decomposition, MUSIC, minimum-norm, and ESPRIT are high-resolution methods which are intended for estimating spectral lines (frequencies). More specifically, for the estimation of complex exponentials in noise. Signals in the fields of e.g. communications, radar, sonar, and geophysical seismology can be described with this sinusoidal model [77, pp. 614–655].

These methods are based on an *eigenvector decomposition* of autocorrelation matrix of the data into two *subspaces*, one associated with the signal and the other associated with the noise. *Eigenvalues* relate to the noise variance and the methods utilize the orthogonality property between signal vectors and noise subspace eigenvectors. High-resolution subspace methods provide very accurate frequency estimates with only small differences in statistical performance and computational load. They are able to resolve more closely spaced spectral lines than classical methods. The fundamental difference to classical methods is, that subspace methods are *not* based on the Fourier transform of the data sequence or its estimated correlation function [76, 139–175].

ESPRIT (Estimation of Signal Parameters via Rotational Invariance Techniques) has been developed primarily for spatial direction of arrival (DOA) estimation [8, p. 318], [12]. ESPRIT exploits invariance of two time displaced data sets to determine sinusoid frequencies, powers, and noise variance. The number of sinusoids must be known in advance and the algorithm tries to find this number of sinusoids, the strongest ones. The performance of ESPRIT is in most cases slightly better than the performance of MUSIC and minimum-norm methods. It has lower computational cost and no problems in separating the signal roots from the noise roots [8, p. 318].

Pitch estimation

Pitch or fundamental frequency estimation is essential in a variety of speech and audio processing systems. Applications can be found in the fields of speech analysis-synthesis systems (vocoder), speaker recognition, speech enhancement, and computer music. The problem is to estimate the period of a speech or music waveform, which varies both in period and in the detailed structure within a period. Many pitch estimation algorithms assume short-time signal stationarity [9], while more recent studies have concentrated on continuous pitch estimation [78], [79]. One study has suggested detecting pitch by using a bank of bandpass filters followed by PLLs [80]. Common to all of these methods is the estimation of *instantaneous* pitch, which can change from one cycle to the next.

Phase locked loop

Phase locked loop (PLL) is the traditional and widely used method for estimating *instantaneous* frequency and phase, and to track periodic signals. Both analog and digital implementations exist. In communication systems the PLL is used among others for carrier and symbol synchronization, demodulation, and frequency synthesis [11, pp. 434–464], [81]. In three-phase power electronic applications the PLL is used for detecting rapid changes in the AC frequency and phase in the

presence of grid disturbances, such as voltage harmonics, voltage dips, and frequency variations. Some recent work has suggested improving the performance of the PLL by neural networks and Kalman filters [82], by a digital PLL controlling ADC sampling [83], [84], and by using the DFT as a phase detector [85]. Common to all of these methods is that the frequency is approximately known, and that the PLL tracks the dominant frequency component and is distracted by other frequency components. When closely spaced frequencies with significantly different amplitudes must be distinguished, PLL performance can be improved by using a narrower loop filter at a cost of increased processing load.

Interpolated DFT

Although spectral analysis using the Discrete Fourier Transform (DFT) is straightforward, it has some drawbacks. Frequency resolution of the DFT is related to the measurement time, and the calculated spectrum is equal to the correct spectrum only when the analyzed signal is periodic and an integer number of periods is measured. Spectral leakage occurs when a non-integer number of periods is presented in the sampled data set.

The problem of *non-integer number of periods* has inspired a new method, which is based on interpolation between the discrete points of a DFT spectrum, thus achieving sub-bin resolution. Signal model is either a single [6] or multiple [86], [87] sinusoids in noise. These methods are often called *Interpolated DFT (IDFT)* or *Interpolated FFT (IFFT)*. They all start with an adjacent pair of DFT spectral lines $(X(i), X(i+1))$ which surround the frequency of interest. Typically a Hanning window is used together with an approximate interpolation function to obtain a frequency estimate. Window function is required for reducing spectral leakage which would otherwise disturb this algorithm. The improved resolution is obtained at a cost of increased processing load.

4.4 Phase estimation

Maximum likelihood estimator

The most popular approach for obtaining practical estimators is to use the maximum likelihood principle. It is shown in [14, pp. 157–199], that a *maximum likelihood estimator (MLE)* is asymptotically unbiased and asymptotically achieves the Cramér-Rao lower bound (CRLB), which is a widely used lower bound on the variance of an unbiased estimator. An estimator which is unbiased and attains the CRLB is said to be *efficient* as it efficiently uses the data [14, pp. 27–34]. For most cases of practical interest the performance of the MLE is optimal for large enough data sets.

Signal model (5.1) in this thesis is a *single unmodulated sinusoid in additive white Gaussian noise*

$$x(n) = A\cos(2\pi n f/f_s + \theta) + w(n)$$

where A is signal amplitude, f frequency, f_s sampling rate, θ phase, and $w(n)$ additive white Gaussian noise. In the estimation problem only phase θ is assumed

to be unknown. It is shown in [14, p. 33] that for this problem, a phase estimator does not exist which is unbiased and attains the CRLB.

Assuming that frequency f is not near 0 or $f_s/2$, an approximation can be used to attain the MLE of phase [14, pp. 167–171]

$$\hat{\theta} = -\arctan \frac{\sum_{n=0}^{N-1} x(n) \sin(2\pi n f/f_s)}{\sum_{n=0}^{N-1} x(n) \cos(2\pi n f/f_s)} \tag{4.5}$$

where N is the number of samples. The CRLB for phase estimate variance is given by

$$\mathrm{var}\{\hat{\theta}\} \geq \frac{2\sigma^2}{NA^2} = \frac{1}{N\eta} \tag{4.6}$$

where $\eta = (A^2/2)/\sigma^2$ is the signal-to-noise ratio (SNR) of the signal $x(n)$, and σ^2 is the variance of the white Gaussian noise $w(n)$. The MLE given by (4.5) is valid only for large N, for shorter data records this estimator is considerably biased.

Interpolated DFT

Phase can be estimated in the same way as frequency by interpolating between an adjacent pair of DFT spectral lines $(X(i), X(i+1))$ which surround the frequency of interest [86]. In addition to two-point interpolation, reference [88] proposes improving phase estimates by using three-point $(X(i-1), X(i), X(i+1))$ interpolation, and by considering also long-range leakage contributions. These methods can cope with the problem of *non-integer number of cycles* in the measurement interval at a cost of increased processing load compared to the correlator (DFT).

Phase difference of two equal frequency signals

Methods for estimating phase difference of two equal frequency sinusoids have been developed in the fields of communications, control applications, and power-line signal processing. Time-domain methods are based on measuring the difference of zero-crossings of the two signals. More recent frequency-domain methods [15], [89] are based on the interpolated DFT. Common to these methods is simultaneous sampling of the *two equal frequency signals*, and that the parameter of interest is the phase difference. They are not suitable for estimating the phase of a single sinusoid.

Time-delay estimation

Time-delay estimation (TDE) is a basic tool in various array processing scenarios and has many applications, including tracking in sonar, range finding in radar, seismic exploration, positioning in navigation, synchronization in communications, and medical ultrasound imaging. Signal model is a single source and several time-delayed versions of the same signal. The target is to estimate relative *phase or time-delay difference of two or more signals*. Depending on the application, the signals are either a known reference signal and a time-delayed arriving signal as in radar [90], or several time-delayed sensor signals from a possibly unknown source as in tracking a speaker in a conference room [13]. Received signals may be coherent

(identical at two sensors, except time delay), or random phenomena in the propagation medium may have caused loss of coherence [91]. When the source signal is a sinusoid, DFT or interpolated DFT is often used to estimate the phase [90], [92] providing subsample resolution. Reference [13] uses generalized cross-correlation (GCC) for arbitrary signals providing a resolution of one sample. Reference [93] proposes time-domain spline-based interpolation of one signal and pattern matching with the second one to estimate the time-delay. Common to all of these methods is, that there is one signal source and *several time-delayed versions of the same signal.*

4.5 Methods for communication systems

The rapid development of digital communications has motivated the development of several methods targeted specifically to this application [11], [16], not for estimating the phase or frequency of a single sinusoid.

Carrier frequency estimation

In digital communication systems the receiver needs an estimate of the carrier frequency for frequency offset compensation. In mobile platforms and in particular in low earth orbit (LEO) satellite systems the Doppler effect can be significant. Both the Doppler shift caused by velocity and Doppler rate-of-change caused by accelerative trajectories are of interest [94]. In [95] the interest is in applications where phase varies significantly within a symbol interval. Reference [96] considers carrier frequency estimation in burst-mode digital transmission either from a preamble, or directly from the modulated signal, and [97] controls receiver local oscillator based on frequency offset estimate obtained with interpolated DFT. Common to all of these methods is that the Doppler shift is time varying and may be large, in most cases M-PSK signaling is used, and that the target is to enable symbol detection.

Timing recovery

Symbol synchronization or timing recovery is essential digital communication systems. Reference [98] discusses timing recovery in digital synchronous receivers. The binary or multilevel PAM input signal is sampled at *one-sample-per-symbol.* The synchronizer adjusts receiver clock frequency and phase continuously to optimize sampling instants and to achieve maximum eye opening.

Joint carrier frequency and phase estimation

Joint carrier frequency and phase estimation of M-PSK signals has been widely studied. In this context *frequency offset estimate* is used in the receiver to compensate for the frequency difference between local oscillators of the transmitting and receiving stations. Inaccurate frequency estimate can cause cycle slips which cause errors in signal decoding [99], [100]. *Phase estimation* in this context means symbol detection. Typically perfect timing or symbol synchronization is assumed, and signal model is *one-sample-per-symbol* plus noise for a burst length of a few

symbols. Bit error rate (BER) of the received data stream is often used as the figure-of-merit, but mean and variance of the frequency and phase estimates are also used. Several ways to improve communication link performance have been studied, including algorithms targeted for short bursts [101] and large frequency offsets [102], comparison of data-aided (DA) and non-data-aided (NDA) methods [103], and a study on the effect of reference symbol location within a data burst [104]. Common target of all these methods is *reliable symbol detection from short bursts of data.*

4.6 Applicability of related methods

The *signal model* in Section 5.2 and *estimation problem* in Section 5.3 direct the selection of applicable methods. The problem is to estimate a minute frequency offset due to the Doppler effect in the received signal when the frequency of the transmitted sinusoid is known. For a 10 kHz signal and a wind speed range of 1 to 100 m/s, the corresponding frequency offset is in the order of $3 \cdot 10^{-5}$ to $3 \cdot 10^{-3}$ Hz. Measurement interval is fixed and either 400 ms or 1000 ms, corresponding to the Alpha and Omega transmission sequence. The number of signal cycles in the measurement interval is in the order of 5000 or 12000, accordingly. This estimation problem differs notably from instantaneous frequency estimation from short signal bursts of 10–30 cycles, or even from sub-cycle data. Alpha signals bring the challenge of non-integer number of cycles in the measurement interval, which the selected method must be able to handle. Methods working at low SNR are preferred over methods requiring high SNR to achieve the same performance. Moreover, it is quite common that several interfering transmitters in the received signal are stronger than most of the navigation signals of interest, making algorithms that find the strongest signals unsuitable for this application. Finally, excessive processing load may make an otherwise suitable algorithm impractical.

Table 4.1 gives a summary of related frequency estimation methods. One method is of particular interest: *IDFT* has same signal model as the one used in this thesis, and it has been developed to improve DFT resolution when the signal of interest falls between two bins, i.e. when there is a non-integer number of cycles in the measurement interval. The remaining frequency estimation methods are not applicable due to various reasons. *Classical non-parametric methods*, such as DFT, do not have adequate resolution and can not handle all navigation signals with the said fixed measurement intervals. As the mathematical model of radio signal is not known due to unknown propagation path, *parametric ARMA class of methods* are not likely to succeed. Furthermore, they are no better than the DFT at low SNR encountered in this application. *High-resolution methods* are primarily intended for direction of arrival (DOA) estimation. As they separate the strongest signals from noise, they are distracted by nearby strong interference encountered in this application. Also their higher computational burden compared to the IDFT makes them impractical for the navigation receiver. The estimation problem in *pitch estimation* differs notably from the estimation problem encountered in this application. The *PLL* is impractical due to the requirement of a very narrow loop filter needed for eliminating strong interference close to a navigation signal or when the SNR is low.

Method	Signal model Estimation problem	Remarks
Classical non-parametric DFT Periodogram Correlogram	Sum of sinusoids in noise, power spectral density	No knowledge of signal required, output directly proportional to signal power, computationally efficient (FFT), works well at low SNR, can not exploit high SNR, reasonable resolution for long data records, poor performance for short data records, high variance, leakage caused by strong signals masks weak signals, windowing reduces sidelobes at the expense of resolution, averaging reduces variance
IDFT	Sinusoid in noise, non-integer number of cycles in the measurement interval	Same signal model as in this thesis, interpolate between an adjacent pair of DFT bins, improved resolution at a cost of increased processing load compared to the DFT, sub-bin resolution
Parametric methods	Signal satisfies a known mathematical model	Must determine model order, when the assumed model is a close approximation of the reality, parametric methods provide better performance than non-parametric methods
AR	Autoregressive (all-pole) process, models spectra with narrow peaks	High resolution at high SNR, no better than DFT at low SNR, good spectral fidelity for short data records, no inherent sidelobe artifacts, some AR algorithms exhibit line splitting and bias, AR is the most frequently used in the ARMA class of methods
MA	Moving average (all-zero) process, models spectra with broad peaks and sharp nulls	Broad spectral response (low resolution), has sidelobes, significantly more difficult to resolve MA parameters than AR parameters
ARMA	Rational transfer function (MA order $\neq$ AR order), models spectra with sharp peaks and sharp nulls	Must determine AR and MA orders, models all rational transfer function processes, no well-established algorithm for ARMA parameter estimation
High resolution subspace methods ESPRIT MUSIC Pisarenko	Sum of complex exponentials in noise, eigenvector decomposition of autocorrelation matrix into two subspaces, signal and noise; determine frequency, power, and noise variance of sinusoids	Very accurate frequency estimates, can resolve more closely spaced spectral lines than classical methods, number of sinusoids must be known in advance or determined, developed for spatial direction of arrival (DOA) estimation, the performance of ESPRIT is in most cases slightly better than the performance of MUSIC and minimum-norm methods
Pitch estimation	Pitch or fundamental frequency estimation of speech and audio signals, the waveform varies both in period and in the detailed structure within a period.	Estimate of instantaneous frequency which can change from one cycle to the next, very short data records, assume short-time stationarity
PLL	Track the dominant frequency of the signal, estimate instantaneous frequency and phase	Loop filter required at low SNR, frequency must be approximately known, performance can be improved with a narrow loop filter at a cost of increased processing load and slower tracking speed

Table 4.1: Summary of related frequency estimation methods

Method	Signal model Estimation problem	Remarks
MLE	Sinusoid in noise, frequency known, estimate phase	Same signal model as in this thesis, good performance for long data records, asymptotically unbiased, asymptotically achieves the CRLB
IDFT	Sinusoid in noise, non-integer number of cycles in the measurement interval	Same signal model as in this thesis, interpolate between an adjacent pair of DFT bins, improved resolution at a cost of increased processing load compared to the DFT, sub-bin resolution
Phase difference	Two equal frequency signals, phase difference	Simultaneous sampling of two equal frequency signals, time difference of zero crossings, frequency domain methods are based on the IDFT, not suitable for a single sinusoid
TDE	One signal source and several time delayed versions of the same signal, signal source may be sinusoid or arbitrary, estimate relative phase or time difference of two or more signals	Basic tool in various array processing scenarios

Table 4.2: Summary of related phase estimation methods

Table 4.2 gives a summary of related phase estimation methods. The maximum likelihood estimator (4.5) of phase equals the argument of the DFT [105, p. 401] when there is an integer number of periods in the measurement interval. Otherwise the problem of apparently changing initial phase is encountered as described in Section 5.4. Finally, the estimation problem in *phase difference estimation* and in *TDE* is not the same as this thesis.

Numerous methods have been developed for communications applications to estimate carrier frequency and phase, but they are not applicable for several reasons. The basic difference to the estimation problem in Section 5.3 is, that the signal model is typically one sample-per-symbol of a phase or amplitude modulated signal, assuming perfect receiver synchronization to the incoming data stream, and that the Doppler shift in mobile applications is a few orders of magnitude greater [106] than that encountered in the navigation application. Carrier frequency estimators aim at compensating Doppler shift caused by satellites and mobile platforms to the extent that symbol detection is possible. Phase estimation methods for communication receivers are also not directly applicable, since in this context phase estimation means reliable symbol detection from an M-PSK modulated signal.

4.7 Discussion

Most of the related frequency and phase estimation methods are not applicable to the estimation problem presented in Section 5.3. Interpolated DFT may be feasible, as it can handle the challenge of Alpha signals. A new method is proposed in Chapter 5 and its properties are compared with the Interpolated DFT, the signal model being a single sinusoid in white Gaussian noise.

Chapter 5

Proposed phase estimation method

5.1 Overview

It has been described in the previous sections, how the motion of a radiosonde causes a minute frequency offset in the received navigation signals. Estimates of the frequency offset are further processed to get a wind profile, which in turn is used for weather forecasting. Accuracy of the frequency offset estimate is of utmost importance, as errors made in the early steps can not be eliminated later in the processing chain. By taking advantage of the fact that the frequency offset is small, its estimate can be obtained by observing signal phase change in consecutive time instants. Finally, the estimation method must be computationally efficient so that it can be implemented in a practical receiver.

The main contribution of this thesis is the following *phase corrected correlation (PCC)* algorithm (Section 5.4) for estimating the unknown *phase* of a sampled sinusoid of known frequency (Section 5.2). According to the estimation problem in Section 5.3, the proposed PCC algorithm is targeted specifically for the case, when there is a *non-integer number of cycles in the measurement interval.* Two additional algorithms are proposed for decreasing the mean squared error (MSE) of phase estimates in the presence of disturbances such as lightnings and interfering transmitters. *Burst noise removal* is described in Section 5.5 and *partition outlier removal* in Section 5.6, respectively.

Estimation performance criterion is discussed in Section 5.7. Performance of the *PCC phase estimate* is studied in Section 5.8 by comparing its mean squared error (MSE) with the Cramér-Rao lower bound (CRLB). Two different cases are considered: first, MSE vs. signal-to-noise ratio (SNR) for fixed N; and second, MSE vs. N for fixed SNR, where N is the number of samples in the measurement interval. Additionally, the effect of sampling rate, burst noise removal, and partition outlier removal on phase estimate MSE is studied. *PCC frequency estimate* is obtained by observing signal phase change in consecutive measurement intervals, and its performance is studied in Section 5.9. Frequency estimation performance and computational burden of the PCC is compared with Interpolated DFT (IDFT) in Section 5.10. Finally, Section 5.11 covers various implementation issues which decrease computational burden in a digital signal processor (DSP) implementation.

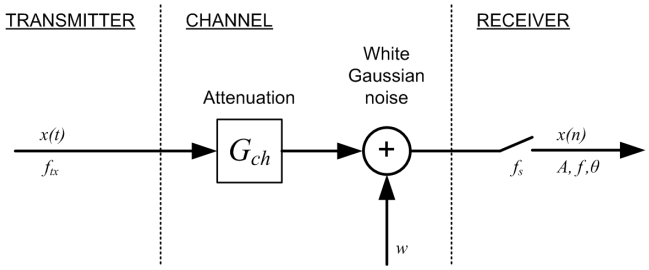

Figure 5.1: Signal model for algorithm performance determination

5.2 Signal model

Signal model which is used for algorithm performance determination is a *single unmodulated sinusoid in additive white Gaussian noise*

$$x(n) = A\cos\left(2\pi nf/f_s + \theta\right) + w(n) \tag{5.1}$$

where A is signal amplitude, f frequency, f_s sampling rate, θ phase, and $w(n)$ additive white Gaussian noise. Signal phase θ is unknown while frequency f is assumed to be known. *Phase θ is the parameter to be estimated.*

The signal model shown in Figure 5.1 is a simplification of the estimation problem shown in Figure 5.2. It is assumed that $f = f_{rx} \approx f_{tx}$, i.e. estimation approach 3 of Section 5.3 is used. It is assumed that receiver sampling clock is perfect and that sampling rate f_s fulfills the Nyquist condition. Although the VLF-band navigation systems transmit multiple sinusoids simultaneously, justification for the simplified single-sinusoid signal model comes from correlation bandwidth, which in this application is in the order of 1 Hz. Correlation bandwidth is discussed in Section 5.11.

5.3 Estimation problem

When a radiosonde flies relative to a fixed ground based VLF band navigation transmitter, the *observed frequency* is changed by the Doppler effect, and by *estimating this change in frequency*, the radial motion of the radiosonde can be determined. By combining observations for several transmitters, the motion of the radiosonde relative to the earth can be determined as described in [17] and [18]. The received radio signal contains not only all navigation signals, but also other VLF-band transmitters, coloured noise, and various types of interference; all summed together.

Figure 5.2 shows how the transmitted sinusoid $x(t)$ is affected by various phenomena in the transmission channel and the receiver: Doppler effect causes a small frequency offset $\Delta f_{doppler}$, attenuation G_{ch} decreases signal-to-noise ratio, time varying channel response H_{ch} distorts both amplitude and phase; coloured noise w_{noise}, lightnings $w_{lightning}$, and narrow band interference from other transmitters w_{narrow} distort the signal; and finally, receiver sampling rate offset Δf_s causes a

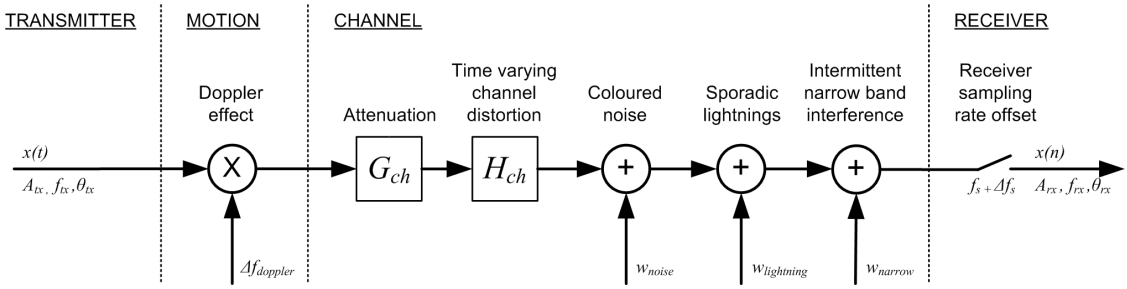

Figure 5.2: Doppler effect causes a small frequency offset, attenuation decreases signal-to-noise ratio and various disturbances distort the signal in the transmission channel

shift in the received frequency f_{rx}. The received signal $x(n)$ can be expressed as

$$x(n) = A_{tx}G_{ch}|H_{ch}(n)|\cos\left(2\pi n\frac{f_{tx}+\Delta f_{doppler}}{f_s+\Delta f_s}+\theta_{tx}+\arg[H_{ch}(n)]\right)+$$
$$+ w_{noise}(n) + w_{lightning}(n) + w_{narrow}(n) =$$
$$= A_{rx}\cos\left(2\pi n f_{rx}/f_s + \theta_{rx}\right) + w_{rx}(n) \quad (5.2)$$

where A_{tx}, f_{tx}, and θ_{tx} are the amplitude, frequency, and phase of the transmitted sinusoid; A_{rx}, f_{rx}, and θ_{rx} are the amplitude, frequency, and phase of the received sinusoid; and $w_{rx}(n)$ contains the sum of all noise and interference sources. *Received phase θ_{rx} is the parameter to be estimated.* Signal model (5.1) for algorithm performance determination uses a simplified model which is shown in Figure 5.1.

The problem of estimating the Doppler shift can be considered from a few different points of view leading to different *estimation approaches*. Estimation approach 3 is used in this thesis.

1. If the transmitted frequency is considered to be unknown, one is directed to try classical or high resolution power spectrum and frequency estimators to estimate the *received frequency* f_{rx}.

2. As the transmitted navigation frequency is in fact known, one is directed to try *frequency offset* estimators to estimate $\Delta f_{doppler}$.

3. By taking advantage of the fact that the frequency offset is small ($f_{tx} \approx f_{rx}$), its estimate can also be obtained by observing signal *phase change* in consecutive time instants; the approach used in this thesis.

Due to the receiver implementation the *measurement interval is fixed* and either 400 ms or 1000 ms, corresponding to the Alpha and Omega transmission sequence. Also due to the receiver implementation the *sampling rate is fixed* (80 kHz) rather than variable. Signal *frequency* can be any of the navigation frequencies listed in Chapter 3. Particularly with Alpha signals, there will be a *non-integer number of signal cycles* in the 400 ms measurement interval. Frequency offset of each navigation transmitter is estimated from the same measurement interval. Finally, low SNR signals must be considered also, since attenuation is high when VLF-signals propagate long distances.

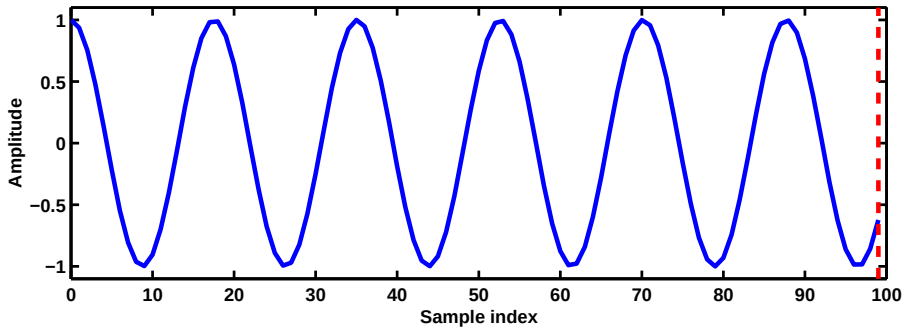

Figure 5.3: Non-integer number of cycles in the measurement interval ($K = 5.7$)

The Doppler effect [107, pp. 706–708] on the *received frequency* can be expressed as

$$f_{rx} = f_{tx} \cdot \left(1 - \frac{v_{rx}}{c} \cos \alpha\right) \tag{5.3}$$

and the observed *frequency offset* as

$$\Delta f_{doppler} = f_{rx} - f_{tx} = -f_{tx} \cdot \frac{v_{rx}}{c} \cos \alpha \quad [Hz] \tag{5.4}$$

In the equations above, f_{tx} is the transmitted frequency, f_{rx} is the received frequency, v_{rx} is the velocity of the radiosonde receiver, c is the velocity of propagation of the electromagnetic wave ($c = 2.9979 \cdot 10^8$ m/s), and α is the angle between the direction of electromagnetic wave propagation and the direction of radiosonde motion. The frequency change to be estimated is small. The Doppler effect causes a 0.003 to 0.3 ppm change in the received frequency for a wind speed range of 1 to 100 m/s. The corresponding frequency offset $\Delta f_{doppler}$ for a transmitted 10 kHz signal is in the order of $3 \cdot 10^{-5}$ to $3 \cdot 10^{-3}$ Hz, assuming that the radiosonde motion is along the line of propagation. When the trajectory is slanted, the change is even smaller.

5.4 Phase corrected correlation

The proposed phase estimation method has three steps: *correlation at signal frequency*, *calculation of a phase correction term*, and *phase correction of the correlation*. This approach enables estimating the phase of signals having properties and limitations presented in the estimation problem, i.e. fixed measurement interval, fixed sampling rate, and non-integer number of cycles in the measurement interval. The concept of non-integer number of cycles in the measurement interval is discussed first, followed by a description of the PCC algorithm. Table 5.1 gives a summary of the algorithm.

Non-integer number of cycles in the measurement interval

Measurement interval is determined by the number of samples N and sampling interval T.

$$T_{meas} = NT \tag{5.5}$$

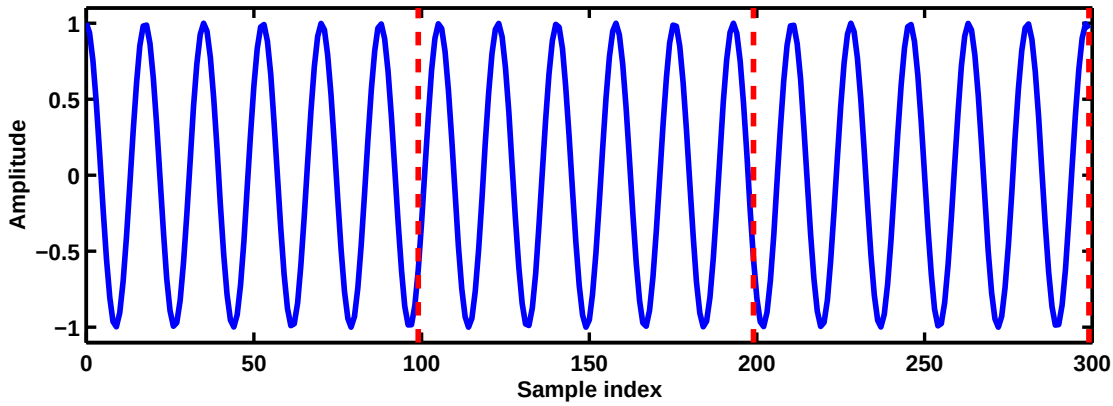

Figure 5.4: Three consecutive measurement intervals with $K = 5.7$ cycles in each measurement interval

Sampling rate $f_s = 1/T$ is selected so that the Nyquist condition is fulfilled. Consider a sinusoid signal which may have a *non-integer number of cycles* in the measurement interval. Let us express this frequency as

$$f = K\frac{f_s}{N} \tag{5.6}$$

where positive real number K is the number of cycles in the measurement interval. K can be written in two parts as

$$K = k + \Delta k, \quad 0 \leq \Delta k < 1 \tag{5.7}$$

where k is the integer part of K and Δk is the fractional part of K.

$$K = f\frac{N}{f_s} \tag{5.8}$$

$$\Delta k = K - \lfloor K \rfloor \tag{5.9}$$

Figure 5.3 shows an example of one measurement interval for $K = 5.7$ and Figure 5.4 shows three consecutive measurement intervals of the same signal.

Correlation at signal frequency

The *first step* of the PCC algorithm is to correlate signal $x(n)$ (5.1) with a sinusoid reference

$$R(f) = e^{-j2\pi nf/f_s}, \quad n = 0, 1, \ldots, N-1 \tag{5.10}$$

to attain *correlation at signal frequency*

$$\begin{aligned} C(f,m) &= \sum_{n=0}^{N-1} x(mN+n) \cdot R(f) \\ &= \sum_{n=0}^{N-1} x(mN+n) \cdot e^{-j2\pi nf/f_s} \end{aligned} \tag{5.11}$$

where f is the known signal frequency and $m = 0, 1, 2, \ldots$ is the measurement interval index. Notice, that Equation (5.11) does resemble the DFT [105, p. 401],

but equals it only, when there is an integer number of cycles of f in the N samples, the measurement interval. Correlation at signal frequency (5.11) does not have this limitation. The same correlation is also found in Equation (4.5), which is the MLE of the phase.

$C(f, m)$ is calculated with the *same reference* $R(f)$ in consecutive measurement intervals. This brings the advantage, that the complex exponential in the reference needs to be calculated only once and the result can be stored and reused when processing subsequent measurement intervals.

Phase correction term

The *second step* is to calculate a phase correction term for each consecutive measurement interval. When there is a non-integer number of cycles in the measurement interval, the initial phase of the signal changes apparently from one measurement interval to the next as shown in Figure 5.4. Correlation (5.11) calculated from the first N samples gives a phase estimate. Correlation of the second measurement interval using the same reference (5.10) as for the first N samples has an apparent

$$\phi = \Delta k \cdot 2\pi \tag{5.12}$$

radian *phase advance*, 2ϕ in the third measurement interval, then 3ϕ, and so on. The apparent phase advance of correlation (5.11) in the mth measurement interval is thus

$$\phi(m) = m \cdot \phi, \quad m = 0, 1, 2, \ldots \tag{5.13}$$

The *phase correction term* for the mth measurement interval can be expressed as

$$PC(m) = e^{-j\phi(m) \bmod (2\pi)} \tag{5.14}$$

when multiples of 2π have been removed.

Phase corrected correlation

The *third step* is phase correction of correlation (5.11) using phase correction term (5.14). The *phase corrected correlation* for the mth measurement interval is given by

$$\begin{aligned} PCC_m(f) &= PC(m) \cdot C(f, m) \\ &= e^{-j\phi(m) \bmod (2\pi)} \cdot \sum_{n=0}^{N-1} x(mN + n) \cdot e^{-j2\pi nf/f_s} \end{aligned} \tag{5.15}$$

and the corresponding *phase estimate* for the mth measurement interval is obtained from

$$\hat{\theta}_m(f) = \arg[PCC_m(f)] \tag{5.16}$$

Notice, that in the special case when there is an integer number of cycles of f in the measurement interval, $\Delta k = 0$, $\phi(m) = 0$, and correction term $PC(m) = 1$ for all m, and thus, phase corrected correlation (5.15) equals the DFT.

Estimation performance of the PCC algorithm is studied in Sections 5.8 and 5.9, its performance is compared with Interpolated DFT (IDFT) in Section 5.10, and a MATLAB example is given in Appendix A.1.

Step 1 Signal model

$$x(n) = A\cos(2\pi nf/f_s + \theta) + w(n) \tag{5.1}$$

Step 2 Number of cycles in the measurement interval

$$K = f\frac{N}{f_s} \tag{5.8}$$

$$\Delta k = K - \lfloor K \rfloor \tag{5.9}$$

Step 3 Correlation at signal frequency

$$R(f) = e^{-j2\pi nf/f_s} \tag{5.10}$$

$$C(f,m) = \sum_{n=0}^{N-1} x(mN+n)\cdot R(f) \tag{5.11}$$

Step 4 Phase advance in the mth measurement interval

$$\phi = \Delta k \cdot 2\pi \tag{5.12}$$

$$\phi(m) = m\cdot\phi, \quad m = 0,1,2,\ldots \tag{5.13}$$

Step 5 Phase correction term

$$PC(m) = e^{-j\phi(m) \bmod (2\pi)} \tag{5.14}$$

Step 6 Phase corrected correlation

$$PCC_m(f) = PC(m)\cdot C(f,m) \tag{5.15}$$

Step 7 Phase estimate

$$\hat{\theta}_m(f) = \arg[PCC_m(f)] \tag{5.16}$$

Table 5.1: Summary of phase estimation using the PCC algorithm

5.5 Burst noise removal

Various disturbances distort the received VLF-band signal as discussed in Section 3.5. One of the major error sources are lightnings, which cause wide band radio interference that can last several milliseconds. During this time the original signal is more or less corrupted by the high energy burst. A correlation receiver performs well in the presence of additive white Gaussian noise, while short duration high energy noise increases MSE of a phase estimate considerably. If these high energy bursts are removed from the samples *before correlation*, overall signal-to-noise ratio is improved and consequently, MSE of the phase estimate is decreased.

Algorithm description

Bursts are removed from the samples by *zeroing a range around a detected burst*. It is assumed, that the length of the burst is short compared to the measurement interval. Variable signal strength is taken into account by calculating standard deviation σ of the signal for each measurement interval. By selecting a detection threshold of 3σ, a 99.7% confidence interval is attained, and the algorithm leaves the signal intact when no bursts are present.

The signal dependent *burst detection threshold* is given by

$$D_{burst} = s_{burst} \cdot \sigma \tag{5.17}$$

where s_{burst} is a fixed threshold scaling factor and σ is the standard deviation of the signal. A *burst is detected* when signal amplitude exceeds the burst detection threshold

$$|x(n)| > D_{burst} \tag{5.18}$$

for some $n = 0, 1, \ldots, N-1$. The detected burst is removed by zeroing a range of $\pm r_{burst}$ samples around it. The size of the zeroing range is adjusted according to the typical burst length.

Figure 5.5 shows a sampled VLF-band antenna signal which has two bursts caused by lightnings, and Figure 5.6 shows the same signal with the two bursts replaced by zeros. The two horizontal dashed lines indicate the signal dependent burst detection threshold $D_{burst} = 3\sigma$. The effect of burst noise removal on phase estimate MSE is studied in Section 5.8 and a MATLAB example is given in Appendix A.2.

5.6 Partition outlier removal

Another error source in the received VLF-band signal is a sudden phase fluctuation caused by the propagation path or by intermittent narrow band interference between Alpha and Omega transmissions as described in Section 3.5. An abrupt change in signal phase increases MSE of the phase estimates. If the duration of the interference is short compared to the measurement interval, the disturbed part of the signal can be removed and the MSE of the phase estimate decreased. In order to be able to detect potential phase fluctuations, the signal in a measurement interval is divided into several partitions, phase of each partition is estimated separately and this set of phase estimates is used as a reference when determining validity of each partition.

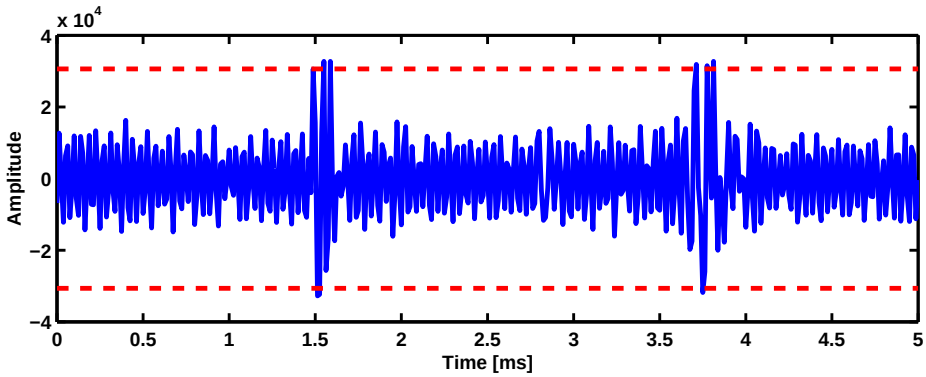

Figure 5.5: A VLF-band antenna signal with two bursts caused by lightnings, burst detection threshold is 3σ

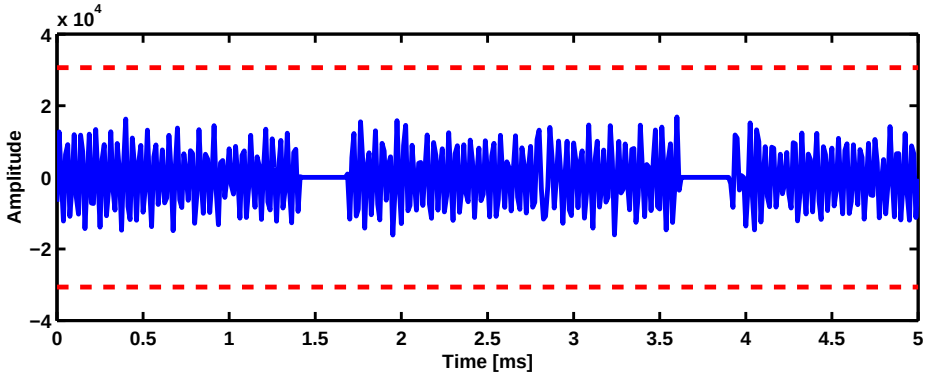

Figure 5.6: Burst noise removal improves signal-to-noise ratio when bursts are present

Algorithm description

Phase fluctuations are removed from the signal by *partitioning the measurement interval* and *discarding erroneous partitions*. Phase estimate for the measurement interval is constructed from the *remaining partitions*. The set of PCC partitions form a cluster in the complex plane. Partition outlier removal is based on the assumption, that less than half of the partitions are affected by the disturbance, which may move some partitions further off from the cluster of remaining partitions. Variable phase noise is taken into account by calculating average deviation of the partition phase estimates. Detection threshold is proportional to the average deviation and can be adjusted for each application with a threshold scaling factor. The size or radius of this cluster depends on the signal-to-noise ratio: with high SNR the cluster is small and gets larger with decreasing SNR. The algorithm leaves the partitions intact when no outliers are present.

Calculate partitioned correlation

Divide the N samples in the measurement interval into L partitions, each containing an integer number of samples

$$N' = \frac{N}{L} \tag{5.19}$$

and calculate phase corrected correlation (5.15) for every partition. Each $PCC_m(f)$ is referred to in the following as the *PCC partition*. As it is now calculated from N' samples, PCC index m increments also every N' samples, and the *partitioned phase corrected correlation* for one measurement interval is thus

$$PCC_{partitioned}(f) = \sum_{m=0}^{L-1} PCC_m(f) \tag{5.20}$$

The first $PCC_{partitioned}(f)$ is formed of partitions $m = 0, 1, \ldots, L-1$, the next one is formed of partitions $m = L, L+1, \ldots, 2L-1$, and so on for each consecutive measurement inteval. A MATLAB example of partitioned PCC is given in Appendix A.3.

Find center of the partition cluster

The set of PCC partitions for one measurement interval forms a cluster in the complex plane. The cluster is small at high SNR and larger at low SNR. A short duration disturbance may move one or several partitions further off from the cluster of remaining partitions. In the presence of a few outliers, median is the preferred method for finding the *center of the partition cluster*.

$$x_{med} = \text{median}(\text{Re}\{PCC_m(f)\}), \quad m = 0, 1, \ldots, L-1 \tag{5.21}$$

$$y_{med} = \text{median}(\text{Im}\{PCC_m(f)\}), \quad m = 0, 1, \ldots, L-1 \tag{5.22}$$

Calculate signal dependent outlier detection threshold

Variable phase noise is taken into account by calculating average deviation (5.52) of the partitions from the center of the cluster

$$ADev_x = \frac{1}{L}\sum_{m=0}^{L-1} |\mathrm{Re}\{PCC_m(f)\} - x_{med}| \tag{5.23}$$

$$ADev_y = \frac{1}{L}\sum_{m=0}^{L-1} |\mathrm{Im}\{PCC_m(f)\} - y_{med}| \tag{5.24}$$

The signal dependent *outlier detection threshold* is given by

$$D_{cluster} = s_{cluster} \cdot \sqrt{ADev_x^2 + ADev_y^2} \tag{5.25}$$

where $s_{cluster}$ is a fixed threshold scaling factor, and $ADev_x$ and $ADev_y$ depend on the partition cluster size.

Discard outliers

Distance of the mth PCC partition from the center of the cluster is

$$r_m = \sqrt{(\mathrm{Re}\{PCC_m(f)\} - x_{med})^2 + (\mathrm{Im}\{PCC_m(f)\} - y_{med})^2} \tag{5.26}$$

Outliers are all partitions whose distance is greater than the detection threshold

$$r_m > D_{cluster} \tag{5.27}$$

and the remaining *valid partitions* are

$$\Lambda = \{m \in \{0, 1, \ldots, L-1\} \mid r_m \leq D_{cluster}\} \tag{5.28}$$

Construct phase estimate from the valid partitions

Phase estimate for the measurement interval is constructed from the valid partitions.

$$PCC_{valid}(f) = \sum_{m\in\Lambda} PCC_m(f) \tag{5.29}$$

$$\hat{\theta}_{valid}(f) = \arg[PCC_{valid}(f)] \tag{5.30}$$

The example in Figure 5.7 shows ten PCC partitions in the complex plane and $\hat{\theta}_{all}$ is the phase estimate using all partitions. When the two outliers in the upper left corner are discarded, the resulting improved phase estimate is $\hat{\theta}_{valid}$. The dashed circle indicates the signal dependent outlier detection threshold $D_{cluster}$. The effect of partition outlier removal on phase estimate MSE is studied in Section 5.8 and a MATLAB example is given in Appendix A.4.

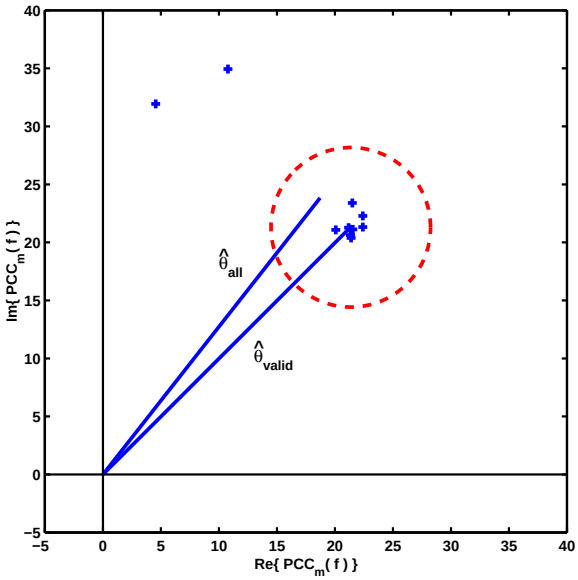

Figure 5.7: Partition outlier removal decreases phase estimate MSE when outliers are present

5.7 Estimation performance criterion

Variance and *bias* are two measures often used to define the performance or quality of an estimator [76, p. 29]

$$\text{var}\{\hat{a}\} = E\left\{(\hat{a} - E\{\hat{a}\})^2\right\} \tag{5.31}$$

$$\text{bias}\{\hat{a}\} = E\{\hat{a}\} - a \tag{5.32}$$

where a is the true value and $\hat{a}$ is an estimate of it. Some additional information on the estimator behavior may be gained by studying its bias and variance separately: a good parameter estimator has small bias and small variance, and it is consistent (estimation error gets smaller as the number of measurements increases) [108, p. 40]. The expectation operator $E\{\cdot\}$ averages over the ensemble of realizations.

It is shown in [14, p. 33] that for the sinusoid in white Gaussian noise problem, a phase estimator does not exist which is unbiased and attains the Cramér-Rao lower bound (CRLB). In this case *mean squared error (MSE)* can be used as a performance criterion

$$\begin{aligned} MSE &= E\{|\hat{a} - a|^2\} \\ &= \text{var}\{\hat{a}\} + \text{bias}^2\{\hat{a}\} \end{aligned} \tag{5.33}$$

Sample mean $\bar{x}$ and sample variance $\text{var}(x)$ are defined in [109, pp. 200–203] as

$$\bar{x} = \frac{1}{N}\sum_{n=1}^{N} x_n \tag{5.34}$$

$$\text{var}(x) = \frac{1}{N-1}\sum_{n=1}^{N}(x_n - \bar{x})^2 \tag{5.35}$$

Being able to place a lower bound on the variance of an unbiased estimator is useful, as it provides a benchmark against which to compare algorithm performance. Although several such variance bounds exist, the CRLB is most widely used [14, pp. 27–62] and is used also in the following as benchmark. For a single real sinusoid in white Gaussian noise (5.1)

$$x(n) = A\cos(2\pi nf/f_s + \theta) + w(n)$$

the *CRLB for phase estimate variance* [14, p. 33] (frequency known and amplitude not known) is

$$\mathrm{var}\{\hat{\theta}\} \geq \frac{2\sigma^2}{NA^2} = \frac{1}{N\eta} \tag{5.36}$$

and the *CRLB for frequency estimate variance* [14, p. 57] (phase and amplitude not known) is

$$\mathrm{var}\{\hat{f}\} \geq \frac{12}{(2\pi)^2\eta N(N^2-1)} \tag{5.37}$$

In the equations above,

$$\eta = \frac{A^2}{2\sigma^2} \tag{5.38}$$

is signal-to-noise ratio (SNR) of the signal $x(n)$, A signal amplitude, N number of samples in the measurement interval, and σ^2 variance of the Gaussian noise $w(n)$. Reference [14] gives the CRLB both for the real and complex case, while in [110] the CRLB is given only for a complex sinusoid.

5.8 Performance of PCC phase estimate

Performance of the PCC phase estimate is studied by comparing its MSE (5.33) with the CRLB (5.36). Two different cases are considered: first, MSE vs. signal-to-noise ratio (SNR) for fixed N; and second, MSE vs. N for fixed SNR, where N is the number of samples in the measurement interval. Additionally, the effect of sampling rate, burst noise removal, and partition outlier removal on phase estimate MSE is studied.

Simulation parameters

An ensemble of $E = 10000$ signal vectors and phase estimates are generated for each x-axis value. MSE of the estimator is calculated for each ensemble. Sampling rate $f_s = 80$ kHz as in the navigation receiver. The following measures are taken to exercise the algorithm in the presence of a *non-integer number of cycles in the measurement interval*: random known frequency f for each signal vector in the ensemble is in the vicinity of Alpha f_1 navigation frequency, $K \in [K_1 - 1/2, K_1 + 1/2]$, uniform distribution, $K_1 = Nf_1/f_s$, $f_1 = 16 * (744 + 1/21) \approx 11904.76$ Hz; measurement interval index m takes a random value $m \in [0, 1, \ldots, E]$, uniform distribution, and signal index $n = mN, mN + 1, \ldots, (m + 1)N - 1$, respectively; correlation reference $R(f)$ is always calculated with indices $n = 0, 1, \ldots, N - 1$; unknown phase θ for each signal vector in the ensemble takes values from $-\pi$ to π in E steps. Noise $w(n)$ is normally distributed random numbers with zero mean. Signal amplitude is one and noise variance σ^2 is adjusted according to SNR.

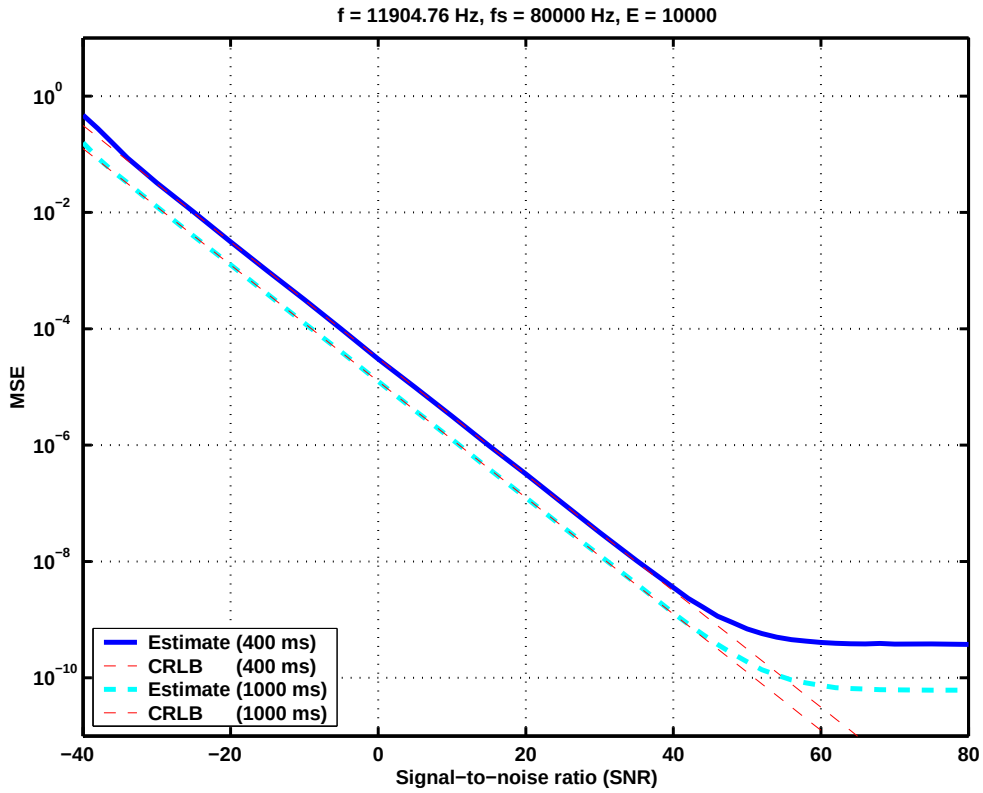

Figure 5.8: MSE of PCC phase estimate vs. SNR

MSE of phase estimate vs. SNR for fixed N

Figure 5.8 shows MSE of the PCC phase estimate versus SNR. Two fixed measurement intervals are shown: 400 ms and 1000 ms according to the Alpha and Omega navigation signals, respectively. N is set according to the sampling rate and measurement interval ($N = 32000$ for $T_{meas} = 400ms$, and $N = 80000$ for $T_{meas} = 1000ms$). MSE is close to the CRLB (5.36) up to about +40 dB SNR.

MSE of phase estimate vs. N for fixed SNR

Figure 5.9 shows MSE of the PCC phase estimate versus N, the number of samples in the measurement interval. Three fixed signal-to-noise ratios are shown: -20 dB, +10 dB, and +40 dB, representing low, medium, and high SNR, respectively. MSE of the phase estimate is close to the CRLB (5.36) when the number of samples in the phase measurement interval is according to the estimation problem ($N \geq 32000$).

The effect of sampling rate

Figure 5.10 shows how MSE of the PCC phase estimate decreases as sampling rate is increased. In this simulation sampling rate is expressed in terms of *samples per cycle (SPC)*

$$SPC = \frac{f_s}{f} \tag{5.39}$$

MSE for three different sampling rates is shown: 3, 7, and 30 samples per cycle. Seven samples per cycle corresponds approximately with the oversampling rate

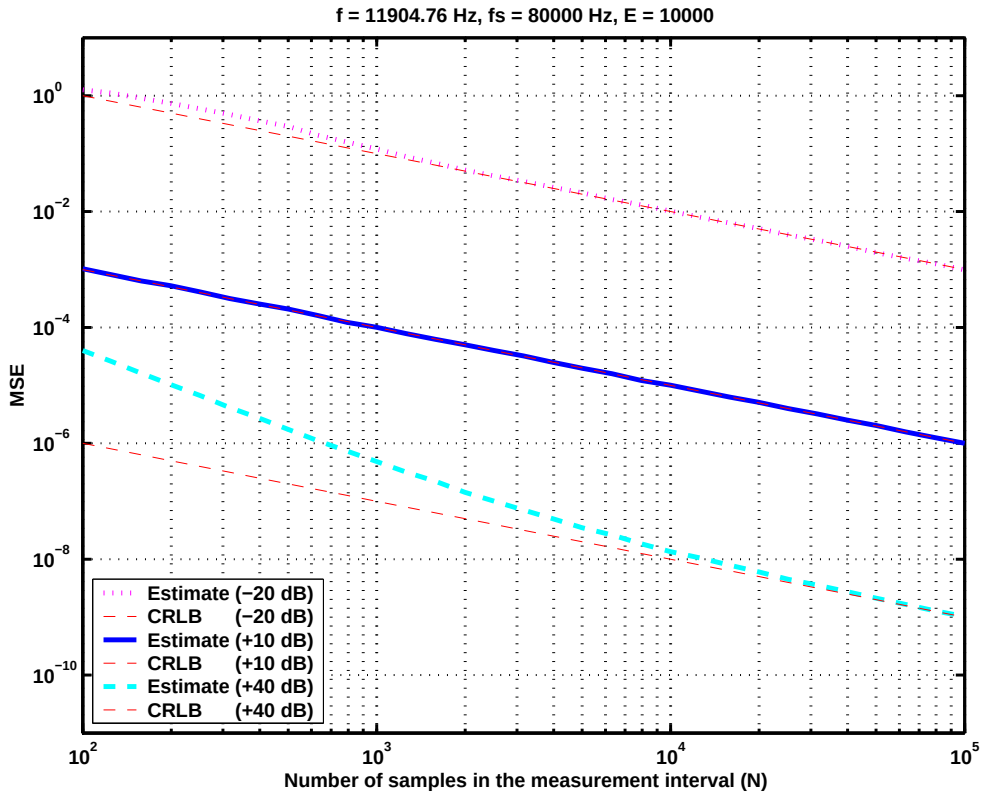

Figure 5.9: MSE of PCC phase estimate vs. N

in the navigation receiver. 400 ms measurement interval is used, otherwise the simulation is as previously.

The effect of burst noise removal

Figure 5.11 shows how two bursts at random locations in a 400 ms measurement interval increase the MSE of the PCC phase estimate, and how MSE decreases when burst noise removal is used. A burst is simulated as additive zero mean white Gaussian noise, amplitude is ten times signal amplitude, and burst length is 1 ms. Otherwise the simulation is as previously.

The effect of partition outlier removal

Figure 5.12 shows how one outlier at a random partition in a 400 ms measurement interval increases the MSE of the PCC phase estimate, and how MSE decreases when partition outlier removal is used. The measurement interval is divided into 40 partitions, 10 ms each. An outlier is simulated as random phase offset $\theta_{outlier} \in [-\pi, \pi]$, uniform distribution; amplitude is not changed. Otherwise the simulation is as previously.

5.9 Performance of PCC frequency estimate

PCC frequency estimate is obtained by observing signal phase change in consecutive measurement intervals as described in Section 4.2. Performance of the estimate is

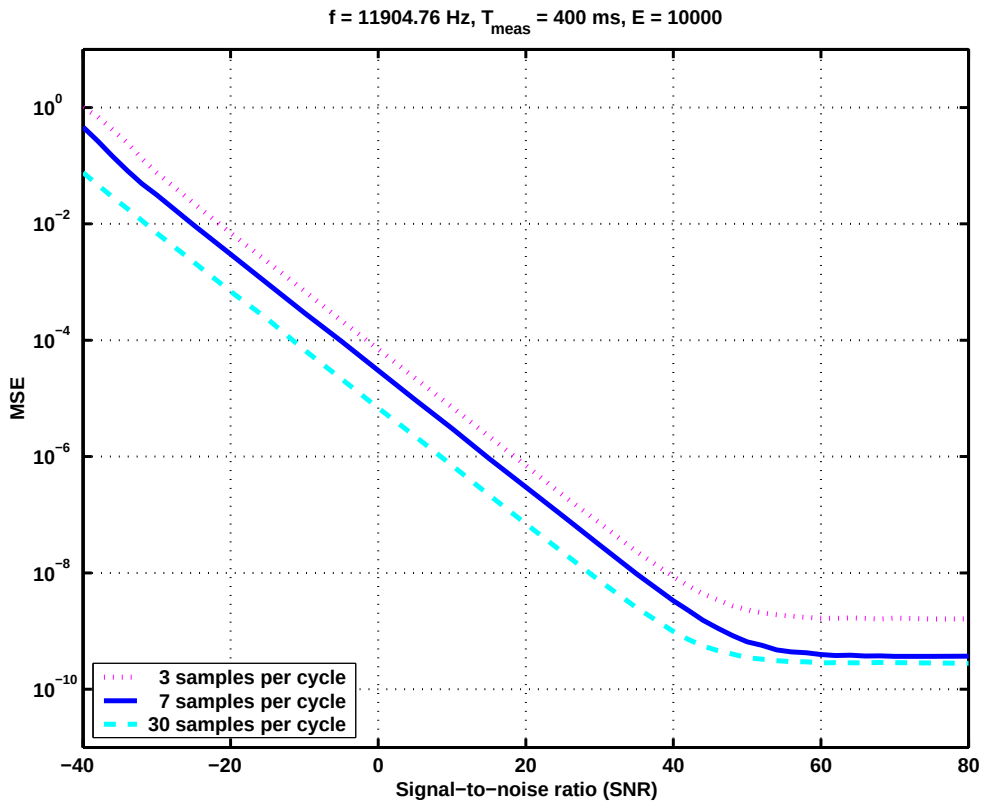

Figure 5.10: Increase in sampling rate decreases MSE of phase estimate

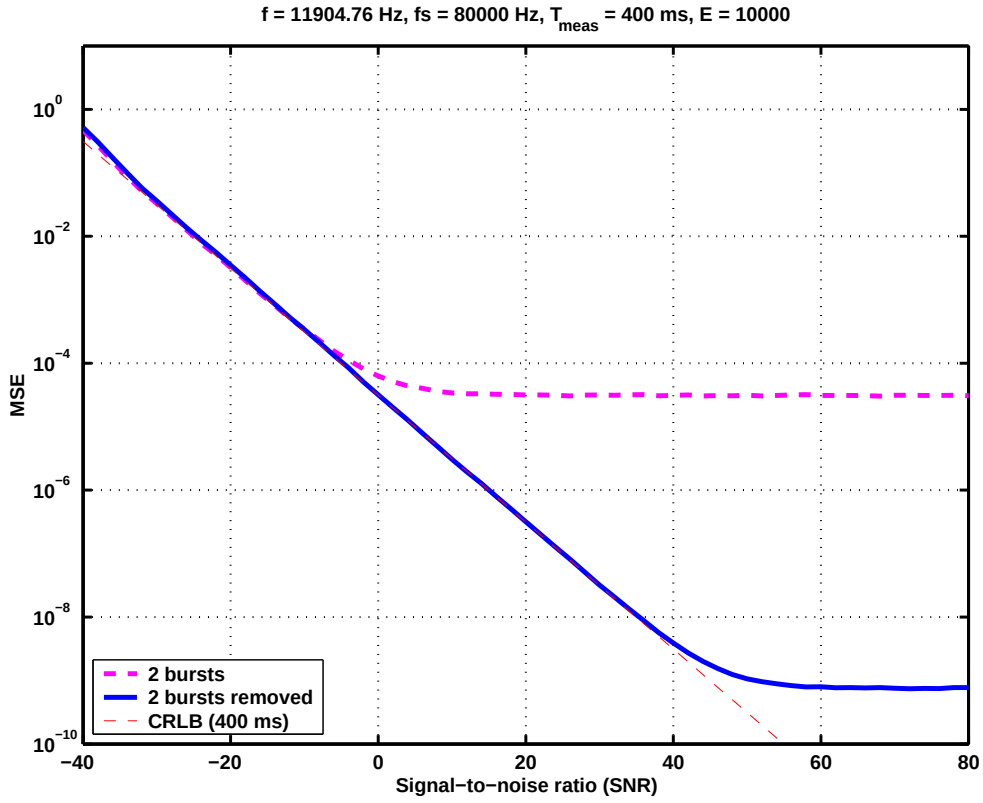

Figure 5.11: Burst noise removal decreases MSE of PCC phase estimate

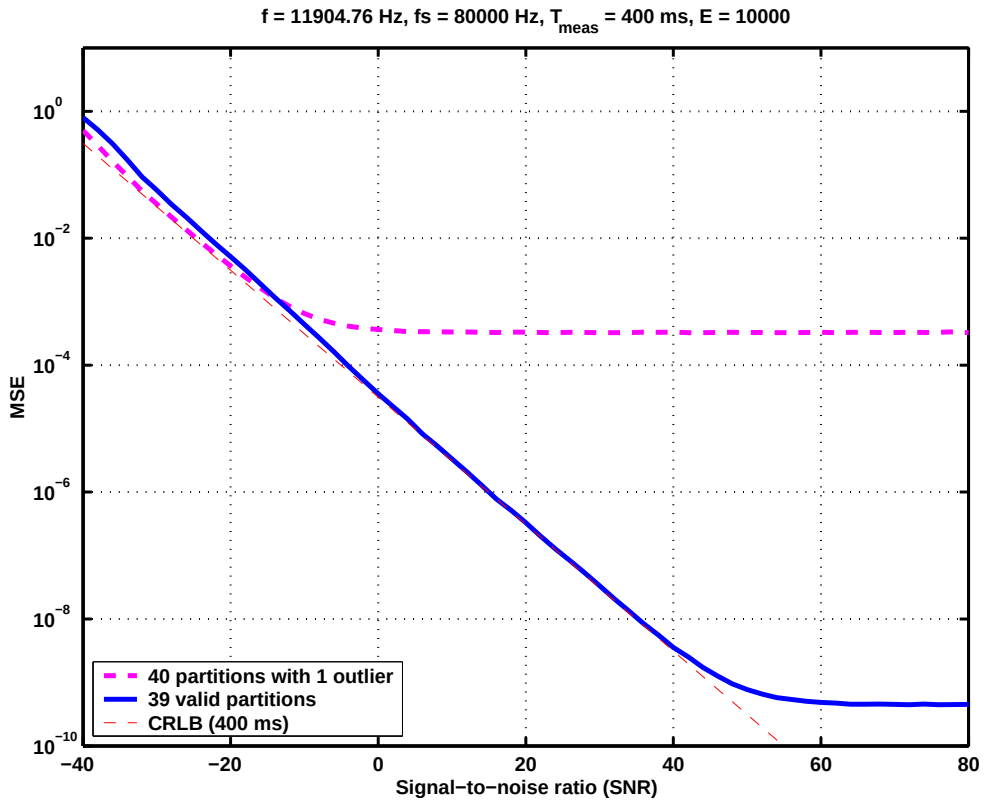

Figure 5.12: Partition outlier removal decreases MSE of PCC phase estimate

studied by comparing its MSE (5.33) with the CRLB (5.37). As two consecutive N-sample phase estimates are used to obtain one $2N$-sample frequency estimate, CRLB is calculated for $2N$ samples, accordingly. Two different cases are considered: first, MSE vs. signal-to-noise ratio (SNR) for fixed $2N$; and second, MSE vs. $2N$ for fixed SNR, where $2N$ is the number of samples in the frequency measurement interval.

Simulation parameters

An ensemble of $E = 10000$ N-sample signal vector pairs and phase estimate pairs are generated for each x-axis value. One phase estimate pair is used to obtain one $2N$-sample frequency estimate. MSE of the estimator is calculated for each ensemble. CRLB is calculated for $2N$ samples, the number of samples used to calculate the frequency estimate. The unknown phase θ for each signal vector pair in the ensemble takes values from $-\pi$ to π in E steps. Otherwise the simulation parameters are the same as for phase estimates in Section 5.8.

MSE of frequency estimate vs. SNR for fixed $2N$

Figure 5.13 shows MSE of the PCC frequency estimate versus SNR. Measurement interval of the $2N$-sample frequency estimate is either 2x400 ms or 2x1000 ms according to the Alpha and Omega navigation signals, which corresponds to 64000 or 160000 samples, respectively. MSE is close to the CRLB (5.37) up to about +40 dB SNR.

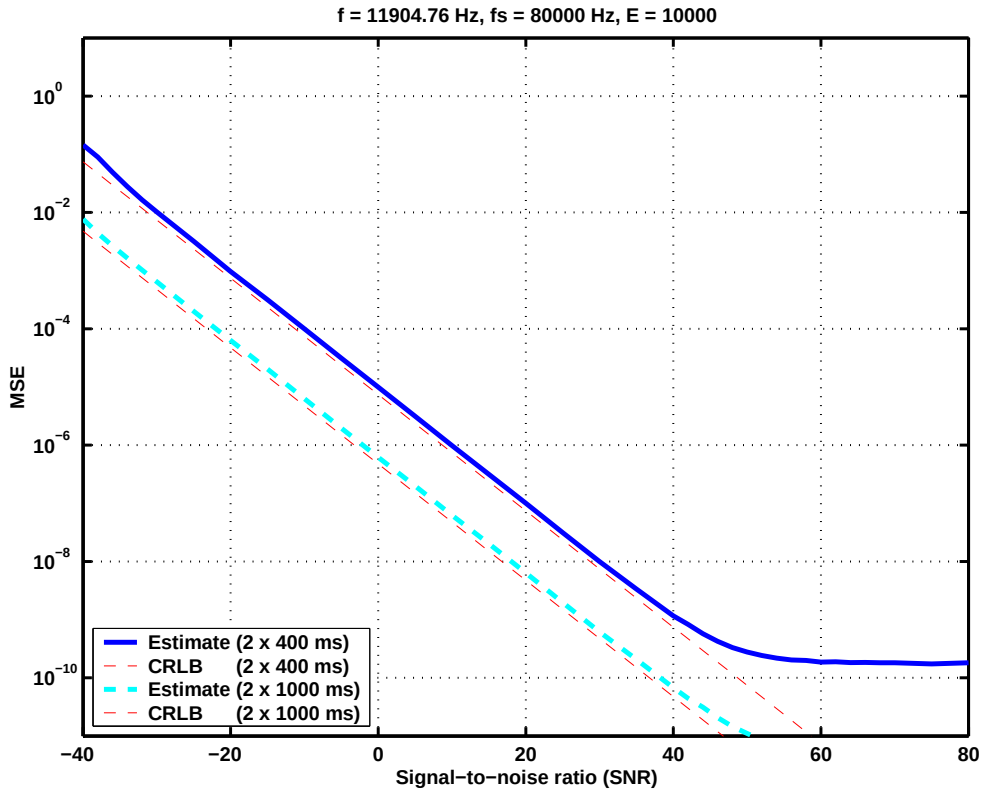

Figure 5.13: MSE of PCC frequency estimate vs. SNR

MSE of frequency estimate vs. $2N$ for fixed SNR

Figure 5.14 shows MSE of the PCC frequency estimate versus $2N$, the number of samples used to calculate the frequency estimate. Three fixed signal-to-noise ratios are shown: -20 dB, +10 dB, and +40 dB, representing low, medium, and high SNR, respectively. MSE of the frequency estimate is close to the CRLB (5.37) when the number of samples in the frequency measurement interval is according to the estimation problem ($2N \geq 64000$).

5.10 Comparison of PCC with Interpolated DFT

Estimation problem presented in Section 5.3 and properties of existing methods discussed in Chapter 4 led to the selection of Interpolated DFT (IDFT) as a prospective alternative method for the navigation receiver. Performance of PCC frequency estimate and IDFT frequency estimate is studied by comparing their MSE (5.33) with the CRLB (5.37).

Simulation parameters

An ensemble of $E = 10000$ frequency estimates is generated for each x-axis value. MSE of the estimator is calculated for each ensemble. PCC frequency estimate is obtained as described in Section 4.2 by using two consecutive 400 ms measurement intervals. IDFT frequency estimate is calculated by taking the average of two 400 ms frequency estimates, as permitted by the Alpha navigation signals. CRLB

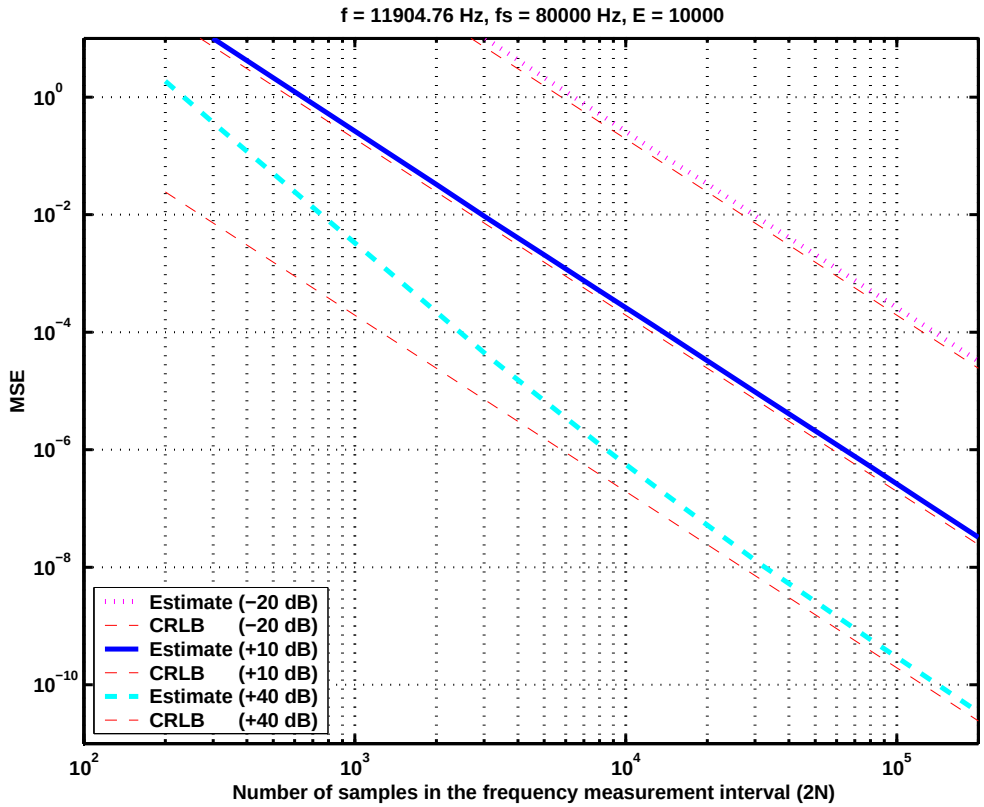

Figure 5.14: MSE of PCC frequency estimate vs. 2N

is calculated for $2N$ samples, according to the 2x400 ms measurement interval used for calculating the frequency estimates. The unknown phase θ for each signal vector pair in the ensemble takes values from $-\pi$ to π in E steps. Otherwise the simulation parameters are the same as for phase estimates in Section 5.8. IDFT algorithm is from [6] and it interpolates the frequency estimate using two adjacent DFT bins.

MSE of frequency estimate vs. SNR

Figure 5.15 shows MSE of PCC and IDFT frequency estimates versus SNR. MSE of the PCC frequency estimate is closer to the CRLB (5.37) as MSE of the IDFT frequency estimate, i.e. PCC has better performance in this application.

Computational burden

Computational burden of IDFT is approximately double compared to the PCC as IDFT requires two correlations (adjacent DFT bins) for one frequency estimate, while PCC manages with one correlation.

5.11 Implementation

Apart from white Gaussian noise, a VLF band navigation receiver is affected by several types of disturbances as discussed in Section 3.5. In the presence of dis-

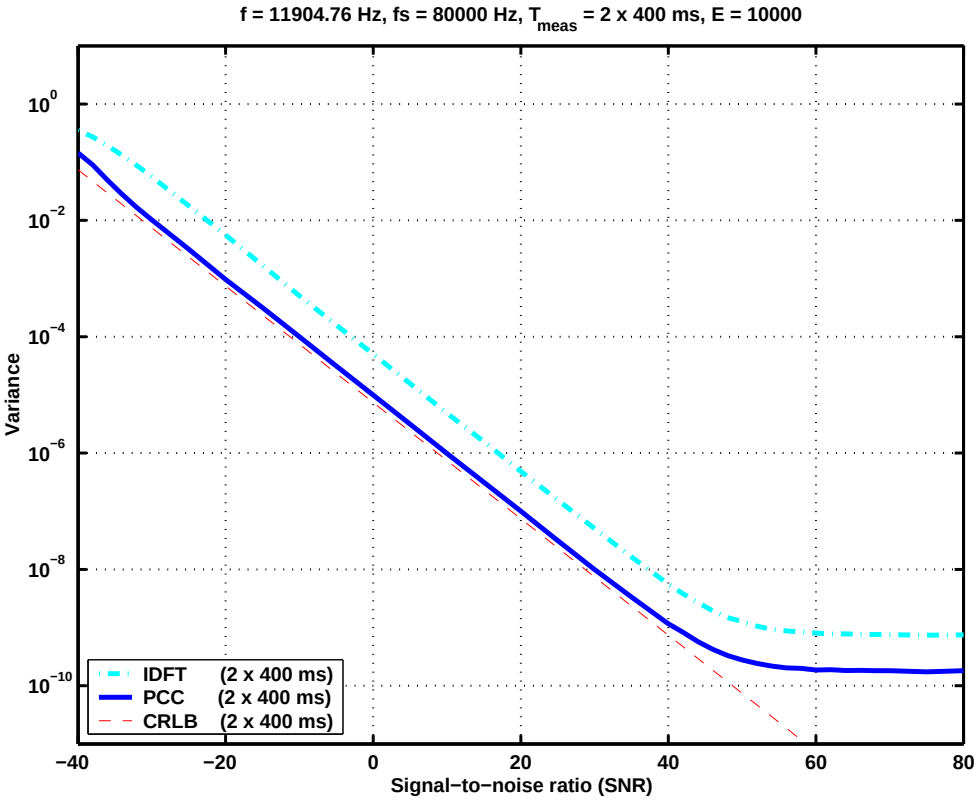

Figure 5.15: MSE of PCC and IDFT frequency estimates vs. SNR

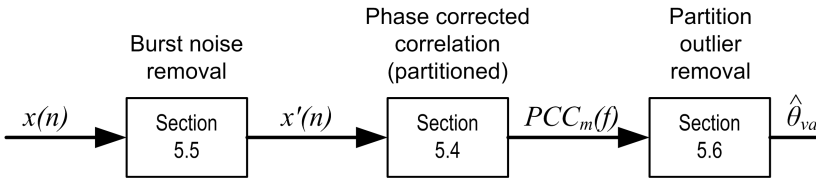

Figure 5.16: Correct processing order for the three algorithms

turbances such as lightnings and interfering transmitters, the proposed burst noise removal and partition outlier removal algorithms improve the phase estimate by decreasing its MSE. Figure 5.16 shows the correct processing order for the three algorithms: remove high energy burst noise from the input signal $x(n)$, calculate a partitioned phase corrected correlation $PCC_m(f)$, and eliminate the effect of short duration phase fluctuations by partition outlier removal. Phase estimate $\hat{\theta}_{valid}(f)$ for the measurement interval is calculated from the remaining valid partitions.

Correlation bandwidth

Phase corrected correlation (PCC) in Equation (5.15) has a characteristic bandwidth that is analogous to the DFT bin width. The correlation can be thought of as a bandpass filter, which is located at the correlation reference frequency [111, pp. 88–91]. As measurement interval becomes longer, the need for a narrow band

prefilter disappears.

$$Bandwidth = \frac{f_s}{N} = \frac{1}{T_{meas}} \tag{5.40}$$

Alpha and Omega radionavigation signals allow correlation lengths of 400 ms and 1000 ms, corresponding to 2.5 Hz and 1.0 Hz receiver bandwidth, respectively! Thus, in this case an additional prefilter only increases computational load with no improvement in performance.

Correlation reference

On-the-fly calculation of correlation reference (5.10) causes additional processing load. When the frequencies of interest are known, it is much faster to access precalculated tables from the processor memory. In a practical implementation the complex exponential is separated into real and imaginary parts and subsequent calculations are done with real numbers.

$$x_R(n) = \mathrm{Re}\{R(f)\} = \cos(2\pi n f/f_s) \tag{5.41}$$
$$y_R(n) = \mathrm{Im}\{R(f)\} = -\sin(2\pi n f/f_s) \tag{5.42}$$

Phase corrected correlation

The real and imaginary parts of the *correlation at signal frequency* (5.11) for the mth measurement interval are

$$x_C = \mathrm{Re}\{C(f,m)\} = \sum_{n=0}^{N-1} x(mN+n)\cdot x_R(n) \tag{5.43}$$

$$y_C = \mathrm{Im}\{C(f,m)\} = \sum_{n=0}^{N-1} x(mN+n)\cdot y_R(n) \tag{5.44}$$

and the real and imaginary parts of the *phase correction term* (5.14) are

$$x_{PC} = \mathrm{Re}\{PC(m)\} = \cos(\phi(m) \bmod (2\pi)) \tag{5.45}$$
$$y_{PC} = \mathrm{Im}\{PC(m)\} = -\sin(\phi(m) \bmod (2\pi)) \tag{5.46}$$

Using these components the phase corrected correlation (5.15) can be expressed as

$$\begin{aligned} PCC_m(f) = {} & (x_{PC}x_C - y_{PC}y_C) + \\ & j(x_{PC}y_C + y_{PC}x_C) \end{aligned} \tag{5.47}$$

A MATLAB example of PCC implementation is given in Appendix A.1.

Phase correction term

Phase correction term (5.14) is a complex exponential. Processing load can be decreased if the phase correction term can be *calculated in advance* and stored in processor memory for later retrieval. A prerequisite for tabulating the values is, that the signal frequency is known and that there exists a finite length repeating sequence of phase correction terms.

A *repeating sequence of phase correction terms* exists if there is an index m for which

$$\phi(m) = 0, \qquad when \quad m > 0 \tag{5.48}$$

Notice, that $\phi(0) = 0$. The condition (5.48) may not be fulfilled due to numerical inaccuracy, even though a repeating sequence exists. The solution is to check the periodicity condition in the vicinity of zero against a small positive number ϵ.

$$\phi(m) < \epsilon \tag{5.49}$$

$$2\pi - \phi(m) < \epsilon \tag{5.50}$$

If either one of the *search rules* (5.49) or (5.50) is satisfied for some index $m > 0$, then a repeating sequence of $M = m$ phase correction terms is found. When *sequence length* M fits in available processor memory, correction term real (5.45) and imaginary (5.46) parts can be tabulated for $m = 0, 1, \ldots, M-1$. The selection of ϵ depends on the numerical precision used. $\epsilon = 10^{-6} \ldots 10^{-9}$ works fine with MATLAB, which uses double precision 64-bit floating point format. A MATLAB example of phase correction term search is given in Appendix A.5.

Partitioned correlation

Although the use of a tabulated correlation reference speeds up processing, the memory size required for a long correlation may be prohibitively large and peak computational load too high. This is especially true for the navigation receiver [1], which must compute continuously 50 parallel phase estimates with correlation lengths of 400 ms and 1000 ms. Partitioning (5.20)

$$PCC_{partitioned}(f) = \sum_{m=0}^{L-1} PCC_m(f)$$

of the phase corrected correlation *reduces memory and peak computational requirements* to a fraction from the original. The correlation reference is the same for each of the L partitions and thus, only length N' cosine and sine tables need to be used. A MATLAB example of partitioned PCC is given in Appendix A.3.

In the special case when there is an integer number of cycles in N and also in $N' = N/L$, the *partitioned correlation* can be expressed as

$$\begin{aligned} X(f_k) &= \sum_{n=0}^{N-1} x(n) \cdot e^{-j2\pi n f_k/f_s} \\ &= \sum_{l=0}^{L-1} \sum_{n=l\frac{N}{L}}^{(l+1)\frac{N}{L}-1} x(n) \cdot e^{-j2\pi\left(n \bmod \frac{N}{L}\right) f_k/f_s} \end{aligned} \tag{5.51}$$

A MATLAB example of partitioned correlation is given in Appendix A.6.

Average deviation

Burst noise removal in Section 5.5 takes variable signal strength into account by calculating standard deviation σ of the signal. When processing load reduction is

of interest, *average deviation* can be used as an alternative estimator of the width of the data around its central value [112, pp. 610–611].

$$ADev = \frac{1}{N}\sum_{n=0}^{N-1}|x(n) - \bar{x}| \tag{5.52}$$

In a radio receiver the input signal $x(n)$ is often AC-coupled. When this is the case, mean $\bar{x}$ is about zero, which gives an opportunity for further processing load reduction.

$$ADev = \frac{1}{N}\sum_{n=0}^{N-1}|x(n)| \tag{5.53}$$

Although bursts may have an unbounded influence on the mean, this approximation works in the burst noise removal algorithm. A MATLAB example is given in Appendix A.2.

5.12 Discussion

A new method for estimating the unknown phase of a sampled sinusoid of known frequency has been introduced. It has been shown with computer simulations, that MSE of the phase estimate is close to the Cramér-Rao lower bound (CRLB). The same applies to frequency estimates obtained by observing signal phase change in consecutive measurement intervals. Interpolated DFT (IDFT) was selected as a prospective alternative method for the navigation receiver out of the numerous existing methods. Simulations show, that MSE of the PCC frequency estimate is closer to the CRLB as MSE of the IDFT frequency estimate, i.e. PCC has better performance in this application. Moreover, PCC achieves this performance with lower computational burden, making it the preferred choice for the navigation application. Furthermore, a number of implementation issues were covered, including computationally efficient digital signal processor (DSP) implementation, removal of natural and man-made interference, and discussion of the effect of sampling rate and measurement interval on estimation performance.

Chapter 6

Conclusions

Estimation of frequency, frequency offset, or phase of a sinusoid signal has applications in many electronic signal processing systems. Numerous approaches have been developed over the years with emphasis on various details depending on the application and signal model. The application domain in this thesis is a meteorological sounding system [2], which is equipped with the navigation receiver by the author [1]. The application is upper-air wind finding using Very Low Frequency (VLF) navigation systems, and the problem is to estimate a minute frequency offset caused by the Doppler effect. In this application the transmitted frequency is known. By taking advantage of the fact that the frequency offset is small, its estimate can be obtained by observing signal phase change in consecutive measurement intervals. According to the application, the viewpoint in this thesis is on estimating the frequency offset or phase of a sinusoid signal from long data records, in the presence of broad-band noise and nearby strong harmonic interference. Suitability of related methods is also considered from this point of view.

Frequencies transmitted especially by the Russian Alpha radionavigation system are challenging: it is not possible to select a fixed measurement interval that would contain an integer number of signal cycles of each and every navigation frequency. Therefore the receiver must be able handle a non-integer number of signal cycles in the measurement interval. Even today very little information has been published on the Russian Alpha radionavigation system. The description in this thesis is to the best of my knowledge the most comprehensive summary. Most references are unpublished and based on observations on the Russian navigation system. Confirmation on details has also been achieved by direct contacts with Russian authorities.

In order to simplify analysis and comparison with known methods, the selected signal model is a single unmodulated sinusoid in additive white Gaussian noise. Although the VLF-band navigation systems transmit multiple sinusoids simultaneously, justification for the simplified single-sinusoid signal model comes from correlation bandwidth, which in this application is in the order of 1 Hz. The correlation can be thought of as a narrow bandpass filter, eliminating most of the broad-band noise and harmonic interference.

The main contribution of this thesis is a new method for estimating the unknown phase of a sampled sinusoid of known frequency. The method is called *phase corrected correlation (PCC)* and it is targeted specifically for the case, when there is a non-integer number of cycles in the measurement interval. It is shown with

computer simulations, that MSE of the phase estimate is close to the Cramér-Rao lower bound (CRLB). The same applies to frequency estimates obtained by observing signal phase change in consecutive measurement intervals. Furthermore, two additional algorithms are proposed for decreasing the MSE of phase estimates in the presence of disturbances such as lightnings and interfering transmitters, they are called *burst noise removal* and *partition outlier removal*, respectively. Also here it is shown that MSE of the phase estimate decreases when interference is removed with these algorithms. Finally, to achieve a computationally efficient digital signal processor (DSP) implementation, a number of implementation issues are covered.

Applicability of related methods is limited by the estimation problem and by the navigation receiver application. Interpolated DFT (IDFT) was selected as a prospective alternative method for the navigation receiver out of the numerous related methods. Simulations show, that MSE of the PCC frequency estimate is closer to the CRLB as MSE of the IDFT frequency estimate, i.e. PCC has better performance in this application. Moreover, PCC achieves this performance with lower computational burden, making it the preferred choice for the navigation application. Although the original application is in a meteorological sounding system, the presented algorithms can be used in other applications where very accurate measurement of frequency, frequency offset or phase of individual sinusoids is needed, or error sources have similar properties with the ones presented here.

The proposed three algorithms have been used successfully in a meteorological sounding system [2] and its navigation receiver [1] since 1995. When Omega network was shut down in 1997, the improved performance of the receiver enabled wind finding using only Alpha and Communications VLF signals. Even though the coverage was not quite global, many meteorological institutes could continue operations as before. To publicize this fact, the author wrote several papers during 1995 to 1998 about potential means to continue VLF-based wind finding without Omega: [24], [25], [26], [27], [28], [29], and [30]. By upgrading the sounding systems with the navigation receiver by the author [1], the meteorological institutes obtained a few extra years of time to prepare for the unavoidable instrumentation replacement program.

At the time of finalizing this thesis in 2011, terrestrial Omega radionavigation system has been displaced by GPS satellite navigation system, terrestrial communications VLF transmitters operated by the U.S. Navy have largely been replaced by satellite-to-submarine and aircraft-to-submarine communication. Alpha is the last remaining VLF radionavigation system. As a consequence of all these changes, the use of very low frequency (VLF) navigation systems for upper-air wind finding has ended during the ten years after Omega termination in 1997.

It is shown in [14, p. 33] that for the sinusoid in white Gaussian noise problem, a phase estimator does not exist which is unbiased and attains the CRLB. As computer simulations have shown, MSE of the PCC phase estimate is close to the CRLB. One topic for further research would be to make a statistical analysis of the PCC, including finding an explanation for the behavior above +40 dB SNR. Another topic would be to develop an optimal method with probabilistic justification for determining burst detection and outlier detection thresholds. One could also consider the complex observations in partition outlier removal as a bivariate observation and find the bivariate median in order to avoid chance of artifacts.

Appendix A

Matlab examples

These examples illustrate how to use the various algorithms that are presented in Chapter 5. The examples are calculated using MATLAB and double precision (64-bit) floating-point format.

A.1 Phase corrected correlation

The following MATLAB example illustrates PCC and its DSP implementation which are discussed in Sections 5.4 and 5.11, respectively. This example produces the following output:

```
Unknown phase that is being estimated: theta     = 1.0000
Phase estimate (m = 0, 1, ..., 6)    : theta_hat =
   0.9998, 1.0000, 1.0002, 0.9999, 1.0001, 1.0002, 0.9999
Phase correction term                : phi_m     =
   0.0000, 5.6848, 5.0864, 4.4880, 3.8896, 3.2912, 2.6928
```

```
%%%%%%%%%%%%%%%%%%%%%%%%%%%%%%%%%%%%%%%%%%%%%%%%%%%%%%%%%%%%%%%%%%%%%%%
%   Description :   Phase corrected correlation (PCC)
%
%                   This example uses real numbers which
%                   is efficient in a DSP implementation.
%
%   2009-07-30 / Juhana Jaatinen
%%%%%%%%%%%%%%%%%%%%%%%%%%%%%%%%%%%%%%%%%%%%%%%%%%%%%%%%%%%%%%%%%%%%%%%
clc
clear all

%-----------------------------------------------------------------
% Parameters
%-----------------------------------------------------------------
% Unknown phase that is being estimated
theta = 1               % [rad]

% Number of PCCs to calculate
NumPcc = 7;

% Sampling rate and measurement interval
fs = 80000;             % [Hz]
N  = 0.4 * fs;          % 400 ms measurement interval
n  = 0 : N-1;

% Sinusoid signal with additive white Gaussian noise,
% non-integer number of cycles in N samples
f = 16 * (744 + 1/21);  % Alpha f1~11904.7619 Hz

SNR = 30;               % [dB]
AwgnAmplitude = sqrt(1/(2*10^(SNR/10)));


%-----------------------------------------------------------------
% Calculate PCC
%-----------------------------------------------------------------
% Correlation reference (same for all measurement intervals)
x_R =  cos(2*pi*n*f/fs);
y_R = -sin(2*pi*n*f/fs);

% Number of cycles in the measurement interval
K   = N*f/fs;

% Phase advance per measurement interval
dk  = K - floor(K);
phi = dk*2*pi;

% Phase corrected correlation
for m = 0 : NumPcc-1

    % Sinusoid signal with additive white gaussian noise
    n  = m*N : (m+1)*N-1;
    xn = cos(2*pi*f*n/fs + theta) + AwgnAmplitude*randn(size(n));

    % Phase correction term for the m-th measurement interval
    phi_m(m+1) = mod( m*phi, 2*pi);
    x_PC =  cos( phi_m(m+1));
    y_PC = -sin( phi_m(m+1));

    % Correlation at signal frequency
    x_C = sum( xn .* x_R);
    y_C = sum( xn .* y_R);

    % PCC for the m-th measurement interval
    PCC_m(m+1) =   (x_PC * x_C - y_PC * y_C) +...
                 i*(x_PC * y_C + y_PC * x_C);
end

% Phase estimate
theta_hat_m = angle( PCC_m)

% Show phase correction term
phi_m

%-----------------------------------------------------------------
% Save result to file
%-----------------------------------------------------------------
fid = fopen( 'matlab_pcc.txt', 'wt');
fprintf( fid, ['Unknown phase that is being estimated: '...
    'theta     = %.4f\n'], theta);
fprintf( fid, ['Phase estimate (m = 0, 1, ..., 6)    : '...
    'theta_hat =\n']);
fprintf( fid, ['   %.4f, %.4f, %.4f, %.4f, %.4f, %.4f,'...
    ' %.4f\n'], theta_hat_m);
fprintf( fid, ['Phase correction term                : '...
    'phi_m     =\n']);
fprintf( fid, ['   %.4f, %.4f, %.4f, %.4f, %.4f, %.4f,'...
    ' %.4f\n'], phi_m);
fclose( fid);


%-----------------------------------------------------------------
% End
%-----------------------------------------------------------------
```

A.2 Burst noise removal

The following MATLAB example illustrates burst noise removal which is discussed in Section 5.5. Output of this example is shown in Figure A.1.

```
%%%%%%%%%%%%%%%%%%%%%%%%%%%%%%%%%%%%%%%%%%%%%%%%%%%%%%%%%%%%%%%%%%%%%%%
%   Description :   Burst noise removal
%
%   2002-07-25 / Juhana Jaatinen
%%%%%%%%%%%%%%%%%%%%%%%%%%%%%%%%%%%%%%%%%%%%%%%%%%%%%%%%%%%%%%%%%%%%%%%
clc
clear all

%------------------------------------------------------------
% Parameters
%------------------------------------------------------------
s_burst = 3.6;
r_burst = 7;


%------------------------------------------------------------
% 1) Get input sample buffer
%------------------------------------------------------------
% Generate a zero mean signal
xn = randn(1,400);

% Add two burst errors
xn(2:7)     = 9 * xn(2:7);
xn(151:161) = 9 * xn(151:161);


%------------------------------------------------------------
% 2) Calculate adaptive burst detection threshold
%------------------------------------------------------------
N = length(xn);
ADev = 1/N * sum( abs( xn));

D_burst = s_burst * ADev;


%------------------------------------------------------------
% 3) Search bursts
%------------------------------------------------------------
BurstIndex = find( abs( xn) > D_burst);
```

```
%------------------------------------------------------------
% 4) Replace bursts with zeros
%------------------------------------------------------------
yn = xn;
for n = 1 : length( BurstIndex)
    % Zeroing range
    First = BurstIndex(n) - r_burst;
    if (First < 1), First = 1; end

    Last = BurstIndex(n) + r_burst;
    if (Last > N), Last = N; end

    % Replace burst with zeros
    yn( First:Last) = zeros(1, Last-First+1);
end


%------------------------------------------------------------
% Figure
%------------------------------------------------------------
figure

subplot(2,1,1)
plot(xn)
a=axis;
title('Signal with two bursts')

subplot(2,1,2)
plot(yn)
axis(a)
title('Bursts removed')

% Encapsulated Level 2 Color PostScript
print -depsc2 Fig_MatlabBurst.eps


%------------------------------------------------------------
% End
%------------------------------------------------------------
```

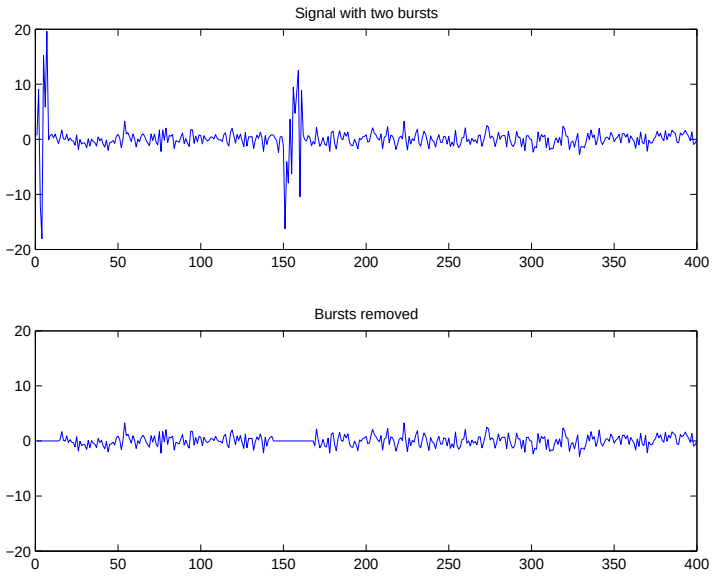

Figure A.1: Burst removal example

A.3 Partitioned phase corrected correlation

The following MATLAB example illustrates PCC partitioning which is discussed in Section 5.6. This example produces the following output:

```
Unknown phase that is being estimated: theta     = 1.0000
Phase estimate                       : theta_hat = 1.0000
```

```
%%%%%%%%%%%%%%%%%%%%%%%%%%%%%%%%%%%%%%%%%%%%%%%%%%%%%%%%%%%%%%%%%%%%%%%
%   Description :   Partitioned PCC
%
%                   This example uses complex numbers which
%                   is efficient in a Matlab implementation.
%
%   2009-07-30 / Juhana Jaatinen
%%%%%%%%%%%%%%%%%%%%%%%%%%%%%%%%%%%%%%%%%%%%%%%%%%%%%%%%%%%%%%%%%%%%%%%
clc
clear all

%-------------------------------------------------------------
% Parameters
%-------------------------------------------------------------
% Unknown phase that is being estimated
theta = 1               % [rad]

% Sampling rate and measurement interval
fs = 80000;             % [Hz]
N  = 0.4 * fs;          % 400 ms measurement interval
n  = 0 : N-1;

% Sinusoid signal with additive white Gaussian noise,
% non-integer number of cycles in N samples
f = 16 * (744 + 1/21);  % Alpha f1~11904.7619 Hz

SNR = 30;               % [dB]
AwgnAmplitude = sqrt(1/(2*10^(SNR/10)));
xn = cos(2*pi*f*n/fs + theta) + AwgnAmplitude*randn(size(n));

% Number of PCC partitions
L  = 10;
Np = N/L;
np = 0 : Np-1;


%-------------------------------------------------------------
% Calculate partitioned PCC
%-------------------------------------------------------------
% Correlation reference (same for all measurement intervals)
R = exp(-j*2*pi*np*f/fs);

% Number of cycles in the partition
K   = Np*f/fs;

% Phase advance per partition
dk  = K - floor(K);
phi = dk*2*pi;

% Partitioned PCC
for m = 0 : L-1

    % Phase correction term for the m-th partition
    phi_m = mod( m*phi, 2*pi);
    PC_m  = exp( -j*phi_m);

    % NOTICE: x' is the complex conjugate (Hermitian) transpose
    % of x and x.' is the non-conjugate transpose of x. The latter
    % has to be used with complex vectors when simplifying the
    % PCC sum, i.e. X = sum( xn .* exp(-j*w)) is equivalent
    % to            X = xn * exp(-j*w).'

    % Correlation at signal frequency
    np = m*Np+1:(m+1)*Np;
    C  = xn( np) * R.';

    % PCC for the m-th partition
    PCC_m(m+1) = PC_m * C;
end

% Partitioned PCC
PCC = sum( PCC_m);

% Phase estimate
theta_hat = angle( PCC)
```

```
%-------------------------------------------------------------
% Save result to file
%-------------------------------------------------------------
fid = fopen( 'matlab_ppcc.txt', 'wt');
fprintf( fid, ['Unknown phase that is being estimated: '...
    'theta     = %.4f\n'], theta);
fprintf( fid, ['Phase estimate                       : '...
    'theta_hat = %.4f\n'], theta_hat);
fclose( fid);


%-------------------------------------------------------------
% End
%-------------------------------------------------------------
```

A.4 Partition outlier removal

The following MATLAB example illustrates partition outlier removal which is discussed in Section 5.6. This example produces the following output:

```
Unknown phase that is being estimated: theta              = 1.0000
Phase estimate (all partitions)      : theta_hat_all      = 1.5814
Phase estimate (valid partitions)    : theta_hat_valid    = 1.0000
Number of outliers found             : 1
Valid partitions                     : 1, 2, 4, 5, 6, 7, 8, 9, 10
```

```
%%%%%%%%%%%%%%%%%%%%%%%%%%%%%%%%%%%%%%%%%%%%%%%%%%%%%%%%%%%%%%%%%%%%%%%%
%   Description :   Partition outlier removal
%
%                   This example uses complex numbers which
%                   is efficient in a Matlab implementation.
%
%   2009-08-03 / Juhana Jaatinen
%%%%%%%%%%%%%%%%%%%%%%%%%%%%%%%%%%%%%%%%%%%%%%%%%%%%%%%%%%%%%%%%%%%%%%%%
clc
clear all

%-------------------------------------------------------------
% Parameters
%-------------------------------------------------------------
s_cluster = 1.6;

% Unknown phase that is being estimated
theta = 1               % [rad]

% Sampling rate and measurement interval
fs = 80000;             % [Hz]
N  = 0.4 * fs;          % 400 ms measurement interval
n  = 0 : N-1;

% Sinusoid signal with additive white Gaussian noise,
% non-integer number of cycles in N samples
f = 16 * (744 + 1/21);  % Alpha f1~11904.7619 Hz

SNR = 30;               % [dB]
AwgnAmplitude = sqrt(1/(2*10^(SNR/10)));
xn = cos(2*pi*f*n/fs + theta) + AwgnAmplitude*randn(size(n));

% Number of PCC partitions
L  = 10;
Np = N/L;
np = 0 : Np-1;


%-------------------------------------------------------------
% 1) Calculate partitioned correlation
%-------------------------------------------------------------
% Correlation reference (same for all measurement intervals)
R = exp(-j*2*pi*np*f/fs);

% Number of cycles in the partition
K   = Np*f/fs;

% Phase advance per partition
dk  = K - floor(K);
phi = dk*2*pi;

% Partitioned correlation
for m = 0 : L-1

    % Phase correction term for the m-th partition
    phi_m = mod( m*phi, 2*pi);
    PC_m  = exp( -j*phi_m);

    % NOTICE: x' is the complex conjugate (Hermitian) transpose
    % of x and x.' is the non-conjugate transpose of x. The latter
    % has to be used with complex vectors when simplifying the
    % PCC sum, i.e. X = sum( xn .* exp(-j*w)) is equivalent
    % to            X = xn * exp(-j*w).'

    % Correlation at signal frequency
    np = m*Np+1:(m+1)*Np;
    C  = xn( np) * R.';

    % PCC for the m-th partition
    PCC_m(m+1) = PC_m * C;
end

% Make one big outlier
% --------------------
PCC_m(3) = 5*exp(j*2*theta)*PCC_m(3);

% Partitioned PCC
PCC_partitioned = sum( PCC_m);

% Phase estimate from all partitions
theta_hat_all = angle( PCC_partitioned)


%-------------------------------------------------------------
% 2) Find center of the partition cluster
%-------------------------------------------------------------
x_med = median( real( PCC_m));
y_med = median( imag( PCC_m));


%-------------------------------------------------------------
% 3) Calculate signal dependent outlier detection threshold
%-------------------------------------------------------------
% Average deviation
ADev_x = 1/L * sum( abs( real( PCC_m) - x_med));
ADev_y = 1/L * sum( abs( imag( PCC_m) - y_med));

% Outlier detection threshold
D_cluster = s_cluster * sqrt( ADev_x^2 + ADev_y^2);


%-------------------------------------------------------------
% 4) Discard outliers
%-------------------------------------------------------------
% Distance of partition from the center of the cluster
r_m = sqrt(( real( PCC_m)-x_med).^2 + (imag( PCC_m)-y_med).^2);

% Select valid partitions
Lambda = find( r_m <= D_cluster);


%-------------------------------------------------------------
% 5) Construct phase estimate from the valid partitions
%-------------------------------------------------------------
PCC_valid = sum( PCC_m( Lambda));

% Phase estimate from valid partitions
theta_hat_valid = angle( PCC_valid)


%-------------------------------------------------------------
% Save result to file
%-------------------------------------------------------------
fid = fopen( 'matlab_por.txt', 'wt');
fprintf( fid, ['Unknown phase that is being estimated: '...
    'theta              = %.4f\n'], theta);
fprintf( fid, ['Phase estimate (all partitions)      : '...
    'theta_hat_all      = %.4f\n'], theta_hat_all);
fprintf( fid, ['Phase estimate (valid partitions)    : '...
    'theta_hat_valid    = %.4f\n'], theta_hat_valid);
fprintf( fid, ['Number of outliers found             : '...
    '%d\n'], L - length(Lambda));
fprintf( fid, ['Valid partitions                     : '...
    '%d, %d, %d, %d, %d, %d, %d, %d, %d\n'], Lambda);
fclose( fid);


%-------------------------------------------------------------
% End
%-------------------------------------------------------------
```

A.5 Phase correction term search

The following MATLAB example illustrates correction term search which is discussed in Section 5.11. Search rules (5.49) and (5.50) are used to stop the search. This example produces the following output:

```
f1 ~ 11904.7619 Hz,         phi_M = 6.3e-011,   M =  21
f2 ~ 12648.8095 Hz,   2*pi-phi_M = 4.6e-011,   M =  21
f3 ~ 14880.9524 Hz,         phi_M = 1.1e-010,   M =  21
f4 ~ 12090.7738 Hz,         phi_M = 1.1e-011,   M =  42
f5 ~ 12044.2708 Hz,         phi_M = 9.1e-011,   M =  24
f6 ~ 14881.0913 Hz,         phi_M = 1.1e-011,   M = 126
```

These frequencies are transmitted by the Alpha radionavigation system, which is described in Section 3.2. Each one of these frequencies has a non-integer number of cycles in the 400 ms measurement interval.

```
%%%%%%%%%%%%%%%%%%%%%%%%%%%%%%%%%%%%%%%%%%%%%%%%%%%%%%%%%%%%%%%%%%%%%%%%
%   Description :   Correction term search
%
%   2002-07-27 / Juhana Jaatinen
%%%%%%%%%%%%%%%%%%%%%%%%%%%%%%%%%%%%%%%%%%%%%%%%%%%%%%%%%%%%%%%%%%%%%%%%
clc
clear all

%-----------------------------------------------------------------
% Parameters
%-----------------------------------------------------------------
% Alpha frequencies
f0 = 744 + 1/21;        % [Hz]

f1  = 16 * f0;
f2  = 17 * f0;
f3  = 20 * f0;
f4  = 260/16 * f0;
f5  = 259/16 * f0;
f6  = f3 + 5/36;        % Actually called f3P

f = [f1 f2 f3 f4 f5 f6];
NumFreq = length( f);

% Sampling rate and measurement interval
fs = 80000;             % [Hz]
N  = 0.4 * fs;          % 400 ms measurement interval

% Small positive number
epsilon = 1e-9;

% Search limit
MaxM = 10000;

% Save result to file
fid = fopen( 'matlab_cts.txt', 'wt');


%-----------------------------------------------------------------
% Correction term search
%-----------------------------------------------------------------

for n = 1 : NumFreq;

    % Number of cycles in the measurement interval
    K   = N*f(n)/fs;

    % Phase advance per measurement interval
    dk  = K - floor(K);
    phi = dk*2*pi;

    % Search for a repeating sequence of phase correction terms
    % ---------------------------------------------------------
    % Start search from m = 1. Notice, that phi_0 = 0.
    for m = 1 : MaxM

        % Phase correction term for the m-th measurement interval
        phi_m = mod( m*phi, 2*pi);

        % Search rule 1
        % -------------
        if (phi_m < epsilon)

            % Repeating sequence found
            M = m;
            s = sprintf( ['f%d ~ %.4f Hz, '...
                '       phi_M = %.1e,   M = %3d'], ...
                n, f(n), phi_m, M);
            fprintf( fid, '%s\n', s); disp(s)

            % Stop search
            break;
        end

        % Search rule 2
        % -------------
        if (2*pi - phi_m < epsilon)

            % Repeating sequence found
            M = m;
            s = sprintf( ['f%d ~ %.4f Hz, '...
                '  2*pi-phi_M = %.1e,   M = %3d'], ...
                n, f(n), 2*pi-phi_m, M);
            fprintf( fid, '%s\n', s); disp(s)

            % Stop search
            break;
        end
    end % m
end % n

% Close result file
fclose( fid);


%-----------------------------------------------------------------
% End
%-----------------------------------------------------------------
```

A.6 Partitioned correlation

The following MATLAB example illustrates partitioning of the correlation in the special case when there is an integer number of cycles in $N' = N/L$ samples, see Section 5.11. This example produces the following output:

```
Unknown phase that is being estimated: theta     = 1.0000
Phase estimate                       : theta_hat = 1.0000
```

```
%%%%%%%%%%%%%%%%%%%%%%%%%%%%%%%%%%%%%%%%%%%%%%%%%%%%%%%%%%%%%%%%%%%%%%%
%   Description :   Partitioned correlation (DFT)
%
%                   This is a special case when there is an
%                   integer number of cycles in the
%                   measurement interval.
%
%   2002-07-26 / Juhana Jaatinen
%%%%%%%%%%%%%%%%%%%%%%%%%%%%%%%%%%%%%%%%%%%%%%%%%%%%%%%%%%%%%%%%%%%%%%%
clc
clear all

%-------------------------------------------------------------
% Parameters
%-------------------------------------------------------------
% Unknown phase that is being estimated
theta = 1               % [rad]

% Sampling rate and measurement interval
fs = 80000;             % [Hz]
N  = 1.0 * fs;          % 1000 ms measurement interval
n  = 0 : N-1;

% Sinusoid signal with additive white Gaussian noise,
% integer number of cycles in N samples
f = 13600;              % Omega 13.6 kHz

SNR = 30;               % [dB]
AwgnAmplitude = sqrt(1/(2*10^(SNR/10)));
xn = cos(2*pi*f*n/fs + theta) + AwgnAmplitude*randn(size(n));

% Number of DFT partitions
L  = 10;
Np = N/L;
np = 0 : Np-1;


%-------------------------------------------------------------
% Calculate partitioned DFT
%-------------------------------------------------------------
% Correlation reference
R = exp(-j*2*pi*np*f/fs);

% Partitioned correlation
for l = 0 : L-1

    % NOTICE: x' is the complex conjugate (Hermitian) transpose
    % of x and x.' is the non-conjugate transpose of x. The latter
    % has to be used with complex vectors when simplifying the
    % DFT sum, i.e. X = sum( x( n) .* exp(-j*a)) is equivalent
    % to X = x( n) * exp(-j*a).'

    % DFT partition
    np = l*Np:(l+1)*Np-1;
    X_l(l+1) = xn( np+1) * R.';
end

% Partitioned DFT
X = sum( X_l);

% Phase estimate
theta_hat = angle( X)


%-------------------------------------------------------------
% Save result to file
%-------------------------------------------------------------
fid = fopen( 'matlab_pcorr.txt', 'wt');
fprintf( fid, ['Unknown phase that is being estimated: '...
    'theta     = %.4f\n'], theta);
fprintf( fid, ['Phase estimate                       : '...
    'theta_hat = %.4f\n'], theta_hat);
fclose( fid);
```

```
%-------------------------------------------------------------
% End
%-------------------------------------------------------------
```

Bibliography

[1] Vaisala Oy, Helsinki, Finland. *VLF-Navaid Processor MWV201*, May 1997. Brochure, Ref. B334en 1997-05.

[2] Vaisala Oy, Helsinki, Finland. *MW15 DigiCORA II Rawinsonde Set*, February 1995. Brochure, Ref. A547en 1995-02.

[3] Jussi Åkerberg. Automatic VLF observing station. Master's thesis, Helsinki University of Technology, Espoo, Finland, February 1997.

[4] Erkka Pälä. Estimation of upper air windfinding accuracy. Master's thesis, Helsinki University of Technology, Espoo, Finland, November 1997.

[5] Ismo Haanaho. Frequency estimation of radiosonde signal. Master's thesis, Helsinki University of Technology, Espoo, Finland, March 2000.

[6] J. Schoukens, Rik Pintelon, and Hugo Van Hamme. The interpolated fast fourier transform: A comparative study. In *IEEE Transactions on Instrumentation and Measurement*, volume 41, pages 226–232, April 1992.

[7] Steven M. Kay, and Stanley Lawrence Marple, Jr. Spectrum analysis–A modern perspective. In *Proceedings of the IEEE*, volume 69, pages 1380–1419, November 1981.

[8] S. Lawrence Marple Jr. *Digital Signal Analysis.* CEI-Europe, Finspong, Sweden, March 1999. Lecture notes, 512 pages.

[9] Lawrence R. Rabiner, Michael J. Cheng, Aaron E. Rosenberg, and Carol A. McGonegal. A comparative performance study of several pitch detection algorithms. In *IEEE Transactions on Acoustics, Speech, and Signal Processing*, volume ASSP-24, pages 399–418, October 1976.

[10] A. Bruce Carlson. *Communication Systems, An Introduction to Signals and Noise in Electrical Communications.* McGraw-Hill International Editions, 3rd edition, 1986.

[11] Bernard Sklar. *Digital Communications, Fundamentals and Applications.* PTR Prentice Hall, Englewood Cliffs, NJ, 1988.

[12] Richard Roy, and Thomas Kailath. ESPRIT–estimation of signal parameters via rotational invariance techniques. In *IEEE Transactions on acoustics, speech, and signal processing*, volume 37, pages 984–995, July 1989.

[13] Jacob Benesty, Jingdong Chen, and Yiteng Huang. Time-delay estimation via linear interpolation and cross correlation. In *IEEE Transactions on Speech and Audio Processing*, volume 12, pages 509–519, September 2004.

[14] Steven M. Kay. *Fundamentals of Statistical Signal Processing, Estimation theory*. PTR Prentice Hall, Upper Saddle River, NJ, 1993.

[15] Matteo Bertocco, Carlo Offelli, and Dario Petri. Dynamic behavior of a digital phase estimator. In *IEEE Transactions on Instrumentation and Measurement*, volume 41, pages 256–261, December 1992.

[16] H. Meyr, and Gerd Ascheid. *Advanced Digital Receivers for Wireless Communications*. CEI-Europe, Finspong, Sweden, November 1996. Lecture notes, 714 pages.

[17] Pentti Karhunen. Extension of multifrequency composite NAVAID windfinding. *Reprint from Vaisala News No 124/1991*.

[18] Antti Lange. Balloon tracking using a hybrid system. Meteorological publications 37, Finnish Meteorological Institute, Helsinki, Finland, April 1999.

[19] Hannu Karttunen, Jarmo Koistinen, Elena Saltikoff, and Olli Manner. *Ilmakehä ja sää*. Tähtitieteellinen yhdistys Ursa, Helsinki, Finland, 1997. Ursan julkaisuja 62.

[20] Vaisala Oy, Helsinki, Finland. *DigiCORA Rawinsonde Set MW11*, 1991. Brochure, Ref. A0459-1.

[21] U.S. Department of Transportation/U.S. Department of Defense. *1994 Federal Radionagivation Plan*, May 1995. DOT-VNTSC-RSPA-95-1/DOD-4650.5.

[22] U.S. Department of Transportation. Dot summary, 1996 radionavigation conferences. *https://navcen.uscg.gov/ftp/GPS/archives/gpsdoc/frp1994/summ.pdf*.

[23] Vaisala Oy, Helsinki, Finland. *CORA, The Vaisala Upper-Air Wind Finding System*, 1976. Brochure, Ref. No. A 270.

[24] Juhana Jaatinen. Potential means to continue VLF-based wind finding without Omega. In *Extended abstracts, WMO International Conference METEOHYTEC 21*, pages 153–156, Geneva, May 1995. World Meteorological Organization.

[25] Juhana Jaatinen. Potential means to continue VLF-based wind finding without Omega. In *Proc. The First International Radionavigation Conference on Planning for Global Radionavigation*, pages 234–237, Moscow, June 1995. Internavigation RTC.

[26] Juhana Jaatinen. VLF-based wind finding without Omega. In *Preprints, 76th AMS Annual Meeting, 12th International Conference on Interactive Information and Processing Systems (IIPS) for Meteorology, Oceanography, and Hydrology*, pages 113–117. American Meteorological Society, February 1996.

[27] Juhana Jaatinen. VLF and Loran-C based wind finding. In *Proc. 21st annual meeting*, pages 233–238. International Navigation Association (INA), August 1996.

[28] Juhana Jaatinen and Timo Saarnimo. Reliable windfinding after Omega Phase-out. In *Preprints, 77th AMS Annual Meeting, 13th International Conference on Interactive Information and Processing Systems (IIPS) for Meteorology, Oceanography, and Hydrology*, pages 448–454. American Meteorological Society, February 1997.

[29] Juhana Jaatinen and Timo Saarnimo. Reliable windfinding after Omega Phase-out. In *Proc. The Second International Radionavigation Conference on Planning for Global Radionavigation*, pages 366–372, Moscow, June 1997. Internavigation RTC.

[30] Juhana Jaatinen and Erkka Pälä. On the windfinding accuracy of terrestrial navaids. In *Preprints, 78th AMS Annual Meeting, 10th Symposium on Meteorological Observations and Instrumentation*, pages 45–50. American Meteorological Society, January 1998.

[31] Juhani Rinne, Jarmo Koistinen, and Elena Saltikoff. *Suomalainen sääkirja – etanasta El Niñoon.* Otava, Helsinki, Finland, 1998.

[32] Richard A. Anthes. *Meteorology.* Prentice Hall, Englewood Cliffs, NJ, 6th edition, 1992.

[33] Roland B. Stull. *Meteorology for Scientists and Engineers.* Brooks/Cole, 2nd edition, 2000.

[34] Ilmatieteen laitos, Finnish meteorological institute. *http://www.fmi.fi.*

[35] European Centre for Medium-Range Weather Forecasts. *http://www.ecmwf.int.*

[36] World Meteorological Organization. *http://www.wmo.ch.*

[37] Ismo Lindell. *Radioaaltojen eteneminen.* Otatieto Oy, Helsinki, Finland, 5th edition, 1985.

[38] United States Coast Guard, Washington, DC. *Omega Navigation System User's Guide*, 1990.

[39] Juhana Jaatinen and Sakari Kajosaari. Loran-C based windfinding in meteorology. In *Preprints, 29th Annual Convention & Technical Symposium.* International Loran-C Association (ILA), November 2000.

[40] Vaisala Oyj. *http://www.vaisala.com.*

[41] World Meteorological Organization. *Guide to Meteorological Instruments and Methods of Observation*, chapter 12 and 13. WMO-No. 8. World Meteorological Organization, Geneva, 6th edition, 1996.

[42] Vaisala Oy, Helsinki, Finland. *Vaisala RS80 Radiosondes*, 1998. Brochure, Ref. A571en 1998-04.

[43] Vaisala Oy, Helsinki, Finland. *Vaisala RS80 Radiosondes, General information on RS series*, 1992. Brochure, Ref. A0435 9-92.

[44] Vaisala Oy, Helsinki, Finland. *MWV201 VLF-Navaid Processor*, December 1997. Brochure, Ref. B334en 1997-12.

[45] Juhana Jaatinen and Jussi Åkerberg. Automatic Loran-C chain selection. In *Preprints, 79th AMS Annual Meeting, 15th International Conference on Interactive Information and Processing Systems (IIPS) for Meteorology, Oceanography, and Hydrology*, pages 267–270. American Meteorological Society, January 1999.

[46] Juhana Jaatinen and John B. Elms. On the windfinding accuracy of Loran-C, GPS and radar. In *Preprints, 80th AMS Annual Meeting, 16th International Conference on Interactive Information and Processing Systems (IIPS) for Meteorology, Oceanography, and Hydrology*, pages 406–409. American Meteorological Society, January 2000.

[47] John B. Elms, John Nash and J. Stancombe. *Second evaluation of Vaisala GPS radiosonde system, Camborne.* UK Meteorological Office, Bracknell, Berks, 1996.

[48] John Nash. Upper wind observing systems used for meteorological operations. In *Annales Geophysicae 12*, pages 691–710, 1994.

[49] Vaisala Oy, Helsinki, Finland. *CORA General description*, November 1975. Technical note, 750918PK, COPG 003.

[50] Vaisala Oy, Helsinki, Finland. *Marwin MW12, DigiCORA MW11*, April 1988. User's Guide, MW-T0534-1.1.

[51] Pentti Karhunen. Visiting Central Aerological Observatory and Committee Internavigation, Moscow. Travel report (Pentti Karhunen, Tapio Iivonen, Juhana Jaatinen), Vaisala Oy, Answers by Mr. Yuri M. Nikulin, Head of Land RNS Department, and his colleagues., April 1995.

[52] Juhana Jaatinen. Alpha radionavigation system. UAD-314-95-003, Vaisala Oy, May 1995.

[53] Vaisala Oy, Helsinki, Finland. *DigiCORA II MW15*, February 1998. User's Guide, MW15-U110en-1.7.

[54] United States Coast Guard. Questions on the Alpha radionavigation system. Fax, cover page missing, USCG OMEGA NAV SYSCEN, Aug-25-1993.

[55] United States Coast Guard. Informal transcription of verbal translation of Russian Alpha system answers provided by Dean W. Sanders, USCGA for CAPT B. Peterson, USCGA and LCDR C. Dubay, ONSCEN on 26 August 1993.

[56] Anonymous. Radionavigation Alfa system of super long-wave range. Photocopy received in 1995.

[57] Sergei B. Boloshin, and Arkady S. Guzman. Synchronization of stations in the ALPHA RNS and features of its synchronization with the OMEGA RNS. Russian Institute of Radionavigation and Time, Photocopy received in 1992.

[58] Protocol of the Russian-United States Coordination Council Meeting. Annex 7. Russian VLF radionavigation system and some issues of its combining with 'Omega' navigation system. September 1992.

[59] Benjamin B. Peterson. The Soviet VLF Navigation System. *NAVIGATION: Journal of The Institute of Navigation*, 38(3):247–261, 1991.

[60] Juhana Jaatinen. Interview of Mr. Keijo Luukkonen, Vaisala Oyj, May 2002.

[61] Ilkka Ikonen. Laskentamenetelmien ja ohjelmiston suunnittelu automaattiseen ylätuulien mittausjärjestelmään (Algorithm and software development for an automatic uppper-air measurement system). Master's thesis, Helsinki University of Technology, Espoo, Finland, February 1974.

[62] International Telecommunication Union (ITU). *Liste internationale des frequences*. Comité international d'enregistrement des fréquences (I.F.R.B). Sixiéme édition.

[63] Benjamin Peterson, Keith Gross, Eric Chamberlin, and Timothy Montague. Integrated CIS VLF/Omega receiver design. *IEEE AES Systems Magazine*, 8(1):9–20, January 1993.

[64] United States Coast Guard, Washington, DC. *Omega, Facts&Figures*. Brochure, no date, prior to 1992.

[65] United States Coast Guard. *Radionavigation Bulletin*. Spring/Summer Issue 1997, Number 32.

[66] United States Coast Guard. *Radionavigation Bulletin*. Fall/Winter Issue 1995, Number 30.

[67] United States Coast Guard. *Radionavigation Bulletin*. Fall/Winter Issue 1996, Number 31.

[68] United States Coast Guard. *Radionavigation Bulletin*. Fall/Winter Issue 1997, Number 33.

[69] U.S. Department of Transportation. Omega radionavigation system termination. *Federal Register: Notices*, 61(199):53479–53480, October 11 1996.

[70] International Telecommunication Union (ITU). *International Frequency List*. 94-2 edition, 1994. CD-ROM, 1994-09-14.

[71] United States Navy. *http://www.tacamo.navy.mil*.

[72] United States Navy. *http://www.navy.mil/*.

[73] Juhana Jaatinen. Communications VLF stations. UAD-314-97-003, Vaisala Oy, 1997.

[74] Paul Rohan. *Introduction to Electromagnetic Wave Propagation*. Artech House, 1991.

[75] Mac E. Van Valkenburg, and Wendy M. Middleton, Editors-in-chief. *Reference Data for Engineers: Radio, Electronics, Computer, and Communications*. Newnes/Butterworth-Heinemann, Woburn, MA, 9th edition, 2002.

[76] Petre Stoica and Randolph Moses. *Introduction to Spectral Analysis*. Prentice Hall, Upper Saddle River, NJ, 1997.

[77] Charles W. Therrien. *Discrete Random Signals and Statistical Signal Processing*. Prentice Hall, Englewood Cliffs, NJ, 1992.

[78] Barbara Resch, Mattial Nilsson, Anders Ekman, and W. Bastiaan Kleijn. Estimation of the instantaneous pitch of speech. In *IEEE Transactions on Acoustics, Speech, and Signal Processing*, volume 15, pages 813–822, March 2007.

[79] Tim R. Black and Kevin D. Donohue. Pitch determination of music signals using the generalized spectrum. In *Proceedings of the IEEE, Southeastcon 2000*, pages 104–109, 2000.

[80] Patricia A. Pelle. A robust pitch extraction system based on phase locked loops. In *Proc. IEEE International Conference on Acoustics, Speech and Signal Processing, ICASSP 2006*, volume 1, pages 249–252, May 2006.

[81] G. T. Hurst, and S. C. Gupta. On the performance of digital phase locked loops in the threshold region. In *IEEE Transactions on Communications*, volume 22, pages 724–726, May 1974.

[82] Mohamed C. Benhabib, Fei Wang, and Jorge L. Duarte. Improved robust phase locked loop for utility grid applications. In *Proc. 13th European conference on Power Electronics and Applications, EPE '09*, pages 1–8, September 2009.

[83] M. Glickman, S.-c. Kam, and Z. Hussain. The use of digital phase locked loops for estimation of instantaneous frequency rate in distributed power networks. In *Australasian Universities Power Engineering Conference, AUPEC 2007*, pages 1–3, December 2007.

[84] A. W. Krieger, and J. C. Salmon. Frequency locked phase estimation under harmonically distorted conditions. In *Proc. IEEE Power Electronics Specialists Converence, PESC 2007*, pages 2982–2986, June 2007.

[85] F. Cupertino, L. Salvatore, E. Lavopa, M. Sumner, and P. Zanchetta. A DFT-based phase locked loop for phase and amplitude tracking in aircraft electrical systems. In *Proc. IEEE International Electric Machines and Drives Conference, IEMDC '09*, pages 1820–1825, May 2009.

[86] Carlo Offelli, and Dario Petri. The influence of windowing on the accuracy of multifrequency signal parameter estimation. In *IEEE Transactions on Instrumentation and Measurement*, volume 41, pages 256–261, April 1992.

[87] Thomas Grandke. Interpolation algorithms for discrete fourier transforms of weighted signals. In *IEEE Transactions on Instrumentation and Measurement*, number 2, pages 350–355, June 1983.

[88] Dusan Agrez. Imroving phase estimation with leakage minimization. In *Proc. IEEE Instrumentation and Measurement Technology Conference*, volume 1, pages 162–167, May 2004.

[89] Miloš Sedláček. Digital measurement of phase difference of LF signals–A comparison of DSP algorithms. In *Proc. XVII IMECO World Congress*, pages 639–644, Dubrovnik, Croatia, June 2003.

[90] Jiang Chaoshu, Wang Xuegang, and Liu Changzhong. Time-delay estimation for single-frequency pulse signals based on differential maximum likelihood estimation method and DTFT. In *Proc. IEEE International Conference on Communications, Circuits and Systems, ICCCAS2008*, pages 934–936, May 2008.

[91] Brian M. Sadler, and Richard J. Kozick. A survey of time delay estimation performance bounds. In *Fourth IEEE Workshop on Sensor Array and Multichannel Processing*, pages 282–288, July 2006.

[92] Jian Li, Renbiao Wu, and Zheng-She Liu. Efficient super resolution time delay estimation techniques. In *Proc. IEEE International Conference on Acoustics, Speech and Signal Processing*, volume 4, pages 2473–2476, May 1998.

[93] Francesco Viola, and William F. Walker. A spline-based algorithm for continuous time-delay estimation using sampled data. In *IEEE Transactions on Ultrasonics, Ferroelectrics, and Frequency Control*, volume 52, pages 80–93, January 2005.

[94] Filippo Giannetti, Marco Luise, and Ruggero Reggiannini. Simple carrier frequency rate-of-change estimators. In *IEEE Transactions on Communications*, volume 47, pages 1310–1314, September 1999.

[95] José M. N. Leitão, and Fernando M. G. Sousa. Recursive Bayesian phase estimation in ranging and mobile communications. In *Proc. 11th IEEE Signal Processing Workshop on Statistical Signal Processing*, pages 202–205, 2001.

[96] Michele Morelli, and Umberto Mengali. Feedforward frequency estimation for PSK: a tutorial review. In *European Transactions on Telecommunications*, volume 9, pages 103–116. John Wiley & Sons, 1998.

[97] Dai-Ki Hong, and Sung-Jin Kang. Joint frequency offset and carrier phase estimation for the return channel for digital video broadcasting. In *IEEE Transactions on Broadcasting*, volume 51, pages 543–550, December 2005.

[98] Kurth H. Mueller, and Markus Müller. Timing recovery in digital synchronous data receivers. In *IEEE Transactions on Communications*, volume 24, pages 516–531, May 1976.

[99] Christian Bergogne, Philippe Sehier, and Michel Bousquet. A new frequency estimator applied to burst transmission. In *Proc. IEEE International Conference on Acoustics, Speech and Signal Processing, ICASSP-97*, volume 1, pages 267–270, April 1997.

[100] Kittipong Piyawanno, Maxim Kuschnerov, Fabian N. Hauske, Bernhard Spinnler, Ernst-Dieter Schmidt, and Berthold Lankl. Correlation-based carrier phase estimation for WDM DP-QPSK transmission. In *Photonics Technology Letters, IEEE*, volume 20, pages 2090–2092, December 2008.

[101] Benjamin R. Wiederholt, and Mario A. Blanco. Phase estimation algorithm for frequency hopped binary PSK and DPSK waveforms with small number of reference symbols. In *Proc. IEEE Military Communications Conference, MILCOM 2005*, volume 2, pages 845–850, October 2005.

[102] France Mazzenga, and Giovanni Emanuele Corazza. Blind least-squares estimation of carrier phase, doppler shift, and doppler rate for m-PSK burst transmission. In *IEEE Communications Letters*, volume 2, pages 73–75, March 1998.

[103] N. Noels, H. Steendam, M. Moeneclaey, and Herwig Bruneel. Carrier phase and frequency estimation for pilot-symbol assisted transmission: Bounds and algorithms. In *IEEE Transactions on Signal Processing*, volume 53, pages 4578–4587, December 2005.

[104] Feng Rice. Carrier-phase and frequency-estimation bounds for transmissions with embedded reference symbols. In *IEEE Transactions on Communications*, volume 54, pages 221–225, February 2006.

[105] John G. Proakis and Dimitris G. Manolakis. *Digital Signal Processing, Principles, Algorithms and Applications*. Prentice Hall International, Upper Saddle River, NJ, 1996.

[106] Irfan Ali, Naofal Al-Dhahir, and John E. Hershey. Doppler characterization for LEO satellites. In *IEEE Transactions on Communications*, volume 46, pages 309–313, March 1998.

[107] Marcelo Alonso and Edward J. Finn. *Fundametal university physics, Fields and waves*, volume II. Addison-Wesley, Reading, MA, 7th printing, 1975.

[108] Jian Li. *EEL 6537–Spectral Estimation*. Department of Electrical and Computer Engineering, University of Florida, Gainesville, FL 32611, USA, 2005. Lecture notes to accompany *Introduction to Spectral Analysis* 2nd ed., 254 pages.

[109] J.S. Milton, and Jesse C. Arnold. *Introduction to Probability and Statistics: principles and applications for engineering and the computer sciences*. McGraw-Hill International Editions, Singapore, 3rd edition, 1995.

[110] David C. Rife, and Robert R. Boorstyn. Single-tone parameter estimation from discrete-time observations. In *IEEE Transactions on Information Theory*, volume IT-20, pages 591–598, September 1974.

[111] Richard G. Lyons. *Understanding Digital Signal Processing.* PTR Prentice Hall, Englewood Cliffs, NJ, 2nd edition, 2004.

[112] W. H. Press and S. A. Teukolsky and W. T. Wetterling and B. P. Flannery. *Numerical Recipes in C.* Cambridge University Press, 1992.